

# 1 Assessing raindrop evolution over northern Western Ghat 2 from stable isotope signature of rain and vapour

3 Sheena Sunil Nimya<sup>1,2</sup>, Sundara Pandian Rajaveni<sup>1</sup>, Saikat Sengupta<sup>1\*</sup>, Sourendra Kumar  
4 Bhattacharya<sup>3</sup>, Nandhini Ananthvel<sup>1</sup>

Formatted: Not Superscript/ Subscript

5 <sup>1</sup>Center for Climate Change Research, Indian Institute of Tropical Meteorology, Ministry of Earth Sciences,  
6 Pune-411008, India

7 <sup>2</sup>Department of Earth, Atmospheric and Planetary Sciences, Purdue University, West Lafayette, IN, USA

8 <sup>3</sup> Institute of Earth Sciences, Academia Sinica, Taipei 11529, Taiwan

9 \*Correspondence to: Saikat Sengupta; email: (saikat@tropmet.res.in)

Formatted: Font: Not Italic

Formatted: Font: Not Italic

Formatted: Font: Not Italic

## 10 Abstract.

Formatted: Font: Not Bold

11 Rain and vapour isotopes were analyzed in samples collected simultaneously from Pune, India during the 2019  
12 summer monsoon. The heavy isotopes of both oxygen and hydrogen ( $\delta^{18}\text{O}$  and  $\delta\text{D}$ ) were significantly depleted  
13 in four events when the Outgoing Longwave Radiation showed strong negative anomaly suggestive of large-  
14 scale convection. The  $\delta^{18}\text{O}$  of the rain samples are negatively correlated with d-excess indicative of modification  
15 of rain drops by evaporation. Analysis of the isotope data indicates isotope exchange between rain and ambient  
16 vapour and significant raindrop evaporation in the sub-cloud layer. The data plotted in terms of  $\Delta\delta-\Delta d$ , where  $\Delta$   
17 indicates difference between rain-equilibrated vapour and the surface vapour, show equal number of points lying  
18 in the 3rd and 4th quadrants, suggesting equal share of two effects: equilibrium exchange with ambient vapour  
19 and drop evaporation.

Formatted: Font: Not Bold

Formatted: Font: Not Bold

Formatted: Font: Symbol, Not Bold

Formatted: Font: Not Bold, Superscript

Formatted: Font: Not Bold

Formatted: Font: Not Bold

Formatted: Font: Symbol, Not Bold

Formatted: Font: Not Bold

Formatted: Font: Symbol, Not Bold

Formatted: Font: Not Bold, Superscript

Formatted: Font: Not Bold

Formatted: Font: Symbol, Not Bold

Formatted: Font: Not Bold

Formatted: Font: Symbol, Not Bold

Formatted: Font: Not Bold

20 operating equally

21 We used one-dimensional Below Cloud Interaction Model to quantify sub-cloud processes affecting raindrop  
22 evolution. A Rayleigh ascent assumption in BCIM overestimates rain isotope values, although model and  
23 observed values are well correlated. Using radiosonde-based temperature and humidity profiles and constructing  
24 vapour isotope profiles from a combination of satellite (Tropospheric Emission Spectrometer) data and a global  
25 circulation model (LMDZ) output, simulations improve and good agreement of model with observed values are  
26 obtained. Sensitivity studies reveal that model outputs are strongly influenced by vapour isotope profiles, and  
27 moderately by drop size, temperature and relative humidity. Raindrop evaporation estimated from mass change  
28 in the model shows that, on average, 23 % of drop mass evaporated in this regionarea.

29

30

31

32

33

34

35

36

37

38

39 ~~Abstract. Isotope exchange between vapor and rain critically influences rain isotope values, which are useful in~~  
40 ~~modeling raindrop evolution. A one-dimensional Below-Cloud Interaction Model (BCIM) has been used to~~  
41 ~~quantify sub-cloud processes affecting raindrop evolution in extratropical regions. However, its applicability has~~  
42 ~~not been tested in a tropical monsoon region, where both advection of moisture and raindrop evaporation are~~  
43 ~~significant. Here, we evaluate the applicability of BCIM using simultaneous surface measurements of rain and~~  
44 ~~vapor isotopes over Pune, a tropical rain-shadow region, during the 2019 Indian Summer Monsoon. Analysis of~~  
45 ~~these data indicates strong isotope exchange and significant raindrop evaporation in the sub-cloud layer. A~~  
46 ~~Rayleigh ascent in BCIM overestimates rain isotope values (by about 6 ‰ for  $\delta D$ ), although model and~~  
47 ~~observed values are well correlated. Using radiosonde-based temperature and humidity profiles and constructing~~  
48 ~~vapour isotope profiles from a combination of satellite (Tropospheric Emission Spectrometer) data and the~~  
49 ~~LMDZ model outputs, simulations improve. Further tuning of vapour isotope inputs while preserving the shape~~  
50 ~~of the profiles yields still better agreement. Sensitivity studies reveal that model outputs are strongly influenced~~  
51 ~~by vapour isotope profiles, and moderately by drop size and relative humidity. We used BCIM to estimate~~  
52 ~~raindrop evaporation, which shows that, on average, 23 % of rain mass evaporated over Pune. Our results~~  
53 ~~emphasize the importance of rain evaporation over the Indian continent during the Monsoon season, in~~  
54 ~~particular, over complex orography, and illustrate the use of water isotopes to constrain this key process.~~

Formatted: Line spacing: 1.5 lines

55  
56  
57  
58  
59  
60  
61  
62  
63  
64  
65  
66  
67  
68  
69  
70  
71  
72  
73  
74

## 75 1. Introduction

76  
77 The Intergovernmental Panel on Climate Change (IPCC) has ~~emphasised~~emphasized the importance of  
78 recycled moisture in the atmosphere (IPCC, 2014). Moisture recycling includes processes by which a fraction of  
79 the precipitated water returns to the atmosphere and ~~adds to the existing vapour that may~~ cause further  
80 precipitation over the same area (Gray, 2012). These processes are soil evaporation, transpiration from plants,  
81 intercepted or condensed water on leaves, and evaporation from falling raindrops (Brubaker et al., 1993;  
82 Trenberth, 1999). The moisture recycling increases with ~~the~~ ambient temperature but ~~is lessened~~decreases with  
83 increasing humidity (Pranindita et al., 2022; Zaitchik et al., 2006; Zhang et al., 2021). It has been seen (Kumar  
84 et al., 2021; Pathak et al., 2014); that ~~Some earlier studies have estimated that a~~ high precipitation recycling

Formatted: Indent: First line: 1.27 cm

85 ratio; (~15%) ~~the ratio of recycled precipitation to total precipitation~~, operates over India (on average 15 %) ~~during the Indian Summer Monsoon (ISM; June-September); this happens despite the high humidity that~~  
86 ~~prevails over the subcontinent (Kumar et al., 2021; Pathak et al., 2014)~~. Among the recycled moisture sources,  
87 raindrop evaporation is difficult to estimate because (1) ~~determination of the~~ parameters needed for  
88 estimating rain evaporation ~~from various satellite data is~~ not ~~sufficiently accurate~~ accurately available from  
89 ~~satellite sources~~; and (2) station-based meteorological observations using Micro rain radars are limited (Dai et  
90 al., 2019; Li and Srivastava, 2001; Xie et al., 2016).

92 Stable isotopologues (~~mainly~~ ( $^1\text{H}_2^{18}\text{O}$ ,  $^1\text{H}_2^{16}\text{O}$ ,  $^1\text{H}_2^{16}\text{O}$ ) of liquid precipitation samples can be used to  
93 assess the magnitude of raindrop evaporation (Crawford et al., 2017; Rahul et al., 2016; Salamalikis et al., 2016;  
94 Wang et al., 2021; Xiao et al., 2021). Falling raindrops exchange isotopes with the ambient vapour; this happens  
95 throughout the fall but occurs mostly in the unsaturated sub-cloud layer. The magnitude of this exchange, which  
96 alters the rain isotope ratios, can, in principle, be used to quantify the extent of raindrop evaporation. Using  
97 satellite-based observations of vapour isotopologues ( $^1\text{H}_2^{16}\text{O}$  and  $^1\text{H}_2^{16}\text{O}$ ) and an isotope mass balance model,  
98 Worden et al. (2007) estimated that in the tropics, during the October to March interval, nearly 20 % of the mass  
99 of ~~a raindrop~~raindrops evaporate. However, they ~~also mentioned~~noted that the satellite data ~~used for~~  
100 ~~this Estimate~~ has limited temporal and spatial coverage. Therefore, ~~these datasets may not be useful for~~  
101 estimating drop evaporation on a daily to monthly scale ~~over is difficult~~some specific locations. ~~In another~~  
102 ~~approach,~~ Raindrop evaporation has ~~also~~ been estimated from ground-based rain isotope observations and a set  
103 of empirical equations (Froehlich et al., 2008; Li et al., 2021; Wang et al., 2016; Zhu et al., 2021). However, ~~it~~  
104 ~~remains a challenge to account for all~~such attempts are often inaccurate because they exclude many important  
105 cloud microphysical processes and ~~their~~ associated isotopic fractionations. Normally, these processes are  
106 considered for simulating rain isotope values in various General Circulation Models (GCM; Risi et al., 2019;  
107 Yoshimura et al., 2008, Stewart, 1975). ~~The GCMs incorporate the isotope exchange scheme associated with~~  
108 ~~evaporation (Stewart, 1975)~~. ~~Nevertheless~~However, recent studies have shown that most of these GCMs over or  
109 underestimate raindrop evaporation in tropical India (Nimya et al., 2022; Sengupta et al., 2023). This is possibly  
110 due to the coarseness of grid sizes used in these GCMs, which are inadequate to capture the region-specific  
111 complexities of processes controlling the evaporation. This necessitates controlled isotope observations and  
112 region-specific models for a reasonable estimation of this parameter (Aemisegger et al., 2015).

113 Various ~~modelling~~ approaches have been followed to estimate raindrop evaporation using paired  
114 observations of rain and vapour isotopes. For example, a bin resolved microphysical model was used to quantify  
115 drop evaporation during the Atlantic Tradewind Ocean–Atmosphere Mesoscale Interaction Campaign  
116 (ATOMIC; Sarkar et al., 2023). Graf et al. (2019), based on surface rain and vapour isotope observations in  
117 Zurich, Switzerland, provided a rationale to evaluate various processes controlling the isotope values. They  
118 developed a simple one-dimensional model (Below Cloud Interaction Model, BCIM) which considers essential  
119 cloud microphysical processes during raindrop formation (vapour deposition, ~~rimming-riming~~ etc.) as well as  
120 evaporative exchange processes within and below the cloud. That model; ~~in principle, shows~~as ~~determines~~ the  
121 isotopic evolution of an ice/liquid drop ~~that is~~ released from a desired altitude ~~and~~ ~~and suffers the~~ ~~undergoing~~  
122 ~~exchange~~ ~~mentioned~~ processes enroute its fall to the ground. ~~Although their model is capable of~~  
123 ~~differentiating isotopic signals of different sub-cloud processes~~However, being ~~one-dimensional~~one-dimensional  
124 vertical model, ~~it~~ does not consider any moisture advection, updraft and downdraft. ~~Nevertheless,~~ ~~it~~ is

125 worthwhile ~~to explore~~exploring the efficacy of that model in a semi-tropical region like Pune during the ISM  
126 when advected moisture fluxes play an important role (Das, 1986; Levine and Turner, 2012).

127 In the Western Ghat (WG) region, shallow convective clouds predominate (80 % of clouds occur  
128 below 4 km and 45 % below 2.5 km altitude) during the ISM (Konwar et al., 2014). Faster evaporation of  
129 smaller raindrops associated with intense rainfalls from these clouds provides significant positive energy  
130 feedback to form mesoscale convection (Konwar et al., 2014; Tao et al., 2012). ~~Another study, based on~~A study  
131 of drop size distributions, showed that raindrop evaporation prevails in the warm rain process ~~(shallow clouds)~~  
132 occurring in this region (Murali Krishna et al., 2021). ~~However, these studies were limited to scanty~~  
133 ~~observations~~ It is of interest to know if one can determine the raindrop evaporation and its variation using  
134 measurements of isotope ratios in rain and vapour ~~an independent, accurate, and simpler method. Isotope ratios~~  
135 ~~in rain and vapour provide such a method.~~

136 The current study investigates the applicability of the BCIM in a tropical Indian region using paired  
137 observations of rain and vapour isotopes for a summer monsoon season. ~~By a suitable choice of input~~  
138 ~~parameters for the BCIM, we may be able to estimate the raindrop evaporation in this area.~~

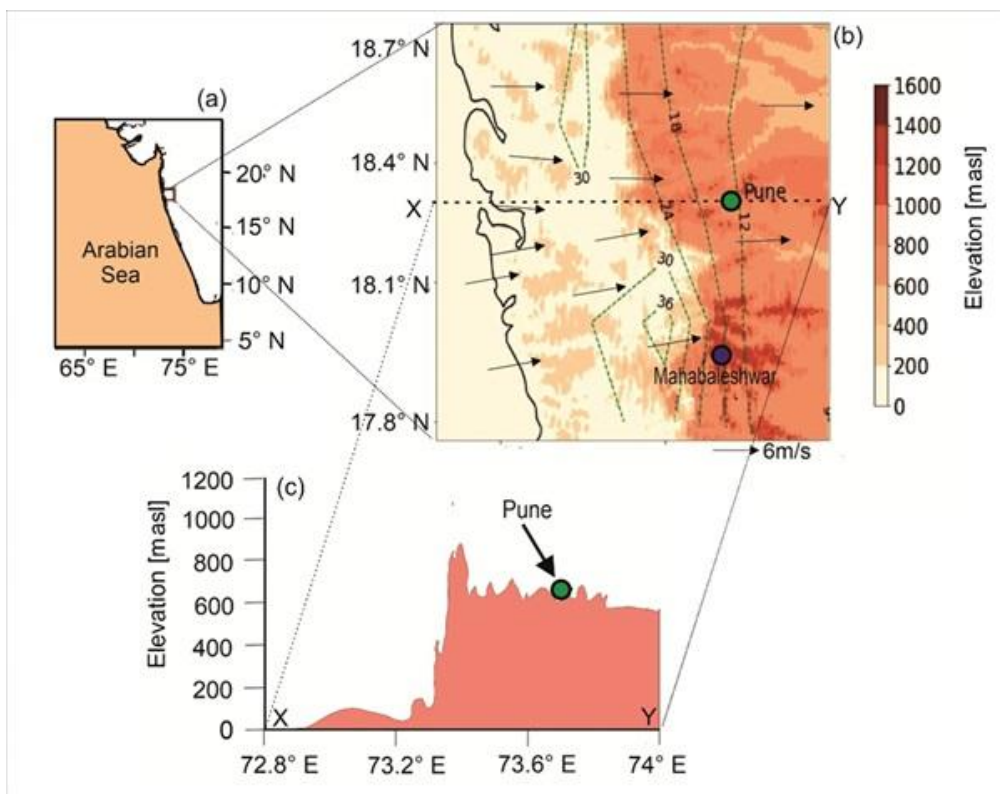
## 140 2. Experimental Methodology

### 141 2.1 Study area

142  
143 Rainwater and vapour samples ~~(mostly on rainy days but even for some non rainy days)~~ were collected  
144 from the ground level at the Indian Institute of Tropical Meteorology (18.53° N, 73.85° E), Pune during the  
145 summer monsoon of 2019. This region receives >90 % rainfall during the ISM and is situated at the lee (rain  
146 shadow) side of the Mountain (Fig. 1). ~~A brief discussion on sources and mechanisms of the ISM rainfall in~~  
147 ~~western India is given below.~~ Rainfall in Western India occurs from mid-tropospheric low-pressure systems in  
148 several episodes, each of which usually lasts for 2–3 days. ~~These systems are locked in place during these~~  
149 periods and fed by moisture derived from the Arabian Sea (Wang et al., 2006; Rao, 1976). The geographic  
150 location of the region, its altitude, ~~(from mean sea level)~~, rainfall variation across the WG mountains, and the  
151 topographic profile across Pune are shown in Fig. 1.

152 There is a sharp variation of rainfall across the mountain from the coastal zone (30 mm day<sup>-1</sup>)  
153 to the lee side (12 mm day<sup>-1</sup>) which is a characteristic of orography-induced rainfall (Fig. 1). The surface air  
154 temperature in Pune varies from 20° C to 30° C during the ISM (Pattanaik et al., 2019).

Formatted: Indent: First line: 1.27 cm



159  
 160 **Figure 1:** (a) The location of the study area in India. (b) Topographic map of the northern Western Ghat, India (prepared  
 161 based on the GTOPO30 digital elevation model). The rainfall contours (long-term (1901-2017) mean June-September  
 162 rainfall in mm/day) were constructed using gridded (0.25°x0.25°) rainfall data (1901-2020) from the India Meteorological  
 163 Department (IMD). (c) A topographic profile along the latitude 18.53° N through Pune (Green circle at altitude of 560 m)  
 164 shows its position ~~in a rain shadow region~~.

165  
 166 **2.2 Sample Collection, Isotope Measurements**

168 The onset and withdrawal dates of ISM (based on wind direction, specific humidity, and outgoing long  
 169 wave radiation OLR; IMD, 2019) at Pune in 2019 were 22 June 2019 and 4 October 2019; respectively. Liquid  
 170 water samples were collected during rains using samplers made following the guidelines of the International  
 171 Atomic Energy Agency ([http://www.naweb.iaea.org/naweb/ih/documents/other/gnip\\_manual\\_v2.02\\_en\\_hq.pdf](http://www.naweb.iaea.org/naweb/ih/documents/other/gnip_manual_v2.02_en_hq.pdf)).  
 172 (see Supplementary Information Fig. SI-1,1). ~~The samples were transferred into 8 ml Polycarbonate bottles and~~  
 173 ~~stored in a dark and cold place. The sampling procedure and storage were such as to ensure negligible~~  
 174 ~~evaporation of the samples after collection (Rajaveni et al., 2024). A total of 59 rain samples were collected. For~~  
 175 ~~vapour samples, An indigenously in-house fabricated glass condenser was used for the vapour sample~~  
 176 ~~collection (see Fig. SI-2-1). One end of the condenser was connected to a diaphragm pump through a PTFE~~  
 177 ~~tube. The ambient air was pulled by the pump through this glass condenser at a flow rate of 800 ml min<sup>-1</sup>. The~~  
 178 ~~glass condenser was immersed in a precooled Dewar flask. The temperature of the flask was maintained at -80°~~  
 179 ~~C by using alcohol slurry. At this temperature, the atmospheric moisture is condensed into water, and all other~~

**Formatted:** Indent: First line: 1.27 cm

**Formatted:** Font: Not Bold

**Formatted:** Font: Not Bold, Not Highlight

**Formatted:** Font: Not Bold, Not Highlight

**Formatted:** Font: Not Bold, Not Highlight

**Formatted:** Superscript

180 ~~non condensable gases are pumped out. The sampling was usually carried out for 3-4 hours, which was~~  
181 ~~sufficient to obtain an adequate amount of water (the collected sample was about 1 ml, which is at least double~~  
182 ~~the amount required for one analysis).~~ Most of the vapour samples were collected during the rainy days  
183 (avoiding direct raindrop entry), but some were also collected during the non-rainy period. [The collection](#)  
184 ~~efficiency was estimated from the amount collected as against the amount expected (see Table SI-2-1). The~~  
185 ~~collected samples are transferred to 2 ml glass vials, which are directly used for isotopic measurement.~~ Due to  
186 logistical problems, vapour samples could not be collected before mid-July. A total of 50 vapour samples were  
187 collected ~~during the study period,~~ and 29 of them coincided with [the rain sampling](#) days. ~~These 29 sample pairs~~  
188 ~~are considered for the present study.~~

Formatted: Not Highlight

189 The liquid samples (~~both rain~~ water and condensed vapour) were measured using a Liquid Water  
190 Isotope Analyser (Model Number TIWA-45-EP, ~~manufactured by~~ Los Gatos Research (LGR). This instrument  
191 measures liquid samples using Off-Axis integrated cavity output spectroscopy (OA-ICOS) with a routine  
192 precision of 0.1 ‰ and 1 ‰ for  $\delta^{18}\text{O}$  and  $\delta\text{D}$  ([relative to VSMOW](#)), respectively (Rajaveni et al., 2024; [see](#)  
193 [also](#) [Supplementary Information SI-3](#)). The d-excess values defined as:  $\text{d-excess} = \delta\text{D} - 8 \cdot \delta^{18}\text{O}$  (Dansgaard,  
194 2012) have a precision of 1 ‰. The daily rain isotope data are weighted by the amount of rainfall on that day.

Formatted: Indent: First line: 1.27 cm

Formatted: Font: Not Bold, Not Highlight

### 196 2.3 Satellite and ground-based meteorological [observations data](#)

197  
198 The rainfall data (~~accumulated over 24 hours~~) are obtained from the Pune observatories of the IMD,  
199 available at the National Data Centre ([www.imdpune.gov.in/ndc\\_new/ndc\\_index.html](http://www.imdpune.gov.in/ndc_new/ndc_index.html)). Apart from ~~daily~~  
200 ~~rainfall, hourly~~ rainfall, daily average temperature and relative humidity data for Pune observatory were also  
201 obtained ~~from the IMD reports~~. The daily gridded data (zonal and meridional wind, specific humidity, air  
202 temperature, and cloud liquid water content) from the European Centre for Medium-Range Weather Forecasts  
203 Reanalysis (ERA5) dataset with a resolution of  $0.25^\circ \times 0.25^\circ$  (Hersbach et al., 2020) ~~are also used and~~ ~~the~~  
204 ~~Interpolated Outgoing Longwave Radiation (OLR) data ( $2.5^\circ \times 2.5^\circ$ ) from NOAA~~  
205 (<https://psl.noaa.gov/data/gridded/data.olrldr.interp.html>) are used in this study. The upper-air radiosonde  
206 measurements (relative humidity, temperature) carried out over Pune ~~were~~ ~~was~~ obtained from the University of  
207 Wyoming repository (<http://weather.uwyo.edu/upperair/sounding.html>). The vertical variation ([every 50 mb](#)  
208 [interval](#)) of the two parameters (~~profiles~~) was available for two times: at 00 UTC and 12 UTC ~~for the entire~~  
209 ~~study period and~~ ~~for~~ each parameter, the two profiles are averaged to make a representative daily profile. The  
210 typical uncertainty of temperature and relative humidity is  $0.3^\circ\text{C}$  (Sapucci et al, 2005; Jensen et al., 2016) and 8  
211 % (Xu et al., 2023), respectively. ~~(see discussion on uncertainty in section 4.3.5 and also SI-12).~~ Tropospheric  
212 Emission Spectrometer (TES) Level 2 (Nadir-Lite-Version 6) retrievals of HDO and H<sub>2</sub>O profiles for the  
213 available period (2005–2007) are used to construct ~~a~~ mean vapour  $\delta\text{D}$  profiles. The details of quality control  
214 criteria and biases associated with TES observations are discussed by Herman et al. (2014) and Worden et al.  
215 (2011). Grid point observations of  $\delta\text{D}$  by TES have a precision of  $\sim 10\text{--}15\%$ , which reduces to  $1\text{--}2\%$  when  
216 the data are averaged over a larger region (Lee et al., 2011; Pradhan et al., 2019).

Formatted: Indent: First line: 1.27 cm

Formatted: Font: Bold, Not Highlight

Formatted: Font: Bold

217 To decipher the moisture sources for vapour/rain at and around our study area, ~~48-hour~~ air mass back  
218 trajectory analysis was carried out at 850 mb pressure level using the NOAA Hybrid Single-Particle Lagrangian  
219 Integrated Trajectory (HYSPPLIT) model (Draxler and Hess, 1997). The model tracks the movement of air

220 parcels backward from a given location for a desired period: ~~The Global Data Assimilation System (GDAS; 1°×~~  
221 ~~1°; Kanamitsu, 1989) dataset is used for back trajectory analyses(see SI-4-1).~~

Formatted: Not Highlight

Formatted: Font: Not Bold

## 224 2.4 ~~The appropriate~~ input parameters for BCIM

### 226 Isotope Model BCIM

228 ~~As mentioned before, to understand water vapour isotope exchange in the sub-cloud layer, we used the~~  
229 ~~Below-Cloud Interaction Model (BCIM) proposed by Graf et al. (2019).~~ Various parameterisation schemes used  
230 in the BCIM have been discussed ~~in the aforementioned earlier study by Graf et al.~~ A brief description of this  
231 model, as applicable for ~~Pune (the shallow cloud processes over Pune),~~ is provided ~~herefor completeness.~~ The  
232 model comprises a single vertical column that extends from the ground level to the point at which a single  
233 hydrometeor is introduced ~~at the base of the cloud, and follows its fate.~~ Within this column, the hydrometeor  
234 descends under the influence of gravity, undergoes growth or evaporation (depending upon the ambient  
235 humidity and temperature), changes its isotopic composition through equilibrium and kinetic isotope exchange  
236 with surrounding vapour, and finally reaches the surface ~~as raindrop-as-rain.~~ The final isotopic composition of  
237 the hydrometeor is estimated following four steps of calculations: (1) setting up the initial condition ~~involving~~  
238 ~~the drop introduction height and its size,~~ (2) estimation of the initial isotopic composition of the hydrometeor,  
239 (3) micro-physics of falling hydrometeor, and (4) tracking the changes in isotopic composition along the ~~vertical~~  
240 ~~fall trajectory descent.~~ ~~To estimate the initial isotopic composition of the drop and its evolution,For these~~  
241 ~~calculations,~~ the model requires temperature, humidity and vapour isotope ~~depth-altitude~~ profiles for a given day  
242 as input parameters. The drop is assumed to form in equilibrium (at relative humidity, RH=100 %) ~~at the cloud~~  
243 ~~base and starts its journey.~~ The input parameters ~~applicable tofor~~ the vapour can be introduced into the ~~model~~  
244 ~~BCIM~~ in two different ways: (1) the profiles can be calculated based on ~~the assumption of~~ idealised (moist)  
245 adiabatic ascent of an air parcel from the surface to the top of the column following a Rayleigh model; ~~RH, T~~  
246 ~~and~~ isotope values at various pressure levels are then estimated from the Rayleigh distillation equations ~~starting~~  
247 ~~from the measured surface values or, and~~ (2) the pressure level specific values of ~~the aforementioned~~  
248 ~~parameters~~ RH and T, if available from radiosondes and ~~isotope values from any satellite data and/or any model,~~  
249 ~~can be introduced directly into the BCIM.~~

250 ~~Since our aim is to understand the isotopic modification and mass loss suffered by the drops on the way~~  
251 ~~down, we introduce here two parameters  $\Delta\delta$  and  $\Delta d$  expressing the deviation of the final rain composition at the~~  
252 ~~ground from the ambient surface vapour. For this, we use difference between the isotopic composition of vapour~~  
253 ~~in equilibrium with the rain samples and the ambient surface vapour and define:  $\Delta\delta = \delta D$  (rain eq. vapour) -  $\delta D$~~   
254 ~~(surface vapour) and similarly for d-excess,~~

255  ~~$\Delta d = d$ -excess (rain eq. vapour) -  $d$ -excess (surface vapour).~~

Formatted: Indent: First line: 0 cm

Formatted: Indent: First line: 0 cm

Formatted: Font: Bold

Formatted: Indent: First line: 1.27 cm, No widow/orphan control, Don't adjust space between Latin and Asian text, Don't adjust space between Asian text and numbers

#### 258 2.4.1 Drop size assignment

259 ~~Apart from temperature, humidity and vapour isotopes, t~~The model ~~also~~ also requires ~~at the input drop~~

diameter of the initial hydrometeor (~~given in Section 4.3.1.1~~). Unfortunately, no disdrometer or Micro Rain Radar observations are available for Pune during 2019. We, therefore, adopted an empirical procedure, known as the Marshall-Palmer (M-P distribution) relationship (Marshall and Palmer, 1948), to estimate the mean drop size at the ground. First, we estimated the hourly mean drop size of the raindrops at the ground level from the hourly rain rate data, available from the IMD observatory at Shivajinagar, Pune, located about 4 km away from the sampling location. Next, we calculated the 24-hour mean drop size by taking a weighted average of the size using rain rates as the weights. The calculated drop sizes at the ground vary from 0.61 to 1.80 mm for various days. The drop diameter at the ground is next provided as an input and the initial size at the drop introduction height (about 2.0 km above ground) is estimated iteratively in BCIM using the microphysics part of the model using the temperature and RH profiles. This procedure was adopted for each day. The accuracy of the drop size based on the M-P distribution and the rain rate is limited, but this was the only imperative. ~~Unfortunately, since, no drop size (disdrometer) measurements were available over Pune during the 2019 monsoon. Therefore, our choice was guided by earlier modelling and observational studies where the M-P distribution were used (Graf et al., 2019; Sarkar et al., 2023; Morrison et al., 2020; Ryu et al., 2025; Jiang et al., 2024).~~

#### 2.4.2 Drop formation height assignment

The formation height of the drop should be fixed by considering the most probable altitude range where majority of the drops ~~are seen~~ exist in any given day. This was not known a priori and was inferred from the cloud liquid water content analysis. An earlier study by Kumar et al. (2014) showed that a peak of Cloud Liquid Water Content (CLWC) is often present at about 850 mb during the monsoon season over western India. In the present case, the CLWC data for ~~a period of 29 days~~ of the study period obtained from the ERA5 dataset show a peak at  $830 \pm 70$  mb, i.e., about 1650 m above msl (See Table SI-5-1 and ~~See Fig. SI-5-1~~). Here, we consider the CLWC peak of a given day as the drop introduction height for that day. ~~We also impose the condition that the RH at that height has a value of 100 %.~~

In the present study, we consider the cloud base height as the Lifting Condensation Level (LCL) where RH is 100% equilibrium

The RH and T profiles from the ~~fitted~~ radiosonde data at various heights (with extrapolated ground level values; see SI-8b) are used to estimate the LCL using Skew T-Log P diagram for all 29 sampling days. The LCL varies from 820 to 900 mb and the average height is  $890 \pm 20$  mb (about 1050 m; see Table SI-5-1). We notice that the LCL is always below (about 600 m on average) the corresponding day's CLWC peak as it should be and therefore, the drop falls ~~fall some of its fall in~~ through a zone of 100% RH till it emerges below the cloud base or LCL (see SI-5).

~~(Table 1) the altitude of data for the sake of the model~~

#### 2.4.3 Isotopic composition of the ambient vapour and hydrometeor

~~Next,~~ The isotopic composition of the introduced hydrometeors is estimated. ~~They are assumed to be formed by assuming formation~~ in equilibrium from the vapour at ~~this is~~ altitude, ~~at~~ and their composition is calculated from the isotopic composition of this vapour ~~at the~~ ambient temperature. Subsequently, these drops grow or diminish as they fall. The isotopic composition of the falling hydrometeor at ~~a given~~ lower altitudes is

- Formatted: Font color: Auto
- Formatted: Font color: Auto
- Formatted: Font: Times New Roman, 10 pt, Font color: Auto
- Formatted: Font color: Auto
- Formatted: Font: Times New Roman, 10 pt, Font color: Auto
- Formatted: Font: Times New Roman, 10 pt, Font color: Auto
- Formatted: Not Highlight
- Formatted: Not Highlight
- Formatted: Font: Times New Roman, 10 pt, Font color: Auto
- Formatted: Font: Times New Roman, 10 pt, Font color: Auto
- Formatted: Font: Times New Roman, 10 pt, Font color: Auto
- Formatted: Font: Times New Roman, 10 pt, Font color: Auto
- Formatted: Font: Times New Roman, 10 pt, Font color: Auto
- Formatted: Font color: Auto
- Formatted: Indent: First line: 1.27 cm
- Formatted: Not Highlight
- Formatted: Not Highlight
- Formatted: Font: Bold, Not Highlight
- Formatted: Font: Not Bold
- Formatted: Not Highlight
- Formatted: Font: Not Bold
- Formatted: Indent: First line: 1.27 cm
- Formatted: Font: (Default) Times New Roman, 10 pt, Font color: Auto
- Formatted: Font: (Default) Times New Roman, 10 pt, Font color: Auto
- Formatted: Font: (Default) Times New Roman, 10 pt, Font color: Auto
- Formatted: ...
- Formatted: ...
- Formatted: ...
- Formatted: ...
- Formatted: ...
- Formatted: ...
- Formatted: Not Highlight
- Formatted: No widow/orphan control
- Formatted: ...

300 then ~~estimated~~ calculated from the composition of the surrounding vapour by using isotope mass balance and  
301 diffusive transport involving appropriate fractionation factors (Graf et al., 2019).

302  
303 The mass and temperature of the hydrometeor are calculated along its fall trajectory ~~through-using~~ the  
304 microphysics of the falling hydrometeor. The terminal velocities are estimated using Foote and du Toit (1969).  
305 To calculate the change in mass and temperature between two pressure levels, the temperature, pressure, and  
306 humidity values are interpolated between these two levels. These changes are estimated as per Pruppacher and  
307 Klett (2010). It is important to mention here that many processes considered in BCIM do not occur for the  
308 shallow convective clouds in Pune (Utsav et al., 2017). Therefore, the BCIM ~~inputs as given in Graf et al.~~  
309 ~~(2019) are~~ modified taken accordingly in the present study. Below, we explore how accurately the BCIM can  
310 simulate rainwater isotopes in our tropical location.

Formatted: Indent: First line: 1.27 cm

### 311 4.3 Application of BCIM with appropriate input parameters

#### 312 4.3.1 Setting the boundary condition of the model

313  
314  
315 As mentioned before, to estimate hydrometeor isotopic composition, the BCIM requires vertical  
316 profiles of temperature, humidity and vapour isotope as input parameters. The vertical profiles can be introduced  
317 into the model in two ways: (1) Vertical ascent assumption. Here, the profiles can be calculated based on an  
318 idealised Rayleigh model having moist adiabatic ascent of air parcels from the surface to the top of the column,  
319 and (2) the T, RH profiles can be constructed based on available sounding data and isotope profiles can be  
320 derived from simulations conducted using isotope-enabled atmospheric models (Pfahl et al., 2012). These are  
321 discussed below (Sections 4.3.2 and 4.3.3).

Formatted: Indent: First line: 1.27 cm

#### 322 4.3.1.1 Formation height and drop size assignment

323  
324  
325 The formation height of the drop is an important factor and should be fixed by considering the most probable  
326 altitude range. This parameter is not known a priori, but we can infer this from the cloud liquid water content  
327 analysis. An earlier study by Kumar et al. (2014) pointed out that a peak of Cloud Liquid Water Content  
328 (CLWC) is often present at 850 mb during the monsoon season over western India. The CLWC data for a period  
329 of 29 days of the study period obtained from the ERA-5 dataset also show a peak at 850±50 mb (Supplementary  
330 Fig. S2). Here, we consider the CLWC peak at 850±50 mb (about 1 km above ground from Pune) as the drop  
331 introduction height for our case, where the RH reaches the value of 100 % (following Graf et al., 2019).

Formatted: Font: Not Italic

332 The BCIM also requires an initial drop size at the formation height. Unfortunately, no disdrometer or  
333 MRR observations are available in the study area during 2019. We, therefore, adopted an empirical procedure,  
334 known as the Marshall Palmer relationship, to estimate the mean drop size at the ground. This was done by a  
335 weighing procedure. First, we estimated the hourly mean drop size of the raindrops at the ground level from the  
336 hourly rain rate data available from an IMD observatory at Shivajinagar, Pune, located about 4 km away from  
337 our study area. Next, we calculated the 24 h mean drop size by taking a weighted average of the size and using  
338 rain rates as the weights. The surface drop sizes thus calculated vary from 0.61 to 1.80 mm for various days. The  
339 drop diameter at the ground is next provided as an input, and then the initial size at the drop height (about 1.5

340 km above ground) is estimated iteratively in BCIM using the microphysics part of the model dealing with the  
341 major isotope H<sub>2</sub>O (based on temperature and RH profile; Graf et al., 2019). This procedure was adopted for  
342 each day.

### 344 4.3.2 Results of simulation

#### 345 4.3.2.1 Run 1: Rayleigh ascent assumptions

346  
347 As mentioned above, the model needs vertical background profiles of atmospheric temperature (T), relative  
348 humidity (RH),  $\delta D_v$ , and d excess,  $d_v$ . In Rayleigh simulations, various profiles were calculated from the moist  
349 adiabatic ascent of an air parcel with surface values of temperature (T0), relative humidity (h0),  $\delta D_v$  ( $\delta v_0$ ) and  
350  $d_v$  ( $d_v_0$ ) of each sampling day as inputs (see isotope profiles in Supplementary Fig. S4a and b). The surface  
351 values of  $\delta D$  and d excess of vapour were taken from our vapour measurements along with the daily  
352 temperature and humidity data obtained from the IMD publication (Section 2.3). The results for the set of  
353 calculations using the Rayleigh ascent assumption (designated as Run 1) are shown in Fig. 6(a-d). In this set of  
354 figures, we compare observed and model rain  $\delta D$  (Fig. 6a),  $\delta^{18}O$  (Fig. 6b), and d excess (Fig. 6c) values. We  
355 also construct  $\Delta\delta$ - $\Delta d$  diagrams for both observed and model values and compare them in Fig. 6d. Although  
356 observed and model isotope values (Fig. 6a and 6b) show strong correlation ( $R^2=0.86$  and  $0.79$ , respectively),  
357 the model values are mostly overestimated (the plotted points lie below the 1:1 line). The overestimations of  
358 isotopes (for  $\delta^{18}O$  and  $\delta D$ ) affect the d excess values considerably more; the points lie far to the right, and no  
359 correlation exists between the observed and model d excess values (Fig. 6c). This is because the d excess  
360 parameter is more sensitive to departure from equilibration due to dominance of evaporation, which means that  
361 a small departure of delta values would magnify the discrepancy in case of d excess. We also note that most of  
362 the model data points in a  $\Delta\delta$ - $\Delta d$  cross plot do not agree with the observed ones. However, they do fall in the  
363 lower right quadrant, which is consistent with high raindrop evaporation. We also note that the  $\Delta\delta$  and  $\Delta d$  model  
364 values (Fig. 6d, Run 1) show smaller variations compared to the observations. The  $\Delta\delta D$  of the model  
365 simulations varies from 0‰ to 5‰ and  $\Delta d$  from 0‰ to 5‰, while the observed values have variations of  
366 about 25‰ (higher by a factor of 5). These comparisons show that the Rayleigh ascent model fails to reproduce  
367 the evolution of the rain isotopes in our region.

#### 369 4.3.2.2 RH and T from Radiosonde and isotope profiles from TES and LMDZ (Run 2)

370  
371 Rayleigh ascent in Run 1 assumes that the source of vapour aloft is the rising air parcel, and the isotope values  
372 along with RH and T should reflect that. But this did not yield a good fit. The simulation can possibly be  
373 improved if we use RH and T data from local radiosonde observations and different isotope profiles. For the  
374 present period, the radiosonde data were available only at a few specific pressure levels, and hence, appropriate  
375 interpolations were carried out. To obtain the vertical profiles of vapour isotopes, we first use the isotope  
376 outputs of a GCM, LMDZ for Pune (Dr. Camille Risi; personal communication). These values are used in  
377 BCIM as inputs, and the simulated rainwater and vapour composition were compared with the observed values.  
378 We found that a wide difference exists between the observed and model rain/vapour isotopic values. We suspect  
379 that the LMDZ model may not be able to simulate the vapour isotope ratios accurately. This limitation was

380 noted by Risi et al. (2021) in a recent study involving large eddy simulation; they observed that for high  
381 precipitation areas, the convective or mesoscale downdrafts bring more depleted vapour from above into the  
382 sub-cloud layer. Therefore, as an alternative, we used the  $\delta D_v$  profiles modified from TES observations. These  
383 profiles are constrained by using the measured ground level vapour isotope ratios as a boundary condition while  
384 maintaining the shape of the profile. The procedure is discussed below in the light of our analysis period.

385 Firstly, TES vapour  $\delta D$  data are not available for 2019. Moreover, it is also known that the data have  
386 large uncertainty within the boundary layer (Nimya et al., 2022). This necessitates the derivation of vapour  
387 isotope profiles, which would merge with the TES observations at upper layers. The TES provides  $\delta D$  values of  
388 moisture at 17 pressure levels with a 5.3 km  $\times$  8.4 km footprint during the years 2005-2009. Based on these, we  
389 derived an average TES profile, which is deemed to be representative of the mean monsoon values constructed  
390 by averaging TES observations over a box (16°-20° N; 72°-76° E) for the ISM period.

### 393 3. Results

394 We present the results of the present current study in two sections: (1) Results of isotope analysis and  
395 (2) Results of BCIM simulations. The first section presents the measured isotope ratios in the context of  
396 meteorological parameters whereas the BCIM simulations show how accurately we can reproduce are compared  
397 with the measured values in the second section.

#### 399 3.1 Results of isotope analysis

400 Measured rain and vapour isotope ratios ( $\delta^{18}O$  and d-excess) on a daily scale are plotted in Fig. 2a and  
401 2b. The general pattern of variations in vapour and rain  $\delta^{18}O$  values is similar; both decrease significantly and  
402 consistently after mid-August. The vapour  $\delta$ -values are lower than the rain. In contrast, the d-excess values of  
403 vapour are always much higher. The  $\delta^{18}O$  and d-excess values of rainwater range from -10.8 ‰ to 1.5 ‰ and  
404 -2 ‰ to 12 ‰ respectively, while those of the vapour range from -19 ‰ to -9 ‰ and 10 ‰ to 30 ‰,  
405 respectively. The mean and  $0.51\sigma$  standard deviation of  $\delta^{18}O$  and d-excess values of rainwater are  $-1.3 \pm 1.22.6$   
406 ‰ and  $3.9 \pm 1.32.7$  ‰, while those of the vapour are  $-12.5 \pm 1.252.5$  ‰ and  $18.3 \pm 2.555.2$  ‰, respectively. The  
407  $\delta^{18}O$  (Fig. 2a) and d-excess (Fig. 2b) time series show four interesting features: (1) For the four date ranges: 27-  
408 29 July, 24-27 July, 4-8 September, and 19-27 September, significant and consistent decrease in isotope values  
409 are observed in both rain and vapour phases (marked 1, 2, 3, 4 in Fig. 2a; no vapour data available for date range  
410 1). (2) On 19 September, the vapour shows sudden decrease (marked A in Fig. 2a). (3) there is a gradual  
411 decrease in vapour  $\delta^{18}O$  values and an increase in d-excess values with the progress of the monsoon, especially  
412 more in the later part, and (4) rain d-excess values remain constant with time but  $\delta^{18}O$  of both rain and vapour  
413 start decreasing beginning from early September onwards.

Formatted: Font: Not Bold, English (India), Character scale: 100%

Formatted: Font: English (India), Character scale: 100%

Formatted: Font: English (India), Character scale: 100%

Formatted: Justified, Indent: First line: 1.24 cm

Formatted: Font: English (India), Character scale: 100%

Formatted: Font: English (India), Character scale: 100%

Formatted: Font: English (India), Character scale: 100%

Formatted: Font: English (India), Character scale: 100%

Formatted: ...

Formatted: ...

Formatted: ...

Formatted: Font: Not Bold

Formatted: Font: Bold

Formatted: ...

Formatted: Font color: Auto

Formatted: Font: Times New Roman

Formatted: Font color: Auto

Formatted: Font:

Formatted: Font color: Auto

Formatted: Font:

Formatted: Font:

Formatted: Font:

Formatted: Font:

Formatted: Font:

Formatted: Font:

Formatted: Font:

Formatted: Font:

Formatted: Font:

Formatted: Font:

Formatted: Font:

Formatted: Font:

Formatted: Font:

Formatted: Font:

Formatted: Font:

Formatted: Font:

Formatted: Font:

Formatted: Font:

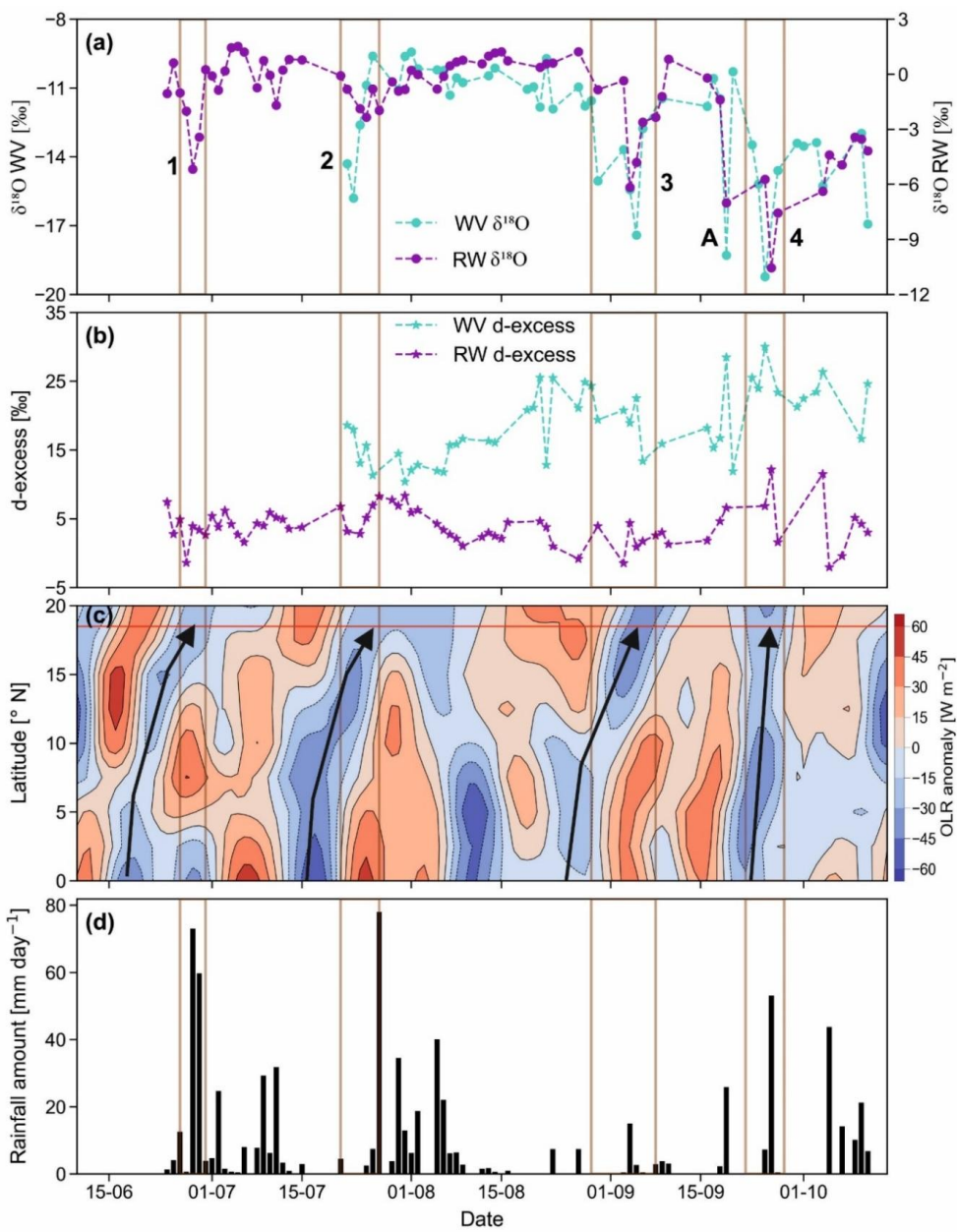
Formatted: Font:

Formatted: Font color: Auto

Formatted: Not Highlight

Formatted: Not Highlight

Formatted: Not Highlight



Formatted: Font: (Default) Times New Roman, 10 pt

414

415

416

417

418

419

420

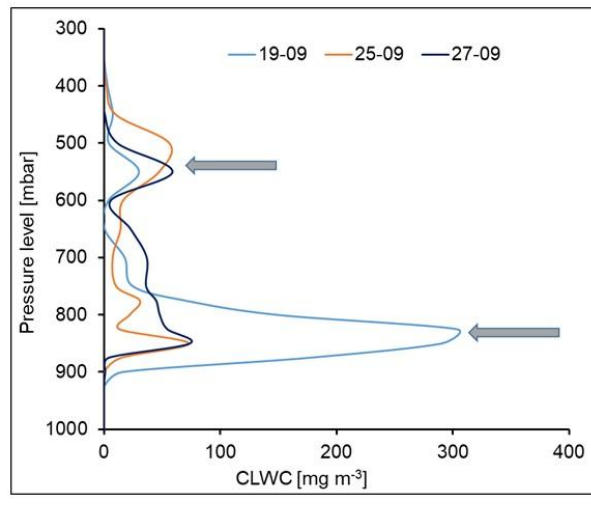
421

422

423

Formatted: Not Highlight

**Figure 2.** The time series of  $\delta^{18}\text{O}$  (a) and d excess values, (b) of the rainwater (RW) and water vapour (WV), (c) OLR anomaly ( $\text{W m}^{-2}$ ), and (d) daily rainfall (mm over 24 h; d) in Pune. The four vertical boxes (numbered 1, 2, 3, and 4) denote synchronous low OLR values and low isotope values (i.e., less than their respective  $\mu - 0.5\sigma$  values). These periods are defined as low isotope events. A indicates one isolated low isotope value without low OLR association. Thick arrows show how convective cloud bands (indicated by low OLR anomaly) traverse to the sampling region over Pune from South-west. Note highly depleted values on 19, 25 and 27 September.



424

425

426 **Figure 3.** Presence of second CLWC peaks at higher altitudes (about 550 mb) on 19, 25 and 27 September 2019  
 427 (beside the first major peaks at lower altitudes) when highly depleted rain  $\delta^{18}\text{O}$  values were observed in  
 428 association with negative OLR anomaly (see Fig. 2). The altitudes of the two sets of peaks are shown by two  
 429 arrows.

Formatted: Not Highlight

Formatted: Superscript

431 phases (marked 1, 2, 3, 4 in Fig. 2a; no vapour data available for date range 1). (2) On 19 September,  
 432 the vapour shows sudden decrease (marked A in Fig. 2a), (3) Gradual decrease in vapour  $\delta^{18}\text{O}$  values and  
 433 increase in  $d$  excess values are observed with progress of monsoon, especially more in the later part, and (4)  
 434 Rain  $d$  excess values remained essentially constant with time but  $\delta^{18}\text{O}$  of both rain and vapour started  
 435 decreasing beginning from early September onwards.

Formatted: No widow/orphan control, Tab stops: 1.24 cm, Left

Formatted: Font:

Formatted: Font color: Auto

Formatted: Font color: Auto

Formatted: Font:

436 The rain and vapour isotopic depletions in rain and vapour samples in the tropics are often associated with  
 437 mesoscale deep convection (Lekshmy et al., 2014; Risi et al., 2008; Sengupta et al., 2020) whose signature is  
 438 possibly present in the present data in the form of depleted-isotope events. We define depleted-isotope events as  
 439 those where isotope ratios of a group of samples fall below the overall mean ( $\mu$ )-0.5 standard deviation ( $\sigma$ );

Formatted: Indent: First line: 0 cm

Formatted: Check spelling and grammar

Formatted: Font color: Auto

Formatted: Font: Times New Roman

Formatted: Font: English (India), Character scale: 100%

Formatted: Font: Times New Roman

Formatted: Font: English (India), Character scale: 100%

Formatted: Font: Times New Roman

Formatted: Font: English (India), Character scale: 100%

Formatted: Not Strikethrough

440 (Sengupta et al., 2020). To examine the extent to which the depleted (more negative) isotope events are related  
 441 to large convective events, a latitude-time Hovmoeller plot of daily OLR anomaly (averaged over the longitude  
 442  $70^\circ\text{E}$  -  $75^\circ\text{E}$ ) is displayed in Fig. 2c. The OLR values are often used as a proxy for convection in tropical and  
 443 subtropical regions. Since the cloud top temperatures are an indicator of cloud height (colder is higher), negative  
 444 OLR anomaly. The OLR values are often used as a proxy for convection in tropical and subtropical  
 445 regions. Since cloud top temperatures (colder is higher) are an indicator of cloud height, negative  
 446 OLR anomaly means colder cloud top temperatures or higher cloud thickness. This, in turn, implies extensive  
 447 coverage by deep cloud systems, characteristic of mesoscale convection and rain. A time synchronous  
 448 association of low OLR and depleted-low isotope events thus indicates indicate mesoscale convection affecting  
 449 isotope values. Fig. 2c indicates four such isotope-depleting mesoscale events (marked as 1, 2, 3 and 4 in  
 450 Fig. 2a). In addition, we also see one depleted-isotope event without such association (marked as A in the Fig.

Formatted: Font: English (India), Character scale: 100%

Formatted: Font: Times New Roman

Formatted: Font: English (India), Character scale: 100%

Formatted: Not Strikethrough

Formatted: Default Paragraph Font, Font: (Default) Calibri, 11 pt, English (India)

449

450

451 2ae). We also note that there were significantly high second CLWC peaks on the three days, 19, 25 and 27  
452 September, at much higher levels (about 550 mbar or about 5.5 km altitude) shown in Fig. 3 (corresponding to  
453 the event number 4 mentioned above).

454 We note from Fig. 2d that major rainfall occurred during the months of July and August; the relative  
455 humidity at the surface during the whole period monsoon season varied from 71.57 % to 97.9 %, and the surface  
456 temperature varied from 25.2° C to 30.2° C (see Fig. S1-10-1 not shown). It is evident from the Fig. 2ured that  
457 deep convection is associated with high rainfall for the three events (1, 2, and 4). A recent study, based on a  
458 year-long continuous measurement of atmospheric vapour in Sri Lanka; (a nearby tropical country under similar  
459 monsoon system) -also noticed found such isotopic depletion during high rainfall events over a northern tropical  
460 station in Sri Lanka (Wu et al., 2025).

461 ~~As mentioned, an increasing trend (13 % to 30 %) in the vapour d excess values associated with a~~  
462 ~~decrease in the  $\delta^{18}\text{O}$  values is noted with the progress of the monsoon (Fig. 2b). In contrast, the rain d excess~~  
463 ~~values were reasonably constant within a small range. The increase in vapour d excess (and decrease in the~~  
464  ~~$\delta^{18}\text{O}$ ) is large and could be ascribed to significant recycling of the moisture with contribution from some~~  
465 ~~evaporative sources (discussed later). We are not certain about the source at this stage. Risi et al. (2023) have~~  
466 ~~discussed the possibility of down drafted vapours as the source of such anomalously low isotope ratios in the~~  
467 ~~case of Sahelian squall lines. Earlier studies over some Indian sites have shown that changes in moisture sources~~  
468 ~~are often associated with a concomitant change in isotope values in rain and vapours (Deshpande et al., 2010;~~  
469 ~~Midhun et al., 2018). We investigated the possibility of this by forty eight hours of air parcel back trajectory~~  
470 ~~analysis (Supplementary Fig. S1), which shows that moisture for the 2019 summer monsoon season was derived~~  
471 ~~mainly from the Arabian Sea. However, this does not rule out the possibility of minor contributions from~~  
472 ~~continental moisture sources or down drafted moisture characterised by low isotope ratios and high d excess~~  
473 ~~values (Risi et al., 2010).~~

Formatted: Font: English (India), Character scale: 100%

Formatted: Font: English (India), Character scale: 100%

Formatted: Font: English (India), Character scale: 100%

Formatted: Font: English (India), Character scale: 100%

Formatted: Font: English (India), Character scale: 100%

Formatted: Font: English (India), Character scale: 100%

Formatted: Not Highlight

Formatted: Font: English (India), Character scale: 100%

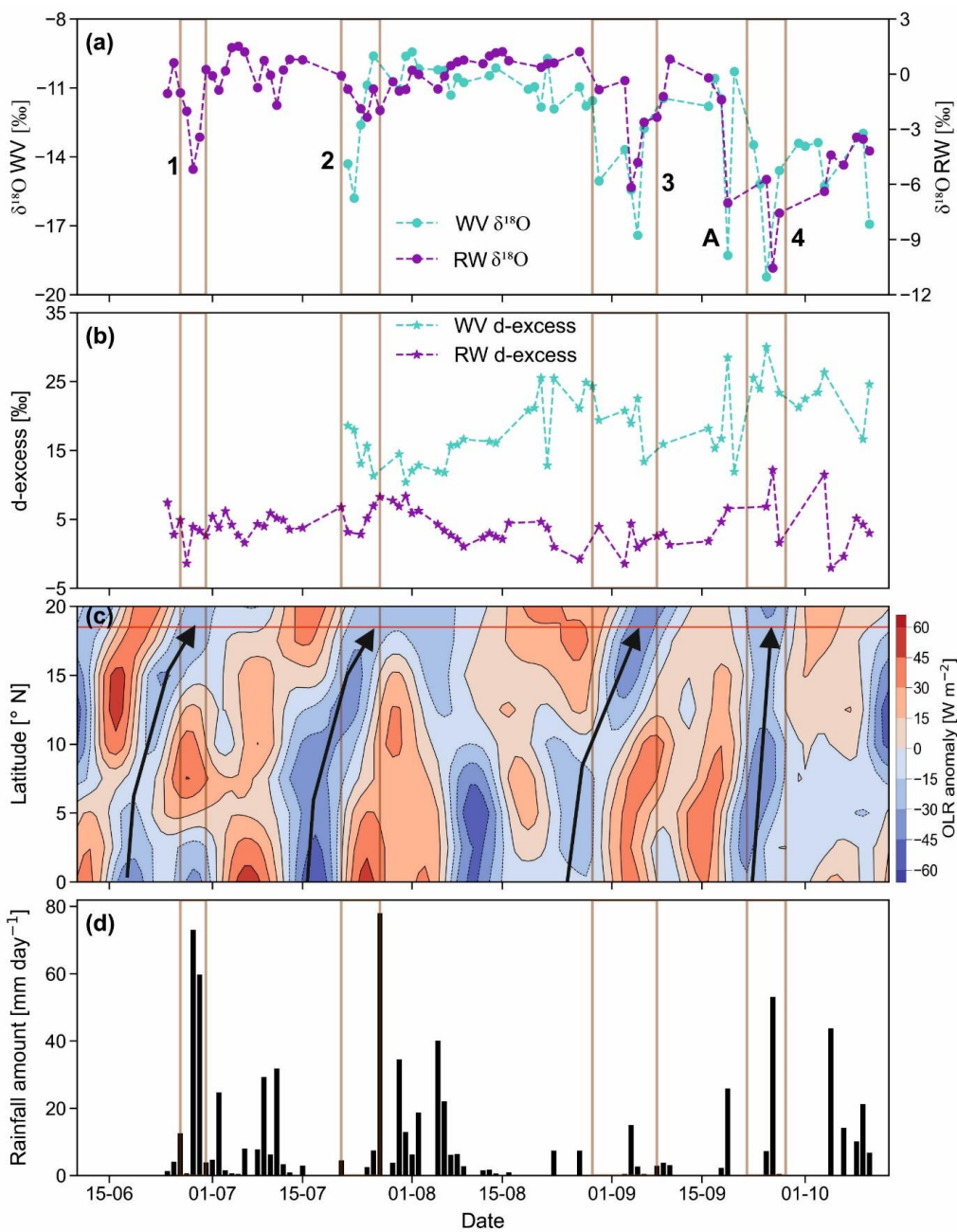
Formatted: Font: English (India), Character scale: 100%

Formatted: Indent: First line: 1.24 cm, No widow/orphan control, Tab stops: 1.24 cm, Left

Formatted: Font: Times New Roman

Formatted: Font: (Default) Times New Roman

Formatted: Font:



Formatted: Font: (Default) Times New Roman, 10 pt

474  
 475 **Figure 2.** The time series of  $\delta^{18}\text{O}$  (a) and d excess values, (b) of the rainwater (RW) and water vapour (WV), (c)  
 476 OLR anomaly ( $\text{W m}^{-2}$ ), and (d) daily rainfall (mm over 24 h; d) in Pune. The four greyshaded vertical bars  
 477 boxes (numbered 1, 2, 3, and 4) denote synchronous low OLR values and low isotope values (i.e., less than their  
 478 respective  $\mu - 0.5\sigma$  values). These periods are defined as low isotope events. A indicates one isolated low isotope  
 479 value without low OLR. Thick arrows show how convective cloud bands (indicated by low OLR anomaly)  
 480 traverse to the sampling region over Pune.

Formatted: Font: 10 pt

Formatted: Left, Line spacing: 1.5 lines, Widow/Orphan control

Formatted: Font: Times New Roman, 10 pt

Formatted: Font: 10 pt

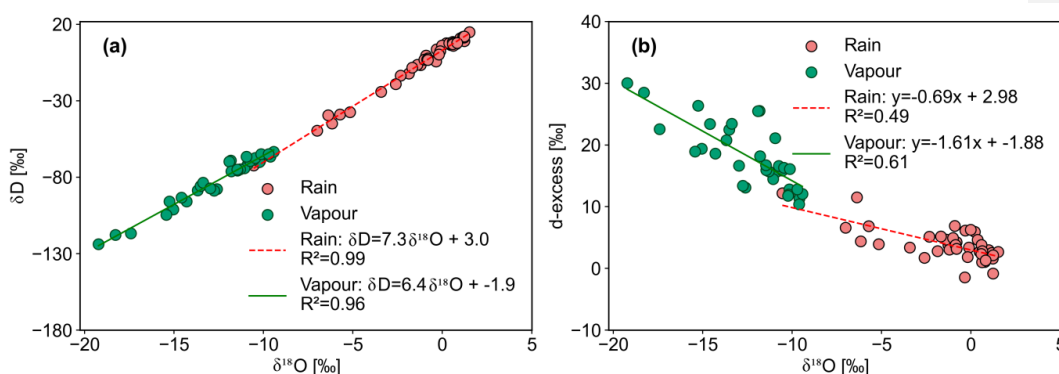
481 Fig. 43a shows the local meteoric water line (LMWL) using rainwater samples and the local water  
 482 vapour line (LWVL) using vapour samples from this study, both pertaining to the monsoon period. The LMWL  
 483 equation is  $\delta D_r = (7.3 \pm 0.1) \delta^{18}O + (3.0 \pm 0.3)$  and the LWVL,  $\delta D_v = (6.4 \pm 0.2) \delta^{18}O - (1.9 \pm 3.0)$ , subscripts r and  
 484 v denote rain and vapour. The slope and intercept of the LMWL values are lower than those of the Global  
 485 Meteoric Water Line (GMWL), which are 8.0 and 10.0, respectively (Dansgaard, 2012; Gat, 1996). This  
 486 difference, though small, suggests some amount of below-cloud evaporation of the rains. At Roorkee, a high-  
 487 latitude Indian Station, Saranya et al. (2018) found an LMWL with a lower slope (5.4) but a higher intercept  
 488 (27) compared to our Pune values. They attributed these changes to the contribution of evaporation from water  
 489 bodies nearby and moisture recycling during the monsoon. Rahul et al. (2016) got a similar slope (7.4) but a  
 490 lower intercept (1.5) in Bangalore (southern central India, at a high altitude of ~1 km). The lower slopes of  
 491 meteoric water lines provide a signature of evaporation processes associated with kinetic fractionations  
 492 occurring during rainfall events.

Formatted: Indent: First line: 1.27 cm, Widow/Orphan control  
 Formatted: Not Highlight

493  
 494  
 495 The d-excess values of rain samples suffering evaporation generally bear a negative relationship with  
 496  $\delta^{18}O$  values (Bonne et al., 2014; Munksgaard et al., 2020). This is also seen in our study (Fig. 43b) where rain d-  
 497 excess increases-decreases with an decrease-increase in  $\delta^{18}O$  values. In addition, the vapour d-excess values also  
 498 show a statistically significant negative correlation with  $\delta^{18}O$  values (Fig. 43b;  $R^2 = 0.61$ ;  $p = 0.001$ ), probably  
 499 indicating contribution of vapour derived from rain evaporation (Kurita, 2013; Risi et al., 2021). Correlation  
 500 studies can be indicative, but the causative factors behind the above variations can be explored only with the  
 501 help of a process-based model like BCIM. Below, the role of local meteorological factors and rain vapour  
 502 isotope exchange will be explored with the help of BCIM.

Formatted: Not Highlight

Formatted: Not Highlight



505  
 506 **Figure 43.** A cross-plot of (a)  $\delta D$  and  $\delta^{18}O$  of rain and vapour; (b) a cross-plot of d-excess and  $\delta^{18}O$  of rain and vapour  
 507 showing anti-correlation. Mean regression lines and correlation coefficients are shown inside the plots.

508  
 509 **3.2 Results of BCIM simulations**

510 As discussed in section 2.4, simulation runs of BCIM were carried out under three assumptions about  
 511 the vertical profiles of RH, T and vapour isotopes. The results are shown as Run-1, Run-2 and Run-3 which  
 512 were designed to make progressive improvement in reproducing the measured rain isotope data.

514 **3.2.1 Run-1: Rayleigh ascent**

515 The sources of input sources of background profiles of atmospheric ambient temperature (T), relative  
 516 humidity (RH), vapour  $\delta D_v$ , and vapour d-excess (dv) required for three BCIM runs are given in Table 21. In  
 517 Rayleigh simulations (designated as Run-1), the profiles were calculated using the formulae equations for moist-  
 518 adiabatic ascent of air parcels (see equations given in Appendix A1 of Graf et al.,2019) starting at the surface  
 519 with values of temperature ( $T_0$ ), relative humidity ( $h_0$ ),  $\delta D_v$  ( $\delta v,0$ ) and dv ( $dv,0$ ) of each sampling day as inputs.  
 520 The surface values of  $\delta D$  and d-excess of vapour (denoted by symbol d) were taken from our vapour  
 521 measurements along with the daily average temperature and humidity values obtained from the Pune surface  
 522 observations of IMD reports (Section 2.3). A dry adiabatic ascent formula is used in the initial phase up to the  
 523 cloud base (LCL). Above the cloud base a moist-adiabatic lapse rate is used. The dry and moist lapse rates are  
 524 calculated using equations based on gravitational constant, specific heat of dry air, mass mixing ratio of vapour,  
 525 latent heat of evaporation, specific gas constant of dry air, temperature, ratio of specific gas constants of dry air  
 526 and water vapour, specific humidity and saturation vapour pressure. The resultant input profiles of RH, T,  $\delta D_v$ ,  
 527 and d-excess for all 29 sampling days are given in Supplementary Information (Fig. SI-8b-1 and Fig. SI-8b-2).

529 Table 21. Input parameters for various BCIM runs

Sl. No	BCIM input	Parameters for Run-1	Parameters for Run-2	Parameters for Run-3
1	Drop size	Marshal-Palmer equation using hourly rainfall data obtained from IMD	Same as Run-1	Same as Run-1
2	RH profile	Rayleigh ascent ~15 % increase per km and 100% above CBH to drop introduction height	Radiosonde values normalized to surface observation and changed to 100% above CBH to drop introduction height	Same as Run-2
3	Temperature profile	Rayleigh ascent Lapse rate ~ 5.6°C km <sup>-1</sup>	Radiosonde normalized to ground value	Same as Run-2
4	$\delta D_{vap}$ profile	Rayleigh ascent ~7 ‰ decrease per km	TES normalized to measured surface value	$\delta D$ values reduced slightly (within ±4‰) keeping the shapes like Run-2
5	d-ex <sub>cap</sub> profile	Rayleigh ascent ~0.1 ‰ increase per km	LMDZ $\delta D$ and $\delta^{18}O$ values used to get d-ex <sub>cap</sub> normalized to measured ground value	d-ex <sub>cap</sub> decreased from Run-2 average of 17‰ to an average ~10‰
6	Rain drop formation height (CLWC peak)	ERA5 Cloud Liquid Water Content peak	Same as Run-1	Same as Run-1

Formatted: Font: Not Bold

Formatted: Font: Not Bold

Formatted: Font: Not Bold

Formatted: Indent: First line: 1.27 cm

Formatted: Font: Not Bold

Formatted: Font: Not Bold

Formatted: Font: Not Bold

Formatted: Indent: First line: 1.27 cm

Formatted: Not Highlight

Formatted: Not Highlight

Formatted: Subscript

Formatted: Subscript

Formatted: Not Highlight

Formatted: Font: Symbol, Not Highlight

Formatted: Not Highlight

Formatted: Not Highlight

Formatted: Not Highlight

Formatted: Not Highlight

Formatted: Font: Not Bold, Not Highlight

Formatted: Not Highlight

Formatted: Font: Not Bold, Not Highlight

Formatted: Not Highlight

Formatted: Font: Not Bold, Not Highlight

Formatted: Not Highlight

Formatted: Font: (Default) Times New Roman, 9 pt, Font color: Auto

Formatted

Formatted

Formatted

Formatted Table

Formatted

Formatted

Formatted

Formatted

Formatted

Formatted: Superscript

Formatted: Not Highlight

Formatted: Not Highlight

Formatted: Superscript

7	Cloud Base Height (LCL)	LCL from radiosonde profiles using skew-T log P diagram	Same as Run-1	Same as Run-1
---	-------------------------	---	---------------	---------------

531  
532 Results of Run-1 calculations are compared with the observed values of rain  $\delta D$  (Fig. 5a),  $\delta^{18}O$  (Fig.  
533 5b), and d-excess (Fig.5c) values. We also construct  $\Delta\delta$ - $\Delta d$  cross plots for both observed and model  
534 values in Fig. 5d. Although observed and model isotope values (Fig. 5a and 5b) show strong correlation  
535 ( $R^2=0.86$  and  $0.79$ , respectively), the model values are mostly overestimated (the plotted points lie below the 1:1  
536 line). The overestimations of isotopes (for  $\delta^{18}O$  and  $\delta D$ ) affect the d-excess values considerably more: the points  
537 lie far to the right, and no correlation exists between the observed and model d-excess values (Fig. 5c). This is  
538 because the d-excess parameter is more sensitive to departure from equilibration, which means that a small  
539 departure of delta values would magnify the discrepancy in case of d-excess. We also note that most of the  
540 model data points in the  $\Delta\delta$ - $\Delta d$  cross-plot do not agree with the observed data points and lie closer to the origin.  
541 However, many of the model points fall in the lower right quadrant, which is expected in case of dominant  
542 raindrop evaporation. We also note that the  $\Delta\delta$  and  $\Delta d$  values (Fig. 6d5d) show smaller variations compared to  
543 the observations. The  $\Delta\delta$  of the model simulations varies from 0 ‰ to 5 ‰ and  $\Delta d$  from 0 ‰ to -5 ‰,  
544 while the observed values have variations of about 25 ‰ (higher by a factor of 5). These comparisons show that  
545 the Rayleigh ascent model with the prescribed inputs fails to reproduce the evolution of the rain isotopes in our  
546 region. We suspect that the vertical profiles of RH, T and vapour isotopes need to be modified to improve the  
547 simulations. Rayleigh ascent in Run-1 assumes that the source of vapour aloft is an unaltered rising air parcel  
548 with constant specific humidity, behind the mismatch between observation and model. But we see from Fig. SI-5-  
549 2 and S8b-1, Figure S7a that for Pune this condition results in unusually low cloud base over Pune (i.e., the  
550 level where RH attains the value of 100%) for Pune which is not seen observed in an earlier study (Naik et al.,  
551 2003). In fact, the ERA5 data show that specific humidity decreases with height (Fig. SI-6-1). It is well known  
552 that decrease of specific humidity is associated with a decrease of the vapour isotope ratios (Noone et al. 2011;  
553 Worden et al., 2007; see SI-6 for details). The simulation can possibly be improved if we use RH and T data  
554 from local radiosonde observations and try out altogether different isotope profiles having realistic vertical  
555 variations.

Formatted: Font: Times New Roman, Not Highlight

Formatted: Not Highlight

Formatted: Not Highlight

Formatted: Not Highlight

Formatted: Not Highlight

### 3.2.2 Run-2: RH and T from Radiosonde and isotope profiles from TES and LMDZ

#### 3.2.2.1 (a) RH and T from Radiosonde

559 For the present study period, the average radiosonde observations were available (see section 2.3) at  
560 every 50 mb pressure interval (about 470 m) but the input for BCIM is required at every 1-meter interval.  
561 Therefore, a linear interpolation between every two consecutive pressure levels in logarithmic scale (Ingleby et  
562 al., 2014) was carried out to obtain RH and T values at meter levels. As the BCIM requires RH=100% for  
563 formation of water droplets (considered to be at CLWC peak level), the RH values above lifting condensation  
564 level (LCL) were considered as 100% disregarding the radiosonde data above the LCL. (see section 2.4.2 and  
565 SI-8b).

Formatted: Font: Bold

Formatted: Font: Bold

Formatted: Font: Bold

Formatted: Font: Not Italic

Formatted: Font: Not Italic

Formatted: Font: Not Italic

Formatted: Font: Not Italic

Formatted: Font: Not Italic

Formatted: Font: Not Italic

Formatted: Font: Not Italic

Formatted: Font: Not Italic

Formatted: Font: Not Italic

Formatted: Font: Not Italic

Formatted: Font: Not Italic

Formatted: Font: Not Italic

Formatted: Indent: First line: 0 cm

Formatted: Font: Bold

#### 3.2.2.2 (b) Use of the TES data to derive vertical profiles of vapour isotopes

567 To obtain the vertical profiles of vapour isotopes, we first tried out the isotope outputs of a General

Formatted: Indent: First line: 1.27 cm

569 Circulation Model, namely, LMDZ. -The output data for our sampling days ~~for Pune-centred grid~~ over Pune was  
570 provided by Dr. Camille Risi (personal communication, 2023) using the LMDZ isotope-enabled general  
571 circulation model (GCM), known as LMDZ-iso (Risi et al., 2010), which is a version of the LMDZ atmospheric  
572 model adapted to simulate the natural variations of water isotopes in precipitation and vapor fields.

Formatted: Font: (Default) Times New Roman, 10 pt, Font color: Auto

Formatted: Font: (Default) Times New Roman, 10 pt, Font color: Auto

Formatted: Font: Times New Roman, 10 pt, Font color: Auto

573 Initially, the LMDZ derived values were also used in BCIM as inputs, but we found that a wide  
574 difference exists between the observed and model isotopic values (results not shown). We suspected that the  
575 LMDZ model did not generate the input vapour isotope profiles accurately. Possibility of such a limitation was  
576 noted by Risi et al. (2021) who observed that for high precipitation areas, the convective or mesoscale  
577 downdrafts bring depleted vapour from above into the sub-cloud layer.

Formatted: Indent: First line: 1.27 cm

Formatted: Not Highlight

Formatted: Font: Not Bold, Not Highlight

Formatted: Font: Not Bold

Formatted: Font: Not Bold, Not Highlight

Formatted: Font: Not Bold

Formatted: Font: Bold

Formatted: Superscript

Formatted: Not Highlight

Formatted: Font: Symbol

Formatted: Superscript

Formatted: Font: Bold

Formatted: Font: Bold

Formatted: Font: Bold

Formatted: Font: Bold

Formatted: Font: Bold

Formatted: Indent: First line: 1.27 cm, Space After: 0 pt, Line spacing: 1.5 lines

Formatted: Font: (Default) Times New Roman, 10 pt, Font color: Auto

Formatted: Font: (Default) Symbol, 10 pt, Font color: Auto

Formatted: Font: (Default) Times New Roman, 10 pt, Font color: Auto

Formatted: Font: (Default) Times New Roman, 10 pt, Font color: Auto

Formatted: Font color: Auto

Formatted: Font: (Default) Times New Roman, 10 pt, Font color: Auto

Formatted: Font color: Auto

Formatted: Font: (Default) Times New Roman, 10 pt, Font color: Auto

Formatted: Font: (Default) Symbol, 10 pt, Font color: Auto

Formatted: Font: (Default) Times New Roman, 10 pt, Font color: Auto

Formatted: Font color: Auto

Formatted: Font: (Default) Times New Roman, 10 pt, Font color: Auto

578 Recognizing the large discrepancies arising out of using a GCM product (LMDZ) directly for both the  
579 isotopes, we tried out next the measured  $\delta D_v$  profiles obtained from Tropospheric Emission Spectrometer (TES)  
580 observations pertaining to the Pune region. We should note here that the TES data were not available for 2019  
581 and the available values must be modified for adapting to 2019 monsoon period. To account for the time  
582 discrepancy, the final profiles are constrained by using the measured daily-scale ground-level vapour isotope  
583 ratios as a boundary condition while maintaining the shapes of the TES  $\delta D_v$  profiles. We should also mention  
584 here that apart from TES the vapour  $\delta D$  data, in principle, can be obtained from one other source, namely,  
585 Atmospheric Infrared Sounder (AIRS). However, isotope vertical profiles obtained from AIRS and used in the  
586 BCIM runs (after suitable modifications) produced rain isotopes which were widely different from the observed  
587 values. ~~These failed trials~~ The analyses with AIRS data See Supplementary Information SI-7 and Fig. S7-1.

588 The derivation of vapour isotope profiles applicable for our sampling days in 2019 requires a  
589 nudging adjustment technique, which would allow merging of lower-level data with the TES observations at  
590 upper layers. This assumes that the shapes of the TES average profiles were applicable as far as the vertical  
591 variation is concerned. The TES satellite provides  $\delta D_v$  values of moisture at 17 pressure levels with a  $5.3 \text{ km} \times$   
592  $8.4 \text{ km}$  footprint during the years 2005-2009 over a box covering the study region ( $16^\circ\text{-}20^\circ \text{ N}$ ;  $72^\circ\text{-}76^\circ \text{ E}$ ).  
593 Using these data sets, we can derive an average TES profile and assume it to be representative of the shape of  
594 the mean monsoon profile Our station at Pune falls within this box but there is an inherent assumption that the  
595 average over a  $\sim 45 \text{ km}^2$  area represents a small sampling location. The only justification is the use of a boundary  
596 constraint where the TES average profile is nudged/adjusted to match the measured ground vapour value at the  
597 sampling location. In addition, the back-trajectory analysis indicates that the moisture source is always from the  
598 Arabian Sea where the vapour is carried inland by the streaming air mass (see Fig. S4-1). Interestingly, an  
599 average of 17 years data of  $\delta^{18}\text{O}$  of rain waters in Bombay (from 1961 to 1978) is  $-1.3\text{‰}$  (Bhattacharya et al.,  
600 2003) close to the Pune average value of  $-1.1\text{‰}$  from the present study. It shows that Pune being located 150 km  
601 upstream of Bombay receives moisture of similar composition as Bombay (possibly added by some evaporation  
602 component on the way). Therefore, our assumption of a large areal average representing a small location is not  
603 expected to be wrong, at least as far as the vertical variation is concerned.

### 605 3.2.2.3 (b) The nudging adjustment technique to derive the vapour isotope profiles

606 The  $\delta D$  and d-excess profiles for each date from the TES data were obtained by adjustment with the  
607 measured surface values. We analysed the available TES  $\delta D$  profiles (digital values) for the years 2005-2007  
608 and adopted three profiles from the data sets which correspond to the Minimum, Mean and Maximum surface

Formatted: Font: (Default) Times New Roman, 10 pt, Font color: Auto

Formatted: Font color: Auto

Formatted: Font: (Default) Times New Roman, 10 pt, Font color: Auto

609 vapour  $\delta D$  values observed in the present study at the surface level. Each of these three profiles was fitted with  
610 polynomials and the coefficients of these polynomials were treated as functions of the surface values. Once we  
611 get these functions, we can obtain the vapour isotope profiles for any day by using that day's surface value. This  
612 exercise was necessary to translate the digital TES values into an analytical form, allowing for the easy  
613 calculation of vapour isotope values at each height (at one meter resolution required for the BCIM inputs) from  
614 the uppermost drop introduction point to the ground level, resulting in a smooth shaped profile.

615 A similar exercise was conducted to obtain the daily d-excess profile from the LMDZ GCM output for  
616 Pune in 2019 and normalising the profile to the measured vapour d-excess value. In brief, this was done by  
617 using the available  $\delta D$  and  $\delta^{18}O$  profiles from LMDZ output for three cases (Mean, Max and Min surface  
618 values), fitting 4<sup>th</sup>-order polynomials;  $Ah^4+Bh^3+Ch^2+Dh+E$ , and then constructing the d-excess profiles for  
619 three cases with five coefficients. Five coefficients were used to get higher precision in fitting. Again, fitting  
620 was done for each of the polynomial coefficients (A, B, C, D and E) as a function of surface value and then use  
621 them to get the dex profile for each day. This procedure is discussed in detail in SI-8a. Fig S8b-1 and Fig S8b-2  
622 in the Supplementary Information SI-8b show the input profiles (RH and T), and (~~and~~  $\delta D_v$  and d-excess)  
623 respectively for the three runs, Run-1, Run-2 and Run-3.

624  
625 The above exercise means that by using the observed ground vapour value as a boundary value we  
626 obtain the desired profiles for  $\delta D$  and dex for each day from an analytical fitting of digital data from TES  
627 (adopted) and LMDZ. We used a multi-order polynomial to get the fitting as accurately as possible, especially  
628 for d-excess. To derive the vertical profiles for each of our sampling days, we use our daily surface  
629 measurements as boundary values. The average TES profile (as mentioned above) is modified through a curve-  
630 fitting technique where the shape of the average profile is slightly altered while being constrained to pass  
631 through the surface value. A 4<sup>th</sup> order Polynomial of the type:  $Ah^4+Bh^3+Ch^2+Dh+E$  (where h is the altitude in  
632 meters) was fitted to the average profile after adjusting its surface value so that a smooth shape is obtained (D/H  
633 decreasing with height following the average pattern). The polynomial coefficients (five in number) were  
634 calculated for three cases: (1) for the maximum observed surface D/H value, (2) for the mean surface value, and  
635 (3) for the minimum observed value, giving us three sets of A, B, C, D and E values. The constants for each day  
636 were next estimated by interpolation using these three sets. Obviously, this method of interpolation, constrained  
637 by surface vapour measurements, assumes that the vapour aloft is related to the surface value, and this  
638 assumption may not be correct. But it, at least, allows us to check if the surface constraints yield better rain  
639 isotope ratios at the ground (using BCIM) while being consistent with the TES measurements of vapour aloft.

640 Unfortunately, the vapour  $\delta^{18}O$  values at various pressure levels are not available from TES (which  
641 gives only the HDO/H<sub>2</sub>O ratio). Therefore, we adopted a derivation technique using the vapour isotope profiles  
642 simulated by the LMDZ model. In this technique, daily average vapour  $\delta^{18}O$  and  $\delta D$  values were obtained from  
643 the LMDZ model outputs over our study region for the sampling dates at each height. For each day, two profiles  
644 (for  $\delta^{18}O$  and  $\delta D$ ) were constructed, and polynomials were fitted. Next, the d excess profiles were constructed  
645 from these two profiles. Each of the daily d excess profiles was then constrained by using the surface d excess  
646 vapour value for that day to obtain the fitted d excess Polynomial for that day. The rationale is that even though  
647 the individual profiles of  $\delta D$  and  $\delta^{18}O$  provided by LMDZ do not predict well the rain isotope ratios (as seen by  
648 our trial), the d excess based on these two isotope ratios should be reasonably good.

Formatted: Font: Symbol, Font color: Auto

Formatted: Font color: Auto

Formatted: Font: (Default) Times New Roman, 10 pt, Font color: Auto

Formatted: Font: (Default) Times New Roman, 10 pt, Font color: Auto

Formatted: Font color: Auto

Formatted: Font: (Default) Times New Roman, 10 pt, Font color: Auto

Formatted: Font: (Default) Times New Roman, 10 pt, Font color: Auto

Formatted: Font: (Default) Times New Roman, 10 pt, Font color: Auto

Formatted: Font: 10 pt, Font color: Auto

Formatted: Font: (Default) Times New Roman, 10 pt, Font color: Auto

Formatted: Font: 10 pt, Font color: Auto

Formatted: Font: (Default) Times New Roman, 10 pt, Font color: Auto

Formatted: Superscript

Formatted: Font: (Default) Times New Roman, 10 pt, Font color: Auto

Formatted: Font: (Default) Times New Roman, 10 pt, Font color: Auto

Formatted: Superscript

Formatted: Font: (Default) Times New Roman, 10 pt, Font color: Auto

Formatted: Font color: Auto

Formatted: Font: (Default) Times New Roman, 10 pt, Font color: Auto

Formatted: Font: Not Bold, Not Highlight

Formatted: Font: Not Bold, Not Highlight

Formatted: Font: Not Bold, Not Highlight

Formatted: Font: Not Bold

Formatted: Font: Symbol

Formatted: Font: (Default) Times New Roman, 10 pt, Font color: Auto

Formatted: Indent: First line: 1.27 cm, Space After: 0 pt, Line spacing: 1.5 lines

Formatted: Indent: First line: 1.27 cm, Adjust space between Latin and Asian text, Adjust space between Asian text and numbers

Formatted

Formatted

Formatted

Formatted

649 ~~The obtained vapour d-excess and δD profiles are shown in Fig. S4c and S4d, Run 2.~~ Obviously, this  
650 method of estimating the vapour profile, constrained by surface vapour measurements, assumes that the vapour  
651 aloft is related to the surface value. This assumption may not be strictly correct. But it allows us to check if the  
652 BCIM, under the surface constraints, yield better rain isotope ratios at the ground compared to the Rayleigh  
653 model while being consistent with the TES measurements of vapour aloft.

Formatted: Widow/Orphan control

#### 654 ~~3.2.2.4 (e) Run-2 results~~

655 The above profiles were subsequently employed in BCIM (named Run 2) to generate the daily-scale  
656 δ<sup>18</sup>O, δD and d-excess values of surface rain isotope ratios surface rains (Fig. 56e-56h). However, the results do  
657 not show much improvement compared to the Run-1 (Fig. 56e-56g) despite showing a larger variability in the  
658 Δδ-Δd plot (Fig. 56h); the Δδ values varied from -4.7 ‰ to 11 ‰ and Δd from -1.8 ‰ to -12.4 ‰. Additionally,  
659 in this case, As in Run-1, all the model data points fell in the 3<sup>rd</sup> quadrant of the Δδ-Δd cross plot (Fig. 56h and  
660 Fig. 56d). Both Run-1 and Run-2 simulations fail to yield a good match between the observations observed and  
661 model values (especially the d-excess) values. The rain δD values differ by about -8 ‰ to 20‰. The model d-  
662 excess values are higher (by 0 to 15‰). Interestingly, the model rain values of Run-1 and Run-2 are quite close  
663 (within ±2.5‰) despite RH and T and isotope profiles being very different. This suggests that the assumption of  
664 surface vapour value as the boundary constraint, as used in both these runs, is the main determinant for rain  
665 isotopes.

Formatted: Not Highlight

Formatted: Not Highlight

Formatted: Font: Bold, Not Highlight

Formatted: Indent: First line: 0 cm

Formatted: Not Highlight

Formatted: Not Highlight

Formatted: Not Highlight

Formatted: Not Highlight

Formatted: Not Highlight

Formatted: Not Highlight

Formatted: Font: Symbol

Formatted: Font color: Auto

Formatted: Font: (Default) Times New Roman, 10 pt, Font color: Auto

Formatted: Font: (Default) Times New Roman, 10 pt, Font color: Auto

Formatted: Font color: Auto

#### 668 ~~3.2.3.4 Tuning of Vapour δ<sup>18</sup>O isotope correction in the profile profile for better matching: Run-3~~

669 The mismatch in case of Run-2, as discussed above, indicates that that we still need to modify the input  
670 profiles to obtain a better match with the observed values. Below we discuss how we go about this task.

Formatted: Indent: First line: 1.27 cm

Formatted: Font: Not Bold

#### 671 ~~3.2.3.1 Possible sources of discrepancy in Run-1 and Run-2 (Run-3 and Run-4)~~

672 Based on the previous discussions we note that the ambient vapour isotope values have the maximum  
673 impact on the model rain isotope values. This can be shown quantitatively by a multiple regression analysis of  
674 rain isotope values with four influencing factors (RH, Temperature, surface δDv and drop diameter) in their  
675 normalised forms. The normalised values of the model rain isotope ratios δD<sub>mod-rain</sub> obtained from Run-2 for the  
676 29 sampling days were regressed with the normalized values of these four variables. We obtain the following  
677 multiple regression equation:

Formatted: Subscript

$$678 \delta D_{\text{mod-rain}} = -0.114 * RH + 0.035 * \text{Temperature} - 0.059 * \text{diameter} + 0.986 * \delta Dv \quad (1)$$

Formatted: Adjust space between Latin and Asian text, Adjust space between Asian text and numbers

681 This equation indicates that the major influence on the model rain isotope value is from the ambient  
682 vapour δDv (with a coefficient of nearly one, meaning +1% change in δDv would result in +1% change in the  
683 rain δDv). In contrast, the influence of RH, for example, is only one-tenth (in opposite direction) for the same  
684 percentage change. The influences of temperature and size are still less. It is logical to assume that the main  
685 source of discrepancy in Run 1 and Run 2 is improper vapour isotope profiles and therefore, for tuning, a change  
686 in the vapour isotope value would be the most effective.

687

688 ~~It seems that the main source of error in Run 1 and Run 2 could be improper vapour isotope profiles. It~~  
 689 ~~is possible that the true profile for a given date may does not coincide with the adopted one based on~~  
 690 ~~extrapolating to the measured surface measured-value-in-extrapolation, as assumed by the boundary constraint.~~  
 691 ~~In other words, the vapour aloft may not be derived entirely from the surface vapour as measured at our~~  
 692 ~~sampling location. One possible explanation could be a significant contribution from the small-scale local~~  
 693 ~~surface moisture having a different isotopic composition (evaporation or evapotranspiration from water bodies~~  
 694 ~~or trees within a few hundred meters). However, this possibility can be ruled out as a study using satellite data~~  
 695 ~~showed that due to high humidity and low temperature during the ISM monsoon season evaporation/~~  
 696 ~~evapotranspiration (~0.5 mm day<sup>-1</sup>) adds a negligible amount of moisture compared to the advective fluxes in~~  
 697 ~~this region (Pathak et al., 2014). Our investigation~~ The search for a true profile in our case is also limited by the  
 698 ~~absence of upper-air high altitude vapour~~ observation of  $\delta D$  and  $\delta^{18}O$  values from an independent source or  
 699 model on a daily scale.

### 701 3.2.3.2 Modification of the isotope ratios

702 Guided by the regression equations, ~~Keeping the D/H ratios nearly the same, we~~ tuned the vapour  
 703  $\delta^{18}O$ - $\delta D$  and dex input profiles to achieve a reasonable agreement in the rain isotope values for each date (Fig.  
 704 5i-5k). ~~Two such tunings are attempted. In both, we reduced~~ The surface  $\delta D$  values were changed by +13.9 to -  
 705 17.8‰ slightly and ~~and increased~~ the  $\delta^{18}O$ -dex moderately values from +3.2 to -17.1‰ while keeping the shapes  
 706 for daily profiles similar to Run-2 (following the ~~adjusting~~ adjustment procedure discussed above).  
 707 Corresponding changes in the vapour  $\delta^{18}O$  is from +2.9 to -1.9‰. Most of the changes were small; in the  $\delta D_v$   
 708 within +4‰ (discarding six large changes) and in the d-excess, within  $\pm 3.4$ ‰ (discarding six large changes).  
 709 These changes improved the results considerably. As a ~~result~~ consequence of this tuning, In Run-3 (Fig. 7a-d),  
 710 the vapour  $\delta^{18}O$  value is increased at each interval in such a way that the average d-excess of the surface  
 711 ~~drop~~ vapour decreased to  $\sim 10.78$ ‰ (on average) from the measured average surface value of ~~about~~ 17.3‰  
 712 (on average). To see these modifications clearly, In the second trial, Run 4 (Fig. 7e-h), the d-excess decrease  
 713 was made slightly less (average d-excess 10.7‰). The Run-3 vapour isotope profiles are shown along with  
 714 those of Run-2se changes are shown in the vapour isotope profiles given in Fig. S1-supplementary 8b-2 Fig.  
 715 S4(f) and S4(h).

716 To check the agreement, a two-tailed Student's t-test was done with observed and modelled  $\delta^{18}O$ ,  $\delta D$ ,  
 717 and d-excess values of 29 rain samples after each of the runs. This test shows that the Run-3 model values are  
 718 close to the observed ones for all three parameters ( $\delta^{18}O$ ,  $\delta D$ , and d-excess) at  $p=0.05$  significance level (see S1-  
 719 9; Table S9). The outputs of Run-1 and Run-2 agree with each other reasonably well (see Fig. S9-1) for all three  
 720 isotopic parameters, but they do not agree well with the observed values.

722 We recognise that it is difficult to validate the vapour  $\delta D$  or d-excess profiles constructed by the above  
 723 method due to a lack of height-specific observations. However, the available aircraft-based vapour isotope  
 724 observations suggest that both d-excess and  $\delta D$  values of vapour decrease with altitude and thus provide some  
 725 evidential support to the assumed decrease (Sodemann et al., 2017). With the above choice, ~~s~~ simulations of  
 726 rain isotopes improve (Fig. 5i-5k7) considerably (both in terms of the uncertainty of the slope of the regression  
 727 line and the correlation coefficient). ~~Between the two alternatives of Run 3 and Run 4, Run 4 is found to be~~

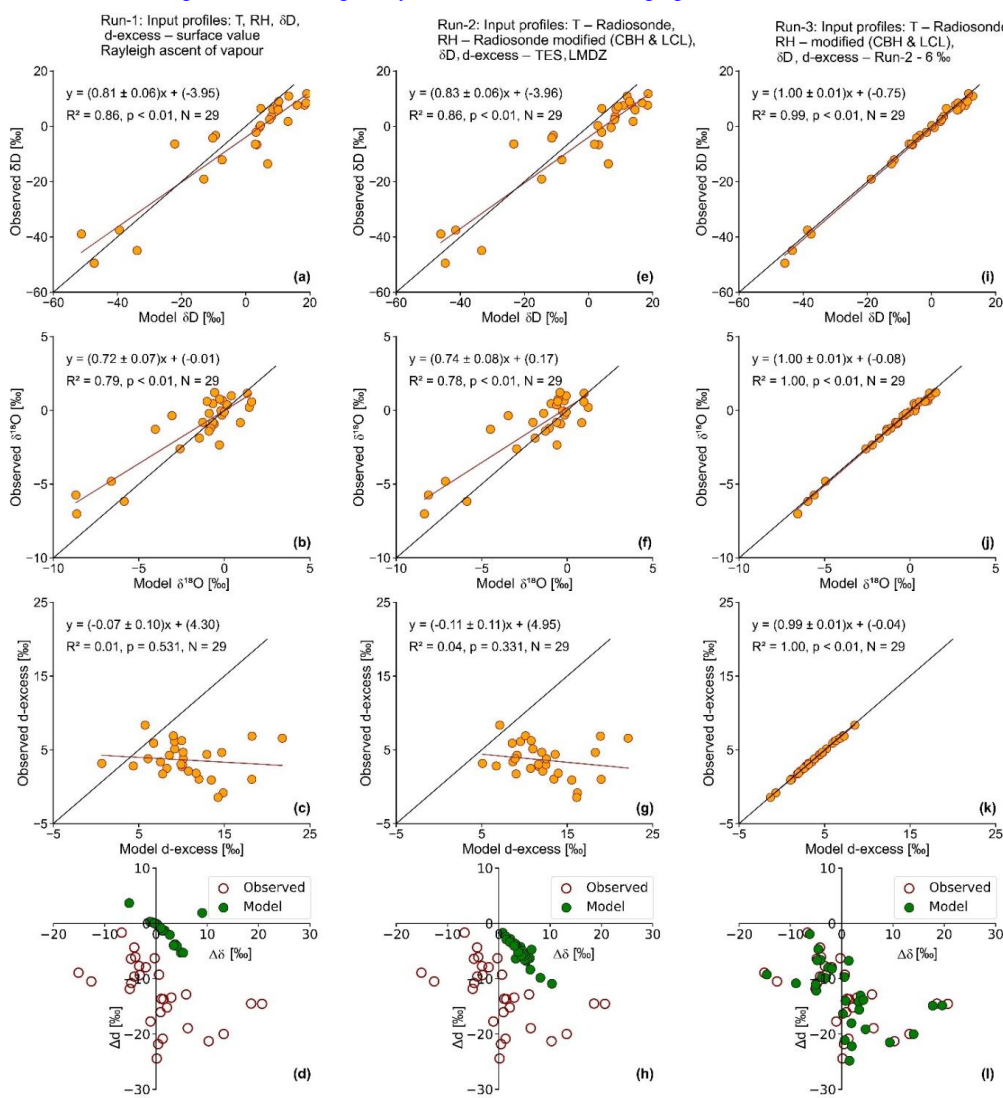
- Formatted: Font: Bold
- Formatted: Font: Bold
- Formatted: Indent: First line: 0 cm
- Formatted: Not Highlight
- Formatted: Font color: Auto
- Formatted: Font: Symbol
- Formatted: Superscript
- Formatted: Font: Symbol
- Formatted: Subscript
- Formatted: Font: Times New Roman
- Formatted: Font: Bold
- Formatted: Font: Not Bold
- Formatted: Not Highlight
- Formatted: Not Highlight
- Formatted: Font: (Default) Times New Roman, 10 pt, Font color: Auto
- Formatted: Font: Symbol
- Formatted: Font: Symbol
- Formatted: Not Highlight
- Formatted: Font: Not Bold, Not Highlight
- Formatted: Font: Not Bold
- Formatted: Font: Not Bold, Not Highlight

728 superior in the matter of comparison of the model with observations; the average  $\Delta d$  (observation-model) d-  
 729 excess difference decreases from 2.1 to 0.4. Additionally, there is considerable improvement in the  
 730  $\Delta\delta$ - $\Delta d$  cross plot (see Fig. 5)7d and 7h).

Formatted: Not Highlight

731  
 732 The tuning exercise suggests that the adoption of the  $\delta^{18}\text{O}$  profiles or the d-excess profiles based on TES  $\delta\text{D}$  and  
 733 LMDZ  $\delta\text{D}/\delta^{18}\text{O}$  values (Run 2) was slightly in error. We found that, on average, the adopted  $\delta^{18}\text{O}$  should be  
 734 increased by about 0.4 ‰, and the adopted  $\delta\text{D}$  decreased by about 3.5 ‰. Consequently, the model d-excess  
 735 should be changed on average by about -7 ‰ (ranging from +3 ‰ to -17 ‰).

Formatted: Font: (Default) Times New Roman, 9 pt



736  
 737  
 738 **Figure 5.** Scatter plots showing observed vs model values for  $\delta\text{D}$ ,  $\delta^{18}\text{O}$ , and d-excess for various runs (Run-1, Run-2 and  
 739 Run-3) of BCIM in the upper nine panels. The lowermost three panels show the  $\Delta\delta$ - $\Delta d$  cross-plots for the runs. The input  
 740 profile sources of T, RH, vapour  $\delta\text{D}$  and d-excess used in the model for the three runs are given in the descriptions above.

741 The best agreement between the observed and model values is achieved in the Run-3. Run 3 uses the same RH and T as Run  
742 2 but  $\delta D$ , and d-excess values are adjusted by tuning which reduces the average vapour d-excess to ~10.7% from an  
743 observed value of ~17.3%.

744  
745 The physical basis behind the good agreement in Run-3 is the validity of the assumptions of the cloud  
746 microphysics of the BCIM, which calculates the evolution of the raindrops as they fall through the cloud and  
747 below-cloud layers. The evolution changes the mass as well as the isotope ratio, finally culminating in the  
748 values that we measure at the ground. We think that a reasonable agreement of the isotope values is proof that  
749 the assumed cloud microphysics of the BCIM (with all assumed input parameter values) holds good for the drop  
750 mass evolution, and therefore the drop evaporation estimated from the same model (see later) can be considered  
751 valid.

### 752 **3.2.3.3 Sensitivity of the model predictions and uncertainty of the predictions**

753 The simulations of BCIM predict the rain isotope ratios based on assumed values of RH, T, drop size  
754 and vapour isotope ratios. We did a sensitivity analysis of the model rain composition using Run-1 to study the  
755 effects of variation in temperature, relative humidity, vapour isotopes, and drop size and the results are given in  
756 Supplementary Information SI-13. Fig. S13-1 shows that vapour isotope value is the most important factor in  
757 controlling the model rain isotope ratios. For +10% change over the reference value of the parameters, the  
758 changes in the rain  $\delta D$  values (in ‰) are: +7.6 (for  $\delta D_v$ ), -4.1 (for RH), +2.6 (for T) and -0.4 (for diameter).

759 We also determined the uncertainty of the model predictions of dD (rain) and d-excess (rain). Using the  
760 Run-3 model output values, we obtained a multi-parameter regression equation for  $\delta D$  (rain) as a function of the  
761 four variables (vapour isotope, relative humidity, temperature and drop diameter)  $\delta D_v$ , RH, T and D. With given  
762 inputs of errors in  $\delta D_v$ , RH, T and D, the uncertainty in the rain isotope value  $\delta D_{rain}$  is 3.5 ‰. Using a similar  
763 exercise for the d-excess<sub>rain</sub> we obtain uncertainty for the d-excess<sub>rain</sub> as 2 ‰. The details of calculations are  
764 given in SI-14.

765 A preliminary inspection has shown that the situation would not improve had we taken another isotope enabled  
766 GCM, IsoGSM2 simulation (instead of LMDZ) for  $\delta^{18}O$  calibration; in fact, IsoGSM2 simulates higher values  
767 for both the vapour isotopes ( $\delta D$  and d-excess; results not shown).

## 768 **4. Discussion**

### 769 **4.1 Influence of local meteorological parameters on isotopes**

770 Water isotopes in the tropics often vary with rainfall, humidity, and temperature (Dansgaard, 2012; Lee  
771 and Fung, 2008). Scatter plots between the vapour d-excess values and local meteorological parameters such as  
772 rainfall amount, relative humidity, specific humidity and temperature are shown in Fig. S10-1. Supplementary  
773 Fig. S2. The d-excess of vapour shows only a marginal positive correlation with temperature ( $R^2=0.16$ ; p-  
774 value=0.03; not significant) and a small negative correlation with relative humidity ( $R^2=0.22$ ; p-value=0.01;  
775 marginally significant).

776 It is known that temperature and relative humidity of air have opposite controls on raindrop  
777 evaporation (Lee and Fung, 2008; Stewart, 1975). If the drop evaporation affects the rainfall significantly, we  
778 should have seen some No significant correlations (not shown) are found relation between the rainwater isotopes  
779 and rainfall. This is contrary to the anti correlation found in other climate zones (Lee and Fung, 2008). The

Formatted: Font: Bold

Formatted: Not Highlight

Formatted: Indent: First line: 1.27 cm

Formatted: Not Highlight

Formatted: Adjust space between Latin and Asian text, Adjust space between Asian text and numbers

Formatted: Indent: First line: 1.27 cm

Formatted: Font: Not Bold

782 absence of correlation in tropics is also found in ~~many recent~~ several other studies (Chakraborty et al., 2016;  
783 Moerman et al., 2013; Vimeux et al., 2011). Even though relation with rainfall in fact is absent, a correlation is  
784 often found with the regional convective activities (Kurita, 2013; Lekshmy et al., 2018). Risi et al. (2023) have  
785 noted that in the tropics, most of the precipitation falls under deep convective systems (see Section 3.1 and Fig.  
786 2), which are controlled by ~~different various~~ microphysical processes (like rain evaporation, diffusive liquid-  
787 vapour exchanges, and mesoscale downdrafts) connected through mesoscale -circulations. These processes  
788 probably override the effect of surface meteorological parameters in our region.

Formatted: Not Highlight

#### 790 **4.2 Rain-vapour isotope exchange and rain evaporation**

Formatted: Font: Not Italic

792 ~~As mentioned, a~~ An increasing trend (13 ‰ to 30 ‰) in the vapour d-excess values associated with a  
793 decrease in the  $\delta^{18}\text{O}$  values is noted with the progress of the monsoon (Fig. 2b). In contrast, the rain d-excess  
794 values were reasonably constant within a small range. The increase in vapour d-excess (and decrease in the  
795  $\delta^{18}\text{O}$ ) is large and could be ascribed to significant recycling of the moisture with contribution from some  
796 evaporative sources (discussed later). We are not certain about the source at this stage. Risi et al. (2023) have  
797 discussed the possibility of down-drafted vapours as the source of such anomalously low isotope ratios in the  
798 case of Sahelian squall lines. Earlier studies over some Indian sites have shown that changes in moisture sources  
799 are often associated with a concomitant change in isotope values in rain and vapours (Deshpande et al., 2010;  
800 Midhun et al., 2018). We investigated the possibility of this by forty-eight hours of air-parcel back trajectory  
801 analysis (Supplementary Fig. S4-1†), which shows that moisture for the 2019 summer monsoon season was  
802 derived mainly from the Arabian Sea. However, this does not rule out the possibility of minor evaporative  
803 contributions from continental moisture sources enroute or down-drafted moisture characterised by low isotope  
804 ratios and high d-excess values (Risi et al., 2010).

Formatted: Not Highlight

805 The micro-physical process of evaporative exchange during the fall of raindrops causes isotopic  
806 enrichment in the rain. Though important, raindrop evaporation cannot be easily quantified. As discussed  
807 before, evaporation is reflected in ~~the~~ higher  $\delta$ -values and lower d-excess values (mean ~2 ‰) of the rain  
808 samples. Froehlich et al. (2008) used d-excess values of precipitation in the Alpine region to derive the extent of  
809 evaporation using assumed end-member values of the regional vapours.

Formatted: Indent: First line: 1.27 cm

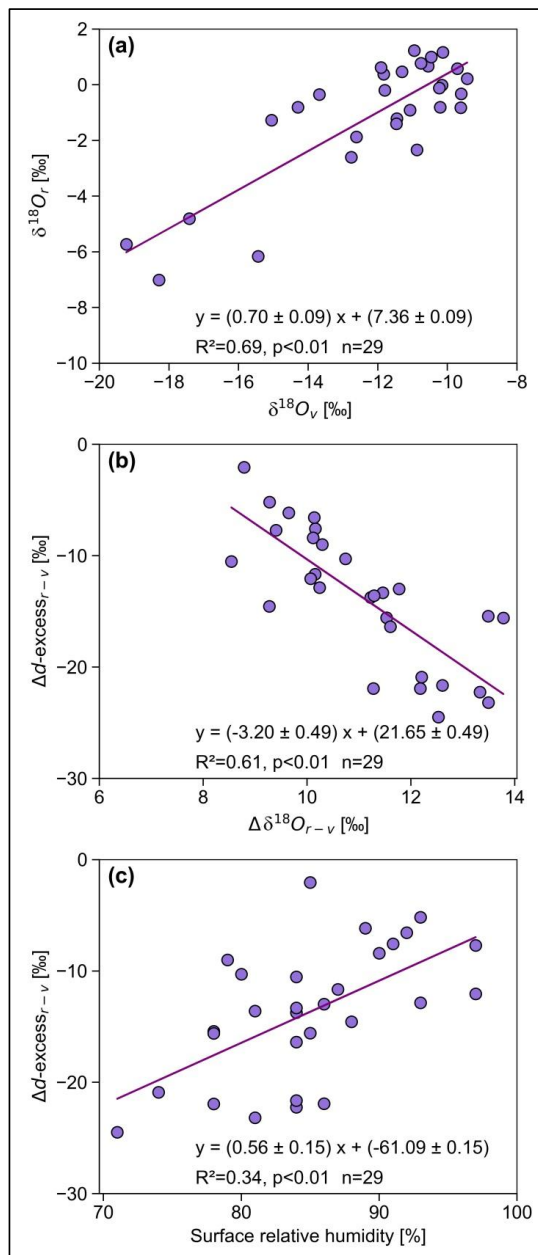
810 ~~To inspect the~~ Any isotope exchange between the rain and ambient vapour would result in correlated  
811 changes, the isotope data for the dates when both rain and vapour samples were collected are analysed here. A  
812 strong correlation between rain and vapour  $\delta^{18}\text{O}$  values is indeed found (Fig. 64a;  $R^2=0.764$ ,  $p < 0.01$ ,  $n=29$ ),  
813 suggesting a ~~genetic~~ connection between them. Sinha and Chakraborty (2020) also found significant positive  
814 relations ( $R^2 > 0.8$ ) between rain and vapour  $\delta^{18}\text{O}$  values over Andaman Island. However, they did not find any  
815 anti-correlation between rain  $\delta^{18}\text{O}$  and rain d-excess, as ~~we did~~ found here (Fig. 43b). The current study exhibits  
816 a reasonable anti-correlation between the ~~absolute value~~ differences in d-excess ( $\Delta d\text{-excess}_{(r-v)}$ ) and  $\delta^{18}\text{O}$   
817 ( $\Delta \delta^{18}\text{O}_{(r-v)}$ ) of rain and vapour (the subscript r-v indicates Rain isotope minus Vapour isotope) (Fig. 64b). This  
818 would be expected if evaporation of rain contributes a significant amount of vapour because the ~~inherited~~  
819 generated vapour is lower in  $\delta^{18}\text{O}$  but higher in  
820 d-excess compared to the rain.

Formatted: Not Highlight

Formatted: Not Highlight

Formatted: Not Highlight

821 | As raindrops evaporate, the newly formed vapour may get down-drafted to ~~the low level vapour~~  
822 | ~~lower~~ levels, and therefore, the two phases at the ground level would exhibit opposite changes. ~~Interestingly,~~  
823 | ~~However,~~ in the case of tropical precipitation, we do not expect a substantial contribution from rain evaporation to the  
824 | ambient vapour because the latter is a large reservoir. It has been shown in several earlier studies that the total  
825 | rain is derived from only a few percent of the overhead vapour mass (Pathak et al., 2014; Rahul et al., 2016).  
826 | Earlier studies have also shown that vapour d-excess values do not exhibit any systematic change in central or  
827 | southern WG stations, although, surprisingly, their rain  $\delta^{18}\text{O}$  values exhibit slight but gradual depletion (1 ‰ to  
828 | -10 ‰) in the later part of the monsoon (Lekshmy et al., 2018; Rahul et al., 2016). The negative correlation  
829 | found in this study suggests that the ground-level vapour gets a significant contribution from drop evaporation.  
830 | How can moisture generated by drop evaporation over the falling path contribute to the ground-level vapour?:  
831 | This is possible when there is a strong downdraft associated with intense monsoon rains (Risi et al., 2023). In a  
832 | modelling study, Mandke et al. (1999) pointed out that deep convective cloud systems contain both upward and  
833 | downward components. The downward motion is driven by the evaporation of falling precipitation and the  
834 | dragging of the ambient air and vapour by big droplets. This downdraft brings moisture down from above and  
835 | increases the vapour d-excess at the surface (Risi et al., 2010; Kurita, 2013; Aemisegger et al., 2015). The  
836 | existence of drop evaporation is further supported by a relation between  $\Delta d\text{-excess}$  ~~( $r_v$ )~~ and surface relative  
837 | humidity (RH;  $R^2=0.31$ ; Fig. 64c). The difference between rain and vapour isotopes is more in lower RH and  
838 | less in higher RH, as expected (Stewart, 1975). A similar analysis (Xing et al., 2020) in China also found that  
839 | the change in isotopic composition is large when RH is less than 60 %.



841  
 842 **Figure 64.** The correlations between (a)  $\delta^{18}O$  of rain ( $\delta^{18}O_r$ ) and  $\delta^{18}O$  of vapour ( $\delta^{18}O_v$ ) at the ground level; (b) the  
 843 difference in d-excess of rain and vapour ( $\Delta d\text{-excess}_{r-v}$ ) and  $\delta^{18}O$  ( $\Delta\delta^{18}O_{r-v}$ ) showing that the rain value is lower in d-  
 844 excess whereas it is higher in  $\delta^{18}O$ ; (c) difference in the d-excess of rain and vapour ( $\Delta d\text{-excess}_{r-v}$ ) and ground level  
 845 relative humidity (RH).

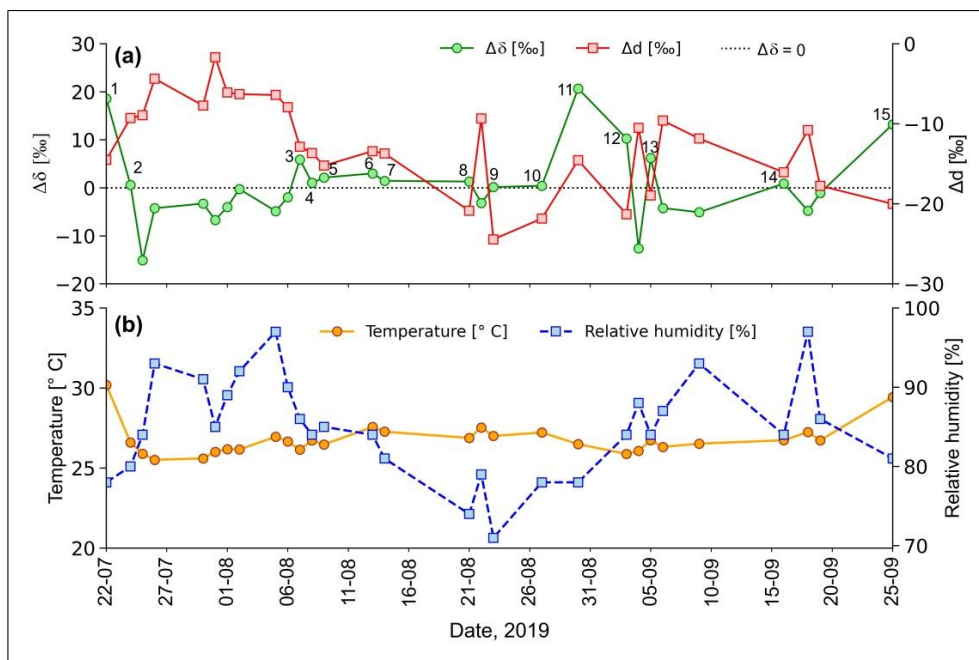
Formatted: Font: 12 pt

Formatted: Font: 12 pt

Formatted: Font: 12 pt

846  
 847 Falling raindrops and the water vapour in the atmospheric column constitute an interacting two-phase  
 848 system, especially below the cloud base. On the way down, the water molecules are constantly exchanged

849 between these two phases depending on the ambient RH and temperature. This makes the system evolve  
 850 towards an isotopic steady state. The difference between isotopes ( $\delta D$  and  $d$ -excess) of vapour in equilibrium  
 851 with raindrops and the observed surface vapour (at the ground level, defined as  $\Delta\delta$  and  $\Delta d$ , respectively) is  
 852 useful to quantify the departure from equilibrium. Graf et al. (2019) demonstrated the importance of a  $\Delta\delta$ - $\Delta d$   
 853 plot to represent the effect of sub-cloud processes, such as evaporation and equilibration, which influence the  
 854 water isotopes. In our case, the expected equilibrium vapour isotope values were estimated by using the standard  
 855 fractionation formula (Horita and Wesolowski, 1994) at the ambient temperature. The time series of  $\Delta\delta$  values  
 856 (Fig. 75a) for the Pune precipitation samples show that the values varied between  $-20$ – $15$  ‰ and  $20$ – $21$  ‰  
 857 (omitting one outlier) respectively. For  $\Delta d$ , the time series shows negative values in all cases (ranging from  $0$ – $2$   
 858 to  $-20$ – $24$  ‰). The close-to-equilibrium samples correspond mostly to the high-humidity period in July (Fig.  
 859 75b). Fifteen samples indicate the influence of below-cloud evaporation with positive  $\Delta\delta$  values associated with  
 860 strongly negative  $\Delta d$  values (up to  $-20$  ‰).  
 861



862  
 863 **Figure 75.** (a) Time series of  $\Delta\delta$  and  $\Delta d$  of the rain samples collected during 2019 monsoon (July to September) in Pune.  $\Delta\delta$   
 864 and  $\Delta d$  values (total points=29) denote rain-equilibrated vapour isotope minus the surface vapour isotopes as defined in the  
 865 text following Graf et al. (2019). The blue dotted line indicates  $\Delta\delta=0$ . All data points where  $\Delta\delta>0$  are marked with numbers  
 866 totaling 15. (b) Time series of daily average surface temperature and relative humidity recorded at IMD Pune-observatory at  
 867 Pune during the study period.

869 A  $\Delta\delta$ - $\Delta d$  scatter plot based on these observed data (Fig. 8)6d and 6h and Fig. 7d and 7h show that none  
 870 of the rain samples is in equilibrium with the corresponding ground-level vapour. If the equilibrium pertained  
 871 the points would plot at the origin. About 63% of the 15-sample pairs points fall in the lower right quadrant of  
 872 the diagram, where the raindrop evaporation is relatively more significant, as per Graf et al. (2019). We note that

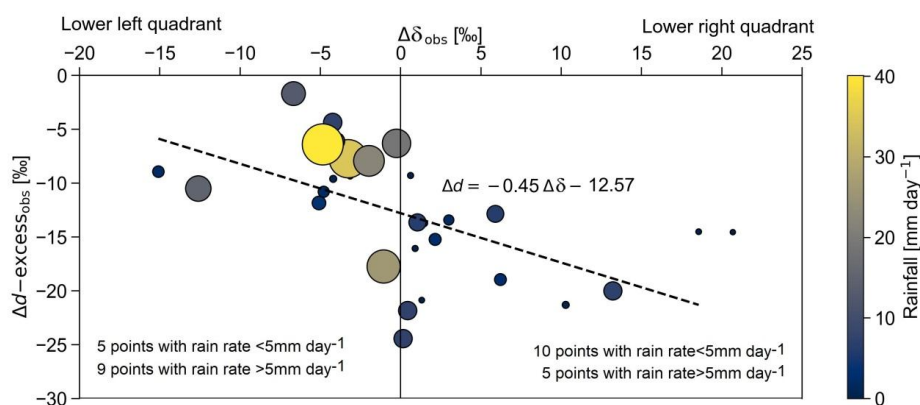
Formatted: Not Highlight

Formatted: Not Highlight

873 the observed rainfall amount was low (less than 5 mm) for these samples, which is consistent with a substantial  
 874 evaporation effect. Nine-14 samples have negative  $\Delta\delta$  and  $\Delta d$  values, indicating incomplete equilibration with  
 875 near-surface vapour. The crucial driving factors for below-cloud processes seem to be the size of raindrops and  
 876 the intensity of precipitation. This is primarily because raindrops with larger diameters correspond to increased  
 877 intensity and have shorter residence times in the atmospheric column. As a result, they experience reduced  
 878 evaporation while descending toward the ground. However, the drop size in this study was not derived by an  
 879 independent method. They were based on rain rates or precipitation intensity through M-P relation and are not  
 880 independent. A clearer demonstration of the relation between rain rate and drop size was provided by Law et al.  
 881 (2020) who showed that higher rainfall intensities are characterized by closer distances among raindrop  
 882 particles. This results in higher chances for smaller raindrops to collide and to coalesce into larger droplets  
 883 before falling from the cloud. We note that our data is consistent with their conclusion.

884 Distribution of points in the  $\Delta\delta$ - $\Delta d$  plot (Fig.8) shows that 10 samples with  $<5\text{mm/day}$  rain rate fall in  
 885 lower right quadrant compared to 5 in the left quadrant. This suggests that drop evaporation is a dominant  
 886 process in low rainfall events (where smaller drop sizes dominate). To see the rainfall or drop size effect more  
 887 clearly the size of the points were characterized in terms of drop size and the colour of the points were varied  
 888 indicative of rainfall (Fig. 8). It seems that larger drop size points with higher rainfall are always in the lower left  
 889 quadrant. This indicates that in such cases, the memory of the isotopes is partly retained even after sub-cloud  
 890 evaporation due to larger sizes. The 29 sampling points are nearly equally distributed in the two quadrants  
 891 suggesting equal number of equilibration-dominant and evaporation- dominant rain events. It is to be noted that  
 892 deep convective rains during the monsoon exhibit significantly higher mass-weighted diameter compared to  
 893 shallow convective rains or stratiform rains (Kumar et al. 2025). The five big diameter points in the lower left  
 894 quadrant correspond to such cases of deep convection.

895 ▲



897

898 Figure 8: The  $\Delta\delta$ - $\Delta d$  plot for various rain rates. The size of the sample circles indicates drop size; their  
 899 variation is also associated with the rain rate (scale on right). We note that most of the 4th quadrant (lower left)  
 900 points are of bigger size and those in the 3rd quadrant (lower right) are of small size. The line shows a good fit to  
 901 the data with a slope of -0.45.



941 ~~As mentioned before, to estimate hydrometeor isotopic composition, the BCIM requires vertical profiles of~~  
942 ~~temperature, humidity and vapour isotope as input parameters. The vertical profiles can be introduced into the~~  
943 ~~model in two ways: (1) Vertical ascent assumption. Here, the profiles can be calculated based on an idealised~~  
944 ~~Rayleigh model having moist adiabatic ascent of air parcels from the surface to the top of the column, and (2)~~  
945 ~~the T, RH profiles can be constructed based on available sounding data and isotope profiles can be derived from~~  
946 ~~simulations conducted using isotope-enabled atmospheric models (Pfahl et al., 2012). These are discussed below~~  
947 ~~(Sections 4.2.2 and 4.3.2).~~

948

#### 949 **4.3.1.1 Formation height and drop size assignment**

950

951 ~~The formation height of the drop is an important factor and should be fixed by considering the most probable~~  
952 ~~altitude range. This parameter is not known a priori, but we can infer this from the cloud liquid water content~~  
953 ~~analysis. An earlier study by Kumar et al. (2014) pointed out that a peak of Cloud Liquid Water Content~~  
954 ~~(CLWC) is often present at 850 mb during the monsoon season over western India. The CLWC data for a period~~  
955 ~~of 29 days of the study period obtained from the ERA-5 dataset also show a peak at 850±50 mb (Supplementary~~  
956 ~~Fig. S3). Here, we consider the CLWC peak at 850±50 mb (about 1 km above ground from Pune) as the drop~~  
957 ~~introduction height for our case, where the RH reaches the value of 100 % (following Graf et al., 2019).~~

958 ~~The BCIM also requires an initial drop size at the formation height. Unfortunately, no disdrometer or MRR~~  
959 ~~observations are available in the study area during 2019. We, therefore, adopted an empirical procedure, known~~  
960 ~~as the Marshall-Palmer relationship, to estimate the mean drop size at the ground. This was done by a weighing~~  
961 ~~procedure. First, we estimated the hourly mean drop size of the raindrops at the ground level from the hourly~~  
962 ~~rain rate data available from an IMD observatory at Shivajinagar, Pune, located about 4 km away from our study~~  
963 ~~area. Next, we calculated the 24 h mean drop size by taking a weighted average of the size and using rain rates~~  
964 ~~as the weights. The surface drop sizes thus calculated vary from 0.61 to 1.80 mm for various days. The drop~~  
965 ~~diameter at the ground is next provided as an input, and then the initial size at the drop height (about 1.5 km~~  
966 ~~above ground) is estimated iteratively in BCIM using the microphysics part of the model dealing with the major~~  
967 ~~isotope H<sub>2</sub>O (based on temperature and RH profile; Graf et al., 2019). This procedure was adopted for each day.~~

968

#### 969 **4.3.2 Results of simulation**

970

##### 970 **4.3.2.1 Run 1: Rayleigh ascent assumptions**

971

972 ~~As mentioned above, the model needs vertical background profiles of atmospheric temperature (T), relative~~  
973 ~~humidity (RH),  $\delta D_v$ , and d excess,  $dv$ . In Rayleigh simulations, various profiles were calculated from the moist~~  
974 ~~adiabatic ascent of an air parcel with surface values of temperature ( $T_0$ ), relative humidity ( $h_0$ ),  $\delta D_v$  ( $\delta v_0$ ) and~~  
975  ~~$dv$  ( $dv_0$ ) of each sampling day as inputs (see isotope profiles in Supplementary Fig. S4a and b). The surface~~  
976 ~~values of  $\delta D$  and d excess of vapour were taken from our vapour measurements along with the daily~~  
977 ~~temperature and humidity data obtained from the IMD publication (Section 2.3). The results for the set of~~  
978 ~~calculations using the Rayleigh ascent assumption (designated as Run 1) are shown in Fig. 6(a-d). In this set of~~  
979 ~~figures, we compare observed and model rain  $\delta D$  (Fig. 6a),  $\delta^{18}O$  (Fig. 6b), and d excess (Fig. 6c) values. We~~  
980 ~~also construct AS-Ad diagrams for both observed and model values and compare them in Fig. 6d. Although~~

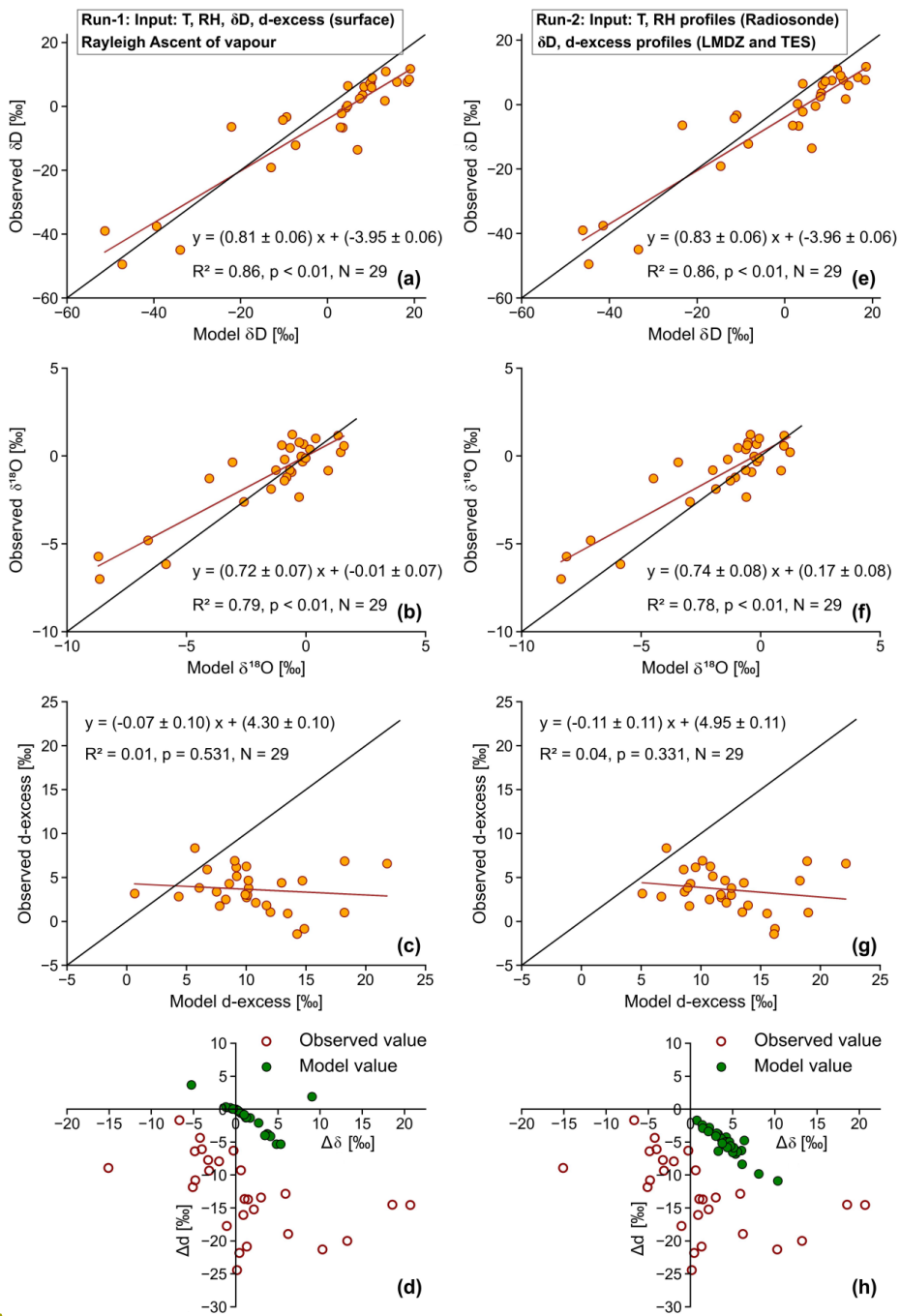
Formatted: Indent: First line: 0 cm

981 ~~observed and model isotope values (Fig. 6a and 6b) show strong correlation ( $R^2 = 0.86$  and  $0.79$ , respectively);~~  
982 ~~the model values are mostly overestimated (the plotted points lie below the 1:1 line). The overestimations of~~  
983 ~~isotopes (for  $\delta^{18}\text{O}$  and  $\delta\text{D}$ ) affect the d excess values considerably more; the points lie far to the right, and no~~  
984 ~~correlation exists between the observed and model d excess values (Fig. 6c). This is because the d excess~~  
985 ~~parameter is more sensitive to departure from equilibration due to dominance of evaporation, which means that~~  
986 ~~a small departure of delta values would magnify the discrepancy in case of d excess. We also note that most of~~  
987 ~~the model data points in a  $\Delta\delta$ - $\Delta\text{d}$  cross plot do not agree with the observed ones. However, they do fall in the~~  
988 ~~lower right quadrant, which is consistent with high raindrop evaporation. We also note that the  $\Delta\delta$  and  $\Delta\text{d}$  model~~  
989 ~~values (Fig. 6d, Run 1) show smaller variations compared to the observations. The  $\Delta\delta\text{D}$  of the model~~  
990 ~~simulations varies from 0 % to 5 % and  $\Delta\text{d}$  from 0 % to 5 %, while the observed values have variations of~~  
991 ~~about 25 % (higher by a factor of 5). These comparisons show that the Rayleigh ascent model fails to reproduce~~  
992 ~~the evolution of the rain isotopes in our region.~~

#### 993 **4.3.2.2 RH and T from Radiosonde and isotope profiles from TES and LMDZ (Run 2)**

994  
995 ~~Rayleigh ascent in Run 1 assumes that the source of vapour aloft is the rising air parcel, and the isotope values~~  
996 ~~along with RH and T should reflect that. But this did not yield a good fit. The simulation can possibly be~~  
997 ~~improved if we use RH and T data from local radiosonde observations and different isotope profiles. For the~~  
998 ~~present period, the radiosonde data were available only at a few specific pressure levels, and hence, appropriate~~  
999 ~~interpolations were carried out. To obtain the vertical profiles of vapour isotopes, we first use the isotope~~  
1000 ~~outputs of a GCM, LMDZ for Pune (Dr. Camille Risi; personal communication). These values are used in~~  
1001 ~~BCIM as inputs, and the simulated rainwater and vapour composition were compared with the observed values.~~  
1002 ~~We found that a wide difference exists between the observed and model rain/vapour isotopic values. We suspect~~  
1003 ~~that the LMDZ model may not be able to simulate the vapour isotope ratios accurately. This limitation was~~  
1004 ~~noted by Risi et al. (2021) in a recent study involving large eddy simulation; they observed that for high~~  
1005 ~~precipitation areas, the convective or mesoscale downdrafts bring more depleted vapour from above into the~~  
1006 ~~sub-cloud layer. Therefore, as an alternative, we used the  $\delta\text{D}_\text{v}$  profiles modified from TES observations. These~~  
1007 ~~profiles are constrained by using the measured ground level vapour isotope ratios as a boundary condition while~~  
1008 ~~maintaining the shape of the profile. The procedure is discussed below in the light of our an~~  
1009 ~~Firstly, TES vapour~~  
1010  ~~$\delta\text{D}$  data are not available for 2019. Moreover, it is also known that the data have large uncertainty within the~~  
1011 ~~boundary layer (Nimya et al., 2022). This necessitates the derivation of vapour isotope profiles, which would~~  
1012 ~~merge with the TES observations at upper layers. The TES provides  $\delta\text{D}$  values of moisture at 17 pressure levels~~  
1013 ~~with a  $5.3\text{ km} \times 8.4\text{ km}$  footprint during the years 2005-2009. Based on these, we derived an average TES~~  
1014 ~~profile, which is deemed to be representative of the mean monsoon values constructed by averaging TES~~  
~~observations over a box ( $16^\circ\text{--}20^\circ\text{N}$ ;  $72^\circ\text{--}76^\circ\text{E}$ ) for the ISM period.~~

Formatted: Indent: First line: 0 cm,  
Widow/Orphan control



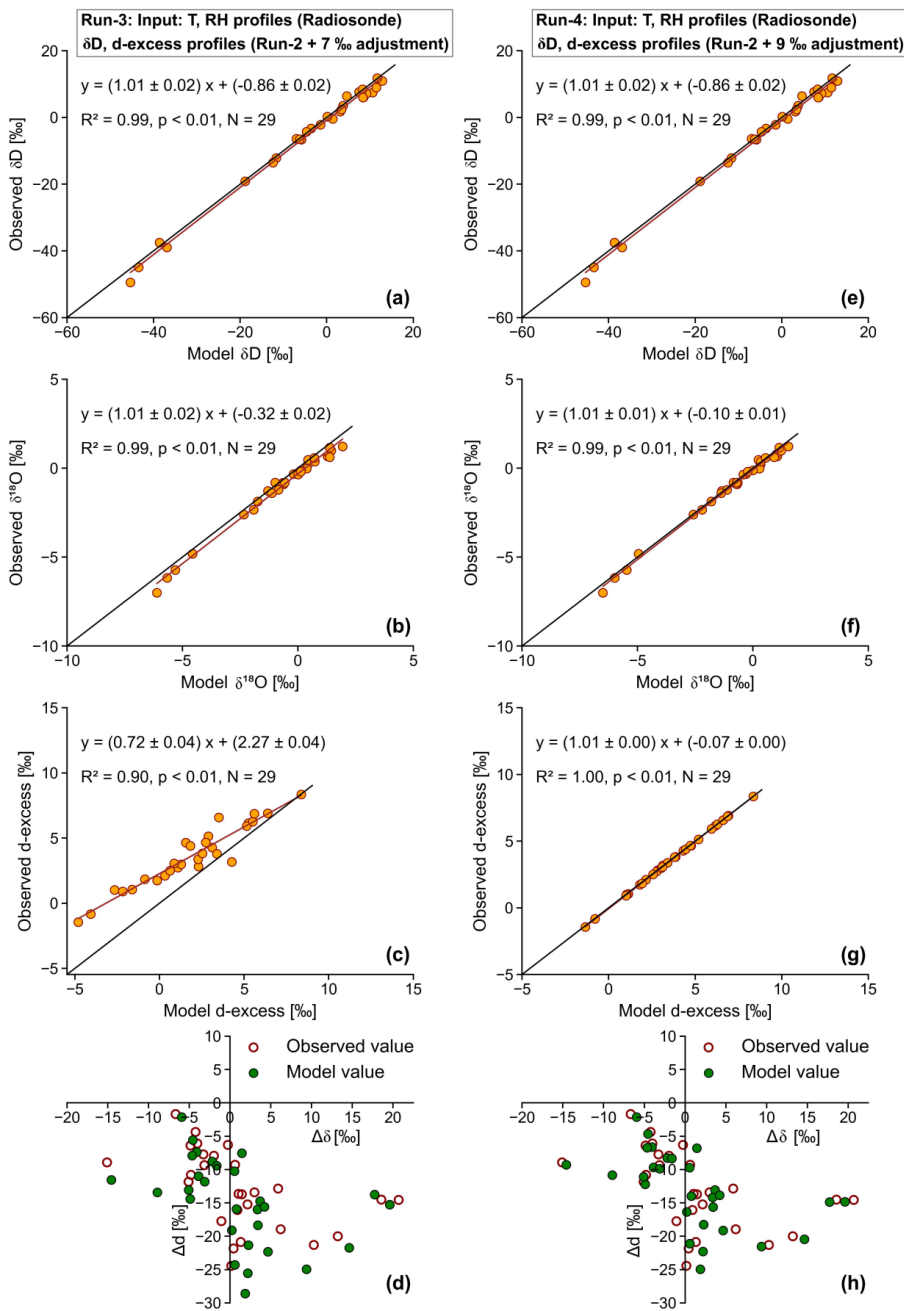
Formatted: Font: (Default) Times New Roman, 10 pt

Formatted: Justified

1015  
1016  
1017  
1018  
1019  
1020

**Figure 6.** Scatter plot showing observed and simulated (a) rain  $\delta^{18}O$ , (b) rain  $\delta D$ , (c) rain d excess, and (d) same data in  $\Delta \delta$ - $\Delta d$  diagram. Rayleigh ascent of a surface air parcel is assumed here (named as Run 1). Similar plots for Run 2 are shown in Fig. 6e-h, in which input profiles of T, RH, and vapour  $\delta D$  and d-excess values are obtained by adopted TES and LMDZ outputs (see text).

1021 To derive the vertical profiles for each of our sampling days, we use our daily surface measurements as  
 1022 boundary values. The average TES profile (as mentioned above) is modified through a curve fitting technique  
 1023 where the shape of the average profile is slightly altered while being constrained to pass through the surface  
 1024 value. A 4<sup>th</sup> order Polynomial of the type:  $Ah^4 + Bh^3 + Ch^2 + Dh + E$  (where h is the altitude in meters) was fitted  
 1025 to the average profile after adjusting its surface value so that a smooth shape is obtained (D/H decreasing with  
 1026 height following the average pattern). The polynomial coefficients (five in number) were calculated for three  
 1027 cases: (1) for the maximum observed surface D/H value, (2) for the mean surface value, and (3) for the  
 1028 minimum observed value, giving us three sets of A, B, C, D and E values. The constants for each day were next  
 1029 estimated by interpolation using these three sets. Obviously, this method of interpolation, constrained by surface  
 1030 vapour measurements, assumes that the vapour aloft is related to the surface value, and this assumption may not  
 1031 be correct. But it, at least, allows us to check if the surface constraints yield better rain isotope ratios at the  
 1032 ground (using BCIM) while being consistent with the TES measurements of vapour aloft. Unfortunately, the  
 1033 vapour  $\delta^{18}\text{O}$  values at various pressure levels are not available from TES (which gives only the  $\text{H}_2\text{O}/\text{H}_2\text{O}$  ratio).  
 1034 Therefore, we adopted a derivation technique using the vapour isotope profiles simulated by the LMDZ model.  
 1035 In this technique, daily average vapour  $\delta^{18}\text{O}$  and  $\delta\text{D}$  values were obtained from the LMDZ model outputs over  
 1036 our study region for the sampling dates at each height. For each day, two profiles (for  $\delta^{18}\text{O}$  and  $\delta\text{D}$ ) were  
 1037 constructed, and polynomials were fitted. Next, the d-excess profiles were constructed from these two profiles.  
 1038 Each of the daily d-excess profiles was then constrained by using the surface d-excess vapour value for that day  
 1039 to obtain the fitted d-excess Polynomial for that day. The rationale is that even though the individual profiles of  
 1040  $\delta\text{D}$  and  $\delta^{18}\text{O}$  provided by LMDZ do not predict well the rain isotope ratios (as seen by our trial), the d-excess  
 1041 based on these two isotope ratios should be reasonably good. The obtained vapour d-excess and  $\delta\text{D}$  profiles are  
 1042 shown in Fig. S4e and S4d, Run 2. These profiles were subsequently employed in BCIM (named Run 2) to  
 1043 generate the daily scale  $\delta^{18}\text{O}$ ,  $\delta\text{D}$  and d-excess values of surface rain isotope ratios (Fig. 6e-6h). However, the  
 1044 results do not show much improvement compared to the Run 1 (Fig. 6e-g) despite showing a larger variability  
 1045 in the  $\Delta\delta - \text{Ad}$  plot (Fig. 6h); the  $\Delta\delta$  values varied from -4.7% to 11% and  $\text{Ad}$  from -1.8% to -12.4%.  
 1046 Additionally, in this case, all the data points fell in the 3<sup>rd</sup> quadrant of the  $\Delta\delta - \text{Ad}$  cross plot (Fig. 6h and Fig.  
 1047 6d). Both Run 1 and Run 2 simulations fail to yield a good match between the observations and model  
 1048 (especially 4.3.4 Vapour  $\delta^{18}\text{O}$  correction in the profile (Run 3). The main source of error in Run 1 and Run 2  
 1049 could be improper vapour isotope profiles. It is possible that the true profile for a given date may not coincide  
 1050 with the surface measured value in extrapolation, as assumed by the boundary constraint. In other words, the  
 1051 vapour aloft may not be derived entirely from the surface vapour as measured at our sampling location. One  
 1052 possible explanation could be a significant contribution from the small-scale local surface moisture having a  
 1053 different isotopic composition (evaporation or evapotranspiration from water bodies or trees within a few  
 1054 hundred meters). However, this possibility can be ruled out as a study using satellite data showed that due to  
 1055 high humidity and low temperature during ISM, evaporation/evapotranspiration ( $\sim 0.5 \text{ mm day}^{-1}$ ) adds a  
 1056 negligible amount of moisture compared to the advective fluxes in this region (Pathak et al., 2014). Our  
 1057 investigation is also limited by the absence of upper air  $\delta\text{D}$ ,  $\delta^{18}\text{O}$  values from an independent observation or  
 1058 model on a daily scale. Due to this limitation, we adopted a forward modelling approach.



Formatted: Font: (Default) Times New Roman, 10 pt, Font color: Black

Formatted: Left

1059  
1060  
1061  
1062  
1063  
1064  
1065

**Figure 7.** Scatter plot showing observed and BCIM-simulated (a, e) rain  $\delta D$ , (b, f) rain  $\delta^{18}O$ , (c, g) rain d-excess; in (d, h) data are cast in the form of  $\Delta \delta - \Delta d$  diagram (for definition of  $\Delta$  values see text). In the panels (a, b, c and d), the input vapour  $\delta^{18}O$  values in the profile are reduced at each level appropriately so that maximum reduction is  $-7 \text{ ‰}$  at the fall height; in the panels (e, f, g and h) the reduction is  $-9 \text{ ‰}$ .

Formatted: Indent: First line: 0 cm

1066  
1067  
1068  
1069  
1070  
1071  
1072  
1073  
1074  
1075  
1076  
1077  
1078  
1079  
1080  
1081  
1082  
1083  
1084  
1085  
1086  
1087  
1088  
1089  
1090  
1091  
1092  
1093  
1094  
1095  
1096  
1097  
1098  
1099  
1100  
1101  
1102  
1103  
1104  
1105  
1106

#### 4.3.5 Sensitivity analysis and uncertainty estimates

meter.....(3)59(

In the context of point #4, we examine the effects of the formation height on isotopes, keeping all other parameters the same. We increase the formation height by 1 km (from 1.5 km to 2.5 km) and run the BCIM. To form the drop at a higher altitude, we need to change the RH profile so that the RH=100 % level is reached at the new height. A simplified RH profile is used by approximating the real profile with a straight line, where the surface RH value is taken as one end member, and the 100 % level is taken at the new height. We found that the simulated values of the rain isotope ratios did not change significantly, and similarly, the raindrop evaporation fraction also did not change (see later).  $\text{drop}^{***} \dots\dots\dots(4) * \text{dexv} + 0.169599 * \text{RH} - 0.31632 * \text{T} + 2.2921 * \text{D} \dots\dots\dots(5)$

Using standard quadratic formula for error (Farrance and Frenkel, 2012) when the dependent variable  $\delta\text{Dr}$  is a function of  $\delta\text{Dv}$ , RH, T and diameter D (using the regression formula as the function) we obtain the error for  $\sigma(\delta\text{Dr})$  given by:

$$\sigma(\delta\text{Dr})^2 = (\partial\delta\text{Dr}/\partial\delta\text{Dv})^2 * \sigma(\delta\text{Dv})^2 + (\partial\delta\text{Dr}/\partial\text{RH})^2 * \sigma(\text{RH})^2 + (\partial\delta\text{Dr}/\partial\text{T})^2 * \sigma(\text{T})^2 + (\partial\delta\text{Dr}/\partial\text{D})^2 * \sigma(\text{dia})^2 \dots\dots\dots(6)$$

Where  $\sigma$  denotes the uncertainties in  $\delta\text{Dv}$ , RH, T and D and the quantities in brackets express partial derivative of  $\delta\text{Dr}$  with respect to the variable. As mentioned earlier, the vapour isotope  $\delta\text{Dv}$  has an error of 2%. We obtained the uncertainties associated with RH and T in Radiosonde observations as 8% and 0.3°C (Sapucci et al.). We provide detailed uncertainty estimates of the model rain isotope values in Supplementary Information (SI 1). The uncertainty values for  $\delta\text{D}_{\text{min}} = 3.5\%$  and  $\text{d excess}_{\text{min}} = 2\%$ .

We also did a detailed sensitivity analysis (see Supplementary information, SI 2) to study the effects of variation in temperature, relative humidity, vapour isotopes, and drop size using the BCIM. These analyses show that vapour isotope values, RH, Temperature and drop sizes are the dominant factors controlling the model rain isotope ratios.

#### 4.3.6 Estimate of raindrop evaporation and its uncertainty

Our analysis shows that with minor tuning of vapour profiles, the BCIM can be used to simulate the rain isotope ratios in Pune. For tuning, the d excess of the vapour needs to be reduced, on average, by about 7% compared to the observed ground vapours. Assuming the validity of this tuning, we find that the rains suffer substantial but variable evaporation in the Pune region. We see from the output of BCIM in Run-3 predicts that the mass of the drop reduces as it falls. The ratio of final mass to the initial mass (or remaining fraction of mass of the hydrometeor relative to the initial mass, i.e.,  $m/m_0$ ) can then be used to estimate the fractional mass loss suffered by the drop on its way down for each day. The difference  $(1-m/m_0)$  of the drop then represents the effective rain evaporation. Defining rain evaporation in this way, With this definition, a time series of evaporation values is displayed in (Fig. 1098a), which varies show variation from 4 % to 6073 % (average ~23 %, omitting one outlier). As expected, drop evaporation is inversely related to the surface humidity (Fig. 1098b) and drop diameter (Fig. 849d) but directly proportional to the temperature (Fig. 1098c).

- Formatted: Indent: First line: 1.27 cm, Widow/Orphan control
- Formatted: Font: Bold
- Formatted: Centered
- Formatted: Not Highlight
- Formatted: Not Highlight
- Formatted: Highlight
- Formatted: Left
- Formatted: Font: 10 pt, English (India), Pattern: Clear
- Formatted: Indent: First line: 0.63 cm
- Formatted: Font: Symbol, 10 pt, English (India), Pattern: Clear
- Formatted: Font: 10 pt, English (India), Pattern: Clear
- Formatted: Font: Symbol, 10 pt, English (India), Pattern: Clear
- Formatted: Font: 10 pt, English (India), Pattern: Clear
- Formatted: Font: Symbol, 10 pt, English (India), Pattern: Clear
- Formatted: Font: 10 pt, English (India), Pattern: Clear
- Formatted: Font: 10 pt, English (India), Pattern: Clear
- Formatted: Font: 10 pt, English (India), Pattern: Clear
- Formatted: Font: Not Italic
- Formatted: Indent: First line: 1.27 cm
- Formatted: Not Highlight
- Formatted: Not Highlight
- Formatted: Not Highlight

1107 The evaporation was ~~particularly relatively~~ high (~~59 % and 60.73 % and 59 %~~) ~~for two days (on~~ 22 July  
1108 and 21 August) when humidity was ~~relatively~~ low (~~74.865 % and 78.14 %~~), and the temperature ~~was~~ high (30° C  
1109 and 27° C) ~~along with drop and the~~ diameter ~~small being small~~; the combined effect resulted in high evaporation  
1110 ~~fraction (Fig. 10.8a). In general, t~~ The deduced evaporation fractions are ~~moderately~~ high (23±16 %) ~~in this~~  
1111 ~~region. This inference which~~ is consistent with the observed anti-correlation between d-excess and  $\delta^{18}\text{O}$  of rain  
1112 samples (Fig. 3.4b) ~~as expected in drop evaporation when d excess of the raindrop decreases while its  $\delta^{18}\text{O}$~~   
1113 ~~increases.~~  
1114

**Formatted:** Not Highlight

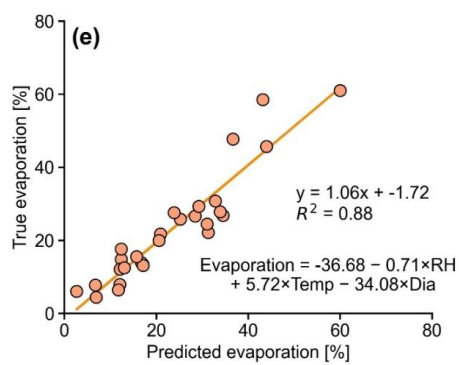
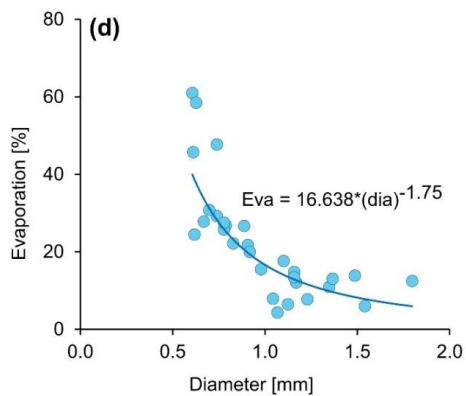
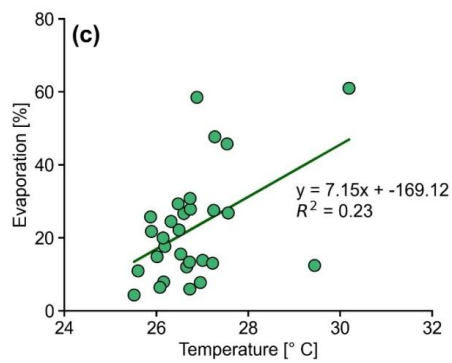
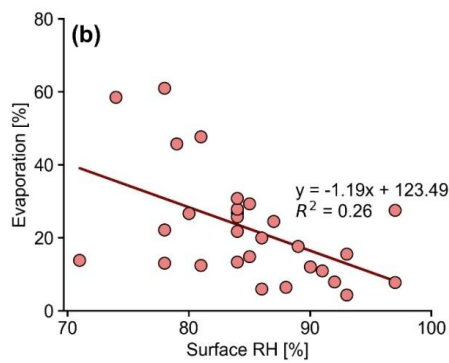
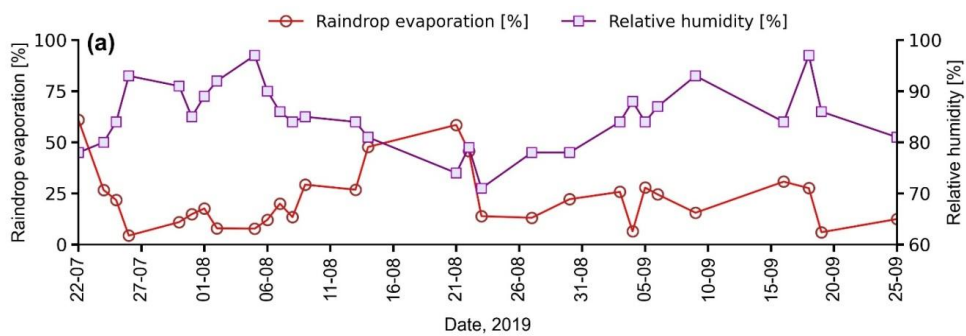
**Formatted:** Justified, Indent: First line: 1.27 cm, Space After: 0 pt, Line spacing: 1.5 lines, Don't adjust space between Latin and Asian text, Don't adjust space between Asian text and numbers

**Formatted:** Not Highlight

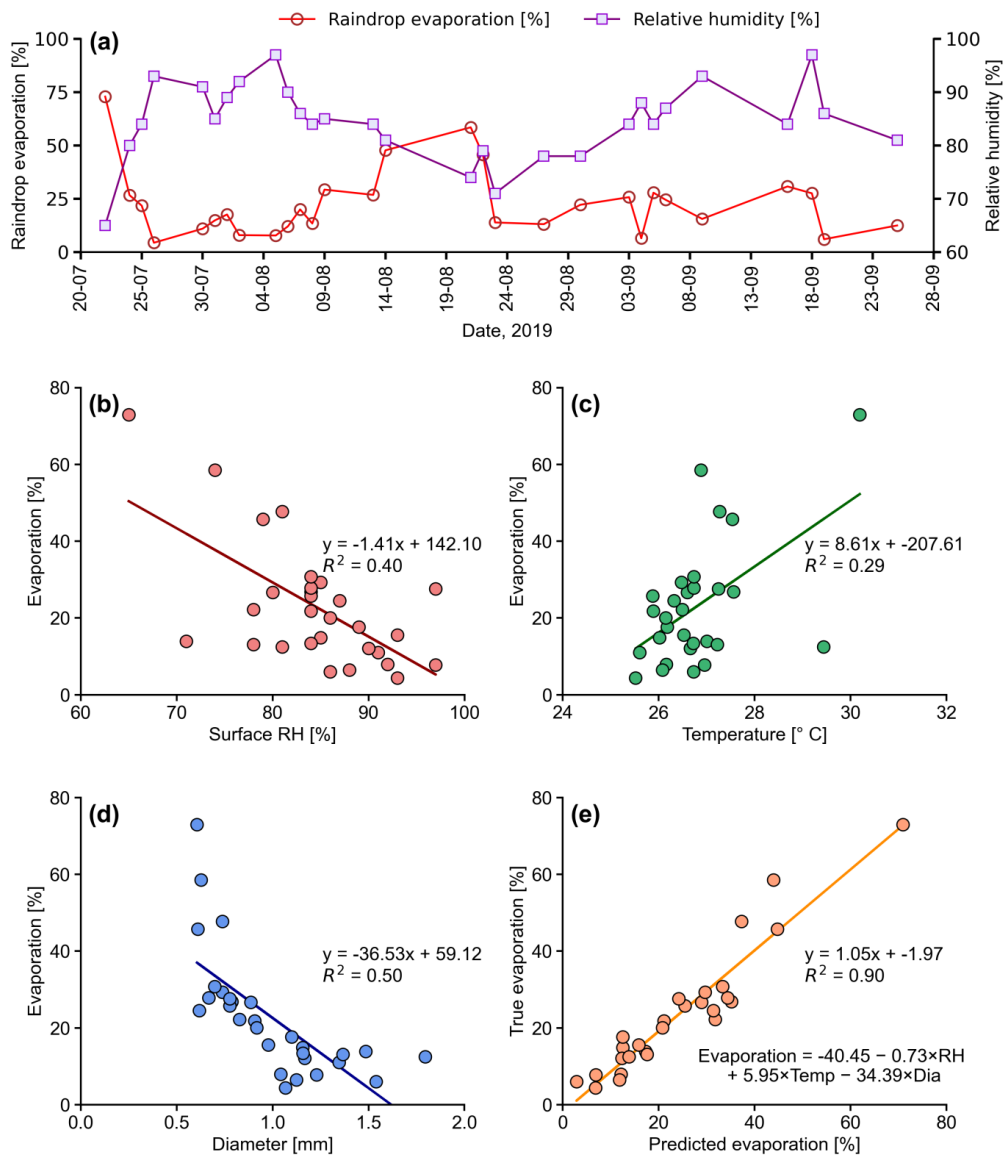
**Formatted:** Not Highlight

**Formatted:** Not Highlight

**Formatted:** Font: (Default) Times New Roman, 10 pt, Font color: Black, English (India), Ligatures: None



1115

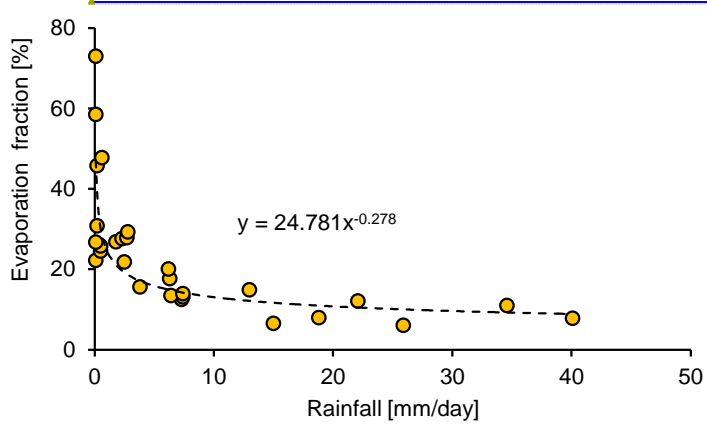
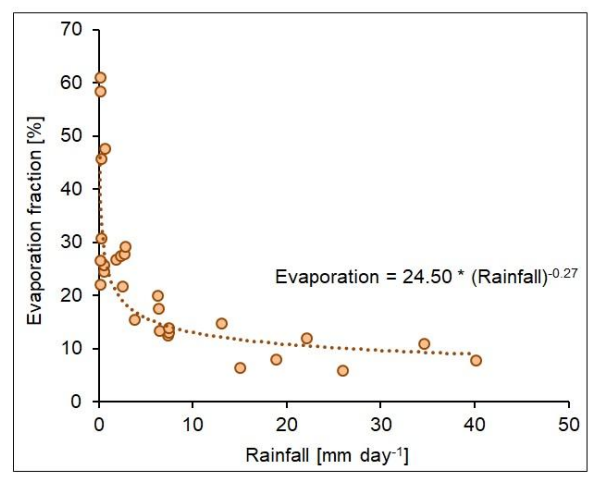


1116 **Figure 109.** (a) Time series of raindrop evaporation using BCIM simulation (Run-3) and surface relative humidity. The  
 1117 regression between raindrop evaporation fraction with (b) RH, (c) temperature, and (d) drop diameter. (e) Multiple  
 1118 regression analysis yields the equation:  $Evaporation (\%) = -36.68 - 0.71 \times RH + 5.72 \times temperature - 34.08 \times drop \ diameter$ . The  
 1119 regression equation prediction explains nearly 88% of the variance.

1120 **Figure 8.** (a) Time series of raindrop evaporation estimated from the BCIM using the simulation in Run 4 and surface  
 1121 relative humidity. The regression between raindrop evaporation with (b) RH, (c) temperature, and (d) drop diameter. (e)  
 1122 Multiple regression analysis yields a joint equation:  $Evaporation (\%) = -40.45 - 0.73 \times RH + 5.95 \times temperature - 34.39 \times drop$   
 1123  $diameter$

1124  
 1125  
 1126 A multi-variate regression analysis shows that we can fit the evaporation fraction (in %) as a function of three  
 1127 surface variables: RH (%), temperature ( $^{\circ}C$ ) and drop diameter (mm) as below (Fig. 8e):





1161

1162

1163

1164

1165

1166

1167

1168

1169

1170

1171

1172

1173

1174

1175

1176

1177

1178

**Figure 1019.** Scatter plot ~~showingshows~~ relationship between the drop evaporation estimated in this study and rainfall in Pune. The black dashed line indicates the best-fit power law. Higher rainfall implies drops of bigger size and hence lower evaporation fraction.

It is instructive to compare our results to the evaporation estimates obtained in similar studies carried out in other climatic regimes. Sarkar et al. (2003), in a steady state one-dimensional model study of rain in the North Atlantic Trade Wind region (Barbados), found a high value of 63% (63+23 %) for raindrop evaporation (using radar reflectivity data on rain evaporation flux) which is three times more than our average value of 23% (23+16 %). We have only four high evaporation days (more than 45%) out of 29 sampling days. The reason for ~~this~~ the large difference of Pune evaporation from Barbados is possibly ~~due~~ due to a large difference in drop size and RH. A comparison reveals that ~~their~~ in Barbados the drop sizes were ~~as~~ much smaller (from 0.125 mm to 0.66 mm) in comparison to ours (from 0.604 to 1.80 mm). Their drops were so small (smaller than 300 μm) in some cases (smaller than 0.3 mm on 4 February, 2020), that the drops ~~are~~ completely evaporated (evaporation ~ 100%) during the fall leading to very small rain. In addition, in their sampling region, the RH was ~~also~~ lower, ranging from 65% to 80%, compared to ours (74.65% to 97%). ~~Smaller~~ Lower drop size and lower RH lead to higher raindrop evaporation. ~~In addition~~ We also note that ~~their~~ drop sizes varied over a ~~larger~~ wider range.



1218 where the ambient vapour isotope ratios are highly depleted. Droplets formed from these vapours are  
1219 correspondingly depleted. The drop isotope values may be so negative that even evaporative exchanges may  
1220 not alter/increase their values much, especially if they are of big size. The high negative isotope values of  
1221 ground vapours could be due to downdrafts associated with strong evaporative cooling of rain drops. The  
1222 proposition that air parcels are lifted to higher altitudes during intense convective events is supported by the  
1223 presence of a second CLWC peak (about 550 mb; see Fig. 3) for 19, 25, 27 Sept, 2019 when the rain and  
1224 vapour isotopes were both highly depleted (rain  $\delta D$  values are -39 ‰, -49 ‰ and -59 ‰ compared to the  
1225 average of -7‰) and associated with the negative OLR anomaly (Fig. 2). It seems that on those days intense  
1226 convection lifted the moist air parcels to about 5.5 km which were responsible for high second CLWC  
1227 peaks.

Formatted

Formatted

Formatted

Formatted

Formatted

1228

1229 3. A gradual increase in the d-excess values of vapour and a small but notable decrease in  $\delta^{18}O$  values in the  
1230 later part of the monsoon (after mid-August) are observed. The high vapour d-excess in September is  
1231 especially noticeable. We also find a strong anti-correlation between vapour  $\delta^{18}O$  and vapour d-excess  
1232 values. Such anti-correlation usually indicates a significant contribution to the ground vapour from  
1233 evaporative sources which, in our case, accumulated slowly with the progress of monsoon. Pathak et al.  
1234 (2014) also found a higher precipitation recycling ratio, that is, the ratio of recycled precipitation to total  
1235 precipitation in central India, at the end of the monsoon (September). In contrast, the rain d-excess values  
1236 are not significantly different because there is no such cumulative effect for the rain.

Formatted: Font: (Default) Times New Roman, 10 pt, Font color: Auto

Formatted

Formatted: List Paragraph, Right: -0.08 cm, Numbered + Level: 1 + Numbering Style: 1, 2, 3, ... + Start at: 1 + Alignment: Left + Aligned at: 0.04 cm + Indent at: 0.68 cm

1237 4. The above observations suggest increased vapour contribution from evaporation of raindrops and/or from  
1238 local evapotranspiration (ET) sources, especially increasing with the monsoon progress. However, vapour  
1239 supply from surface sources cannot be a large factor. Pathak et al. (2014) showed that for central India the  
1240 ET contribution increases with the progress of the Monsoon but can at best account for 5 to 10% of the  
1241 vapour mass. Therefore, we strongly believe that downdraft of depleted vapour (and not local supply) is the  
1242 main source of low  $\delta^{18}O$  (and high d-excess) surface vapour (Risi et al., 2023). The depleted vapour  
1243 in the sub-cloud region can originate from raindrop evaporation and such vapour can be downdrafted by  
1244 the drag of the falling raindrops. However, a single column model like BCIM cannot capture this process.

Formatted: Right: -0.08 cm, Space After: 0 pt, Add space between paragraphs of the same style, Numbered + Level: 1 + Numbering Style: 1, 2, 3, ... + Start at: 1 + Alignment: Left + Aligned at: 0.04 cm + Indent at: 0.68 cm, No widow/orphan control, Don't adjust space between Latin and Asian text, Don't adjust space between Asian text and numbers, Tab stops: 0.56 cm, Left

Formatted

1245 5. In the  $\Delta\delta - \Delta d$  ( $\Delta$  indicates the isotope ratio of vapour in equilibrium with rain minus the ambient vapour  
1246 isotope ratio, following Graf et al., 2019) cross plot, about half of the data points lie in the lower right  
1247 quadrant, which signifies the importance of raindrop evaporation over Pune and the adjoining region during  
1248 our study period. The distribution of points in this quadrant is indicative of drop evaporation, but this fact  
1249 alone cannot quantify the magnitude. We determined the slope  $\Delta d / \Delta\delta$  of the points in the cross plot and  
1250 found a value of -0.45 which suggests that the evaporation in Pune was intense. This is because a higher  
1251 slope in the cross plot is caused by a relatively magnified effect of d-excess difference between the rain (and  
1252 corresponding equilibrated vapour) and the ambient vapour caused by a larger evaporation. A comparison  
1253 can be made with the study of Graf et al. (2019) who found a lower slope at a value of -0.31 for Zurich. The  
1254 slope is essentially due to a differential effect in evaporative fractionation. Evaporation decreases rain d-  
1255 excess but increases rain  $\delta D$ . However, the magnitudes of changes, negative for d-excess and positive for  
1256  $\delta D$ , are not the same. Fractionation values (involving equilibrium and kinetic factors) show that the change

Formatted: Font: (Default) Times New Roman, 10 pt, Font color: Auto

Formatted: Justified, Right: -0.08 cm, Numbered + Level: 1 + Numbering Style: 1, 2, 3, ... + Start at: 1 + Alignment: Left + Aligned at: 0.04 cm + Indent at: 0.68 cm

Formatted



1296 ~~downdraft of depleted vapour is the main source of low isotope (and high d-excess) surface vapour (Risi et~~  
1297 ~~al., 2023). The depleted vapour in the sub-cloud region can originate from raindrop evaporation.~~

1298 5. ~~To quantify the sub-cloud processes altering the rain isotope values, we used the Below Cloud~~  
1299 ~~Interaction Model-BCIM. Upon reasonable tuning of the input parameters, we obtained a notable agreement~~  
1300 ~~between the observed and model rain isotope values at the ground level.~~

1301 6. ~~In the  $\Delta\delta-\Delta d$  ( $\Delta$  is defined by rain-equilibrium vapour minus the ambient vapour following Graf et al)~~  
1302 ~~cross-plot, the majority of the data points lie in the 3<sup>rd</sup>-quadrant, which signifies the dominance of raindrop~~  
1303 ~~evaporation over Pune and the adjoining region during our study period. The cross-plot is indicative of drop~~  
1304 ~~evaporation but cannot quantify the magnitude. The slope of the points (about -0.43), however, suggests~~  
1305 ~~that evaporation is intense. This is because a higher slope in the cross-plot is caused by a relatively~~  
1306 ~~magnified effect of d-excess difference between the rain (and corresponding equilibrated vapour) and the~~  
1307 ~~ambient vapour which is due to a larger evaporation. For reference, Graf et al. (2019) found that the slope~~  
1308 ~~was lower at a value of -0.3 for Zurich.~~

1309 7. ~~Since the BCIM is found to be applicable to our study area, we estimate the raindrop evaporation~~  
1310 ~~parameter from the model output. An event-to-event quantification of raindrop evaporation is the key~~  
1311 ~~finding of our study. The model gives a net reduction of the drop mass at the ground level, and we can~~  
1312 ~~define the relative reduction as a measure of the effective rain evaporation. Using this innovative technique,~~  
1313 ~~the model shows that, on average, about 23% (varying from 4% to 73%) of the rain evaporates in the sub-~~  
1314 ~~cloud layer. There are four abnormally large values (46, 48, 58, and 73%) of evaporation. The largest value~~  
1315 ~~is probably due to low RH (~65%) on that day, but as for the other days, probably a combination of~~  
1316 ~~smaller drop size and lower RH played a role. Excluding these four values, the average evaporation is 18±8~~  
1317 ~~% (range of 4 to 30%).~~

1318 ~~It is instructive to compare our results to the evaporation estimates obtained in similar studies carried out in~~  
1319 ~~other climatic regimes. Sarkar et al. (2002), in a steady state one dimensional model study of rain in the~~  
1320 ~~North Atlantic Trade Wind region (Barbados), found a high value of 63% (63±23%) for raindrop~~  
1321 ~~evaporation which is three times more than our average value of 23% (23±16%). The reason for this is a~~  
1322 ~~large difference in drop size and RH. A comparison reveals that their drop size was much smaller (from~~  
1323 ~~125 μm to 6 μm) in comparison to ours (from 0.61 to 1.80 mm). The drops were so small (smaller than~~  
1324 ~~300 μm) in some cases (1 February, 2020), that they completely evaporated (evaporation = 100%) during~~  
1325 ~~the fall leading to very small rain. In addition, in their sampling region, the RH was also lower, ranging~~  
1326 ~~from 65% to 80%, compared to ours (65% to 97%). Lower drop size and lower RH lead to higher raindrop~~  
1327 ~~evaporation. In addition, the drop sizes varied over a larger range, leading to a larger variability compared~~  
1328 ~~to our study.~~

1329 ~~In another study, rain and vapour isotopes were measured in a cold-front passage over Zurich during 19-25 July~~  
1330 ~~2011, and the data were interpreted by an isotope enabled regional weather prediction model COSMOiso~~  
1331 ~~(Aemisegger et al., 2015). The authors showed that by switching off the raindrop evaporation, the rainfall~~  
1332 ~~increased by about 75% because the cooling induced by evaporation causes diminished convective activity. The~~  
1333 ~~estimated average evaporation in their study was about 40% (Dr. F. Aemisegger, personal comm.). This value is~~  
1334 ~~also twice our value. The reason is probably lower drop size and lower RH; as stated in their paper: “weak~~  
1335 ~~rainfall intensities (small droplets and thus lower falling velocities), and the possibly lower relative humidity in~~

Formatted: Font color: Auto

1336  
1337  
1338  
1339  
1340  
1341  
1342  
1343  
1344  
1345  
1346  
1347  
1348  
1349  
1350  
1351  
1352  
1353  
1354  
1355  
1356  
1357  
1358  
1359  
1360  
1361  
1362  
1363  
1364  
1365  
1366  
1367  
1368  
1369  
1370  
1371  
1372  
1373  
1374

the air column above could have contributed to the evaporative enrichment of precipitation”.

## 5.2 Limitations and uncertainty of the derived parameters

The tracer-based isotope technique and the BCIM, which we used, are associated with a series of the following limitations:-

- (a) We used TES satellite data averaged over 2005-2009 to guide our choice of vapour isotope profiles, but the year of analysis was 2019. In this matter, there is no way to ascertain the degree of deviation of the true profile from the adopted ones in Run-2 and in Run-3.
- (b) There are limitations on use of RH and T from radiosonde. On operating days, the radiosondes are usually launched at 00Z and 1200Z in Pune. Due to operational challenges, these measurements are not generally carried out when there is rain. The radiosonde data for Pune are expected to be reasonable for use in the model, if we can at least show that the difference between the two consecutive available measurements is not large. The difference between RH ( $\Delta$ RH) and temperature ( $\Delta$ T) measured at 1200Z and 00Z are plotted against height in Fig. SI-12-1 for the 29 days which are considered in the BCIM runs. The figure shows that the  $\Delta$ RH values are within  $\pm$  10% on most days (~80% of the total sampling days) and  $\Delta$ T values are within 2°C. This is expected as those parameters over the western India do not vary much during Indian Summer Monsoon (Pathak et al. 2013). We need to check how serious these differences are in the context of their use in the model. We have shown through sensitivity analyses and two multiple regression analyses that the effects of the daily scale variation in RH and T on model rain isotope values and evaporation fraction are not significant. We also demonstrate further that the RH and T data from the radiosonde used in this study is more reliable than the same obtained from any satellite datasets.

The  $\delta^{18}\text{O}$  profiles were adopted based on the  $\delta\text{D}$  and  $\delta^{18}\text{O}$  profiles obtained from the LMDZ model. As noted, this did not give us good agreement with the observations. Run-2 uses radiosonde for the thermodynamic profile,  $\delta\text{D}$  from satellite data from 2005-2009, and  $\delta^{18}\text{O}$  from the d-excess of the GCM extrapolated to the observed vapor measurement at the ground. We realize that there are major concerns with these inputs coming from different data products that all have different spatial/temporal scales and measurement principles. But we would like to emphasize that when any atmospheric model is initialized, by necessity, the input parameters from various sources are used, which may have different spatial and temporal resolutions and measurement principles. Moreover, datasets from various sources are also utilized in the atmospheric model across different parametrization schemes and nudging. Nudging is a well-known technique where the model values are nudged to accord with the observed values where available. For example, Graf et al. (2019) used point-based radiosonde RH and T observations, as well as isotope outputs from a limited-area model (Pfahl et al., 2012; Villiger et al., 2023), with a km-scale resolution, as input to BCIM. These two datasets have different scales and measurement principles. Guided by their argument, we have taken the Radiosonde profiles of each sampling day as our choice and adjusted the lowermost parts to match the measured RH and T values at the ground taken from the IMD.

- Formatted: Indent: First line: 0 cm
- Formatted: Font: Bold
- Formatted: Font: Bold
- Formatted: Font: (Default) Times New Roman, 10 pt, Font color: Black
- Formatted: Font: (Default) Times New Roman, 10 pt, Font color: Black
- Formatted: Font: Symbol
- Formatted: Font: Symbol
- Formatted: Font: Not Bold, Not Highlight
- Formatted: Not Highlight
- Formatted: Font: Not Bold, Not Highlight
- Formatted: Not Highlight
- Formatted: Font: Not Bold, Not Highlight
- Formatted: Font: Symbol
- Formatted: Font: Symbol
- Formatted: Font: Symbol
- Formatted: Font: (Default) Times New Roman, 10 pt, Font color: Black
- Formatted: Indent: Left: 1.9 cm, Right: 0 cm, Line spacing: 1.5 lines, No bullets or numbering, Tab stops: Not at 1.33 cm
- Formatted: Font: (Default) Times New Roman, 10 pt
- Formatted: Font: (Default) Symbol, 10 pt
- Formatted: Font: (Default) Times New Roman, 10 pt
- Formatted: Font: (Default) Symbol, 10 pt
- Formatted: Font: (Default) Times New Roman, 10 pt, Superscript
- Formatted: Font: (Default) Times New Roman, 10 pt
- Formatted: Font: (Default) Times New Roman, 10 pt
- Formatted: Font: (Default) Times New Roman, 10 pt
- Formatted: Font: (Default) Times New Roman, 10 pt
- Formatted: Font color: Auto
- Formatted: Font: (Default) Times New Roman, 10 pt, Font color: Auto
- Formatted: Font color: Auto
- Formatted: Font color: Auto
- Formatted: Font color: Auto
- Formatted: Font color: Auto
- Formatted: Font: (Default) Times New Roman, 10 pt

(c) The isotope profiles were constructed using ground observations as boundary values. However, this also resulted in a mismatch with the observed values (in Run-2), and we had to tune to lower  $\delta^{18}\text{O}$  values and higher d-excess values to achieve good agreement. It should be mentioned here that Risi et al. (2023) also discussed a similar idea in their study of water isotopes in tropical squall lines, that convective downdrafts can introduce depleted vapour produced by rain re-evaporation in the boundary layer. ~~Moreover, Another limitation is that~~ the vapour samples were collected for a duration (about a few hours) that did not coincide exactly with the longer rain collection period (about 24 hours).

(d) The raindrop formation height was assumed to be the ~~same-CLWC peak level~~ for all rainy days, and the drops were all introduced at ~~a constant~~ level, ~~considered to be the cloud base at RH=100 %~~. However, it is well known that raindrops do not all form at the same height, even on a single day. With this assumption, we are neglecting alterations in isotope ratios produced inside the cloud by various microphysical processes. ~~However, since we are concerned with sub-cloud processes, this is not a serious problem.~~

~~(e)~~ ~~Although some studies pointed out that collision-coalescence is an important warm rain process that occurs in various rain shadow region of India (Padmakumari et al., 2024), including those in Western Ghats (Konwar et al., 2014), BCIM neglects the process while estimating rain  $\delta^{18}\text{O}$  isotope values. We admit think that this may introduce some an error in rain evaporation estimation which but that cannot be quantified in the present study. Since collision coalescence is a non-fractionating process, the effect would be only through drop size modification. Therefore, the isotope effect would be a secondary effect and is expected to be small.~~

~~(f)~~ ~~Considering these limitations, we~~ provide detailed uncertainty estimates of the model rain isotope values ( $\delta\text{D}_{\text{rain}}$ ,  $\text{dexcess}_{\text{rain}}$ ) in the Supplementary Information (SI-I) section 3.2.3.3 and raindrop evaporation fractions estimates in the s(Section 4.3.6). Several assumptions are required to calculate the uncertainties in these parameters. The uncertainty values for  $\delta\text{D}_{\text{rain}}$  is= 3.5 ‰, for  $\text{dexcess}_{\text{rain}}$  it is= 2 ‰, and for drop evaporation estimate it is 10%.

### -5.3 Impact of evaporation on rainfall and heat budget

Presence of evaporation of rain drops during the Indian Summer MonsoonISM has been postulated earlier in several theoretical models, but this study provides, for the first time, a quantitative estimate of rain evaporation on a day-to-day basis in the Indian monsoon season using combined rain and vapour isotope data. However, We found that a ~~about~~ 25 % raindrop evaporation ~~applies only to occurred in 2019 monsoon season in~~ the highly humid Pune region. The average seasonal rainfall in Pune is about 55 cm (during monsoon for ISM), and if ~25 % of this is evaporated, it would mean considerable cooling of the boundary layer leading to localized downdrafts, formation of cold pools, and changes in atmospheric stability. ~~The cooling~~ Cooling can also hinder efficient formation of convection (Hwong and Muller, 2024) and can have a large effect on the precipitation patterns in the tropics (Bacmeister et al., 2006; Sarkar et al., 2023). Given the large share of precipitation recycling found in this study for Pune, the question arises, how large is the precipitation recycling is at larger scales, i.e., regional or continental scales, as well as in other seasons over India. We need to have a

Formatted: Normal, Indent: Left: 1.27 cm, No bullets or numbering

Formatted: Font color: Auto

Formatted: Font color: Auto, Not Highlight

Formatted: Font color: Auto

Formatted: Font: Times New Roman, Font color: Auto

Formatted: Font color: Auto

Formatted: Font: Times New Roman

Formatted: Font color: Auto

Formatted: Font: (Default) Times New Roman, 10 pt, Font color: Black

Formatted: Font: (Default) Symbol, 10 pt, Font color: Black

Formatted: Font: (Default) Times New Roman, 10 pt, Font color: Black

Formatted: Subscript

Formatted: Font: (Default) Times New Roman, 10 pt, Font color: Black

Formatted: Subscript

Formatted: Font: (Default) Times New Roman, 10 pt, Font color: Black

Formatted: Not Highlight

Formatted: Font: (Default) Times New Roman, 10 pt, Font color: Black

Formatted: Font: (Default) Times New Roman, 10 pt, Font color: Black

Formatted: Font: (Default) Times New Roman, 10 pt, Font color: Black

Formatted: Font: (Default) Times New Roman, 10 pt, Font color: Black

Formatted: Font: (Default) Times New Roman, 10 pt, Font color: Black, Highlight

Formatted: Font: (Default) Times New Roman, 10 pt, Font color: Black

Formatted: Font: Not Bold

Formatted: Font: (Default) Times New Roman, 10 pt, Font color: Black

Formatted: Font: Not Bold

Formatted: Font: (Default) Times New Roman, 10 pt, Font color: Black

Formatted: Font: (Default) Times New Roman, 10 pt, Font color: Black

Formatted: Font: Bold

Formatted: Font: (Default) Times New Roman, 10 pt, Bold, Font color: Black

1415 comprehensive program for carrying out such analysis, aided with appropriate BCIM input parameters, to  
1416 understand the evaporation of raindrops over various climatic subdivisions in India. Moreover, high-frequency  
1417 observation of vapour and rain isotopes would be useful to quantify this fraction during various convective  
1418 events associated with low-pressure systems during [the monsoonISM](#). ~~As mentioned above, A quantitative~~  
1419 ~~estimate of~~ raindrop evaporation ~~is an important parameter~~ [would be of great help](#) in modelling the energy and  
1420 moisture budget ~~in during the monsoon season rainfall prediction~~.

1421

#### 1422 **Data Availability**

1423 Observed rain and vapour isotope data are available upon communication with the corresponding author. The  
1424 upper-air radiosonde measurements were obtained from the University of Wyoming repository  
1425 (<http://weather.uwyo.edu/upperair/sounding.html>). The daily gridded data (zonal and meridional wind, specific  
1426 humidity, air temperature, and cloud liquid water content) are available from the European Centre for Medium-  
1427 Range Weather Forecasts Reanalysis (ERA-5; [https://www.ecmwf.int/en/forecasts/datasets/reanalysis-](https://www.ecmwf.int/en/forecasts/datasets/reanalysis-datasets/era5)  
1428 [datasets/era5](https://www.ecmwf.int/en/forecasts/datasets/reanalysis-datasets/era5)). The rainfall data (cumulated over 24 hours) are obtained from the Pune observatories of the IMD  
1429 (available at the National Data Centre ([www.imdpune.gov.in/ndc\\_new/ndc\\_index.html](http://www.imdpune.gov.in/ndc_new/ndc_index.html))). Apart from daily  
1430 rainfall, hourly rainfall data and daily average temperature and relative humidity data for the Pune observatory  
1431 were also obtained from the IMD using the above link. The datasets for 48 h air mass back trajectory analysis at  
1432 850 mb pressure level are obtained from the NOAA Hybrid Single-Particle Lagrangian Integrated Trajectory  
1433 (HYSPPLIT) model (<https://www.ready.noaa.gov/HYSPLIT.php>). We received daily outputs of LMDZ isotope-  
1434 enabled GCMs, which were provided by Dr. Camille Risi by personal communication. The Interpolated  
1435 Outgoing Longwave Radiation (OLR) data from NOAA  
1436 (<https://psl.noaa.gov/data/gridded/data.olrcdr.interp.html>) is used in this study. Tropospheric Emission  
1437 Spectrometer (TES) Level 2 (Nadir-Lite-Version 6) retrievals of HDO and H<sub>2</sub>O profiles for the available period  
1438 (2005–2007; <https://tes.jpl.nasa.gov/tes/data>) are used to construct the vapour  $\delta D$  profile.

1439

#### 1440 **Author Contribution**

1441

1442 SSN carried out all rain and vapour isotopic measurements and part of the data analyses, installed and ran the  
1443 model BCIM. SPR ~~analysed~~ [analyzed the majority of most of the samples to get the](#) isotopic data, performed all  
1444 controlled runs in the BCIM, and constructed most of the figures. SS conceptualized the scientific plan and  
1445 methodology and wrote the initial draft of the manuscript. SKB contributed to data analysis and interpretation of  
1446 model outputs, corrected the manuscript, and provided useful comments and suggestions. [NA contributed to](#)  
1447 [data analysis, and running of the BCIM.](#)

1448

#### 1449 **Code Availability**

1450 We carried out data analysis and plots using licensed versions of Microsoft Excel and Python, the latter being  
1451 freely available from <https://www.python.org/downloads/>. The code of the model, BCIM, is freely available  
1452 from <https://git.app.uib.no/Harald.Sodemann/bcim>.

1453

#### 1454 **Competing interests**

1455 The authors declare that they have no conflict of interest.

1456

1457 **Acknowledgements**

1458 The Indian Institute of Tropical Meteorology, Pune (IITM), is fully supported by the Earth System Science  
1459 Organization (ESSO) of the Ministry of Earth Sciences, India. This work forms part of the Ph.D. thesis of SSN,  
1460 who thanks IITM for a fellowship. SPR thanks IITM for a research associateship. We thank Director IITM for  
1461 his constant encouragement. The NASA Langley Research Centre and the Atmospheric Science Data Centre are  
1462 acknowledged for the TES dataset. A fruitful discussion with Dr. Camille Risi is also acknowledged. [We thank](#)  
1463 [Dr. Pallab Roy for helping with the Bootstrap analysis and making several plots.](#)

1464

1465 **References**

1466 [Aemisegger, F., Spiegel, J. K., Pfahl, S., Sodemann, H., Eugster, W., and Wernli, H.: Isotope meteorology of](#)  
1467 [cold front passages: A case study combining observations and modeling, Geophys. Res. Lett., 42, 5652–5660,](#)  
1468 <https://doi.org/10.1002/2015GL063988>, 2015.

1469 [Bacmeister, J. T., Suarez, M. J., and Robertson, F. R.: Rain re-evaporation, boundary layer–convection](#)  
1470 [interactions, and Pacific rainfall patterns in an AGCM, J. Atmos. Sci., 63, 3383–3403, 2006.](#)

1471

1472 [Bhattacharya S.K., K. Froehlich, P. K. Aggarwal, and K. M. Kulkarni Isotopic variation in Indian Monsoon](#)  
1473 [precipitation: Records from Bombay and New Delhi, Geophysical Research Letters, 30\(24\), 2285,](#)  
1474 <doi:10.1029/2003GL018453>, 2003

1475

1476 [Bonne, J. L., Masson-Delmotte, V., Cattani, O., Delmotte, M., Risi, C., Sodemann, H., and Steen-Larsen, H. C.:](#)  
1477 [The isotopic composition of water vapour and precipitation in Ivittuut, southern Greenland, Atmos. Chem.](#)  
1478 [Phys., 14, 4419–4439, https://doi.org/10.5194/acp-14-4419-2014, 2014.](#)

1479 [Brubaker, K. L., Entekhabi, D., and Eagleson, P. S.: Estimation of Continental Precipitation Recycling, J.](#)  
1480 [Climate, 6, 1077–1089, https://doi.org/10.1175/1520-0442\(1993\)006<1077:EOCPR>2.0.CO;2, 1993.](#)

1481 [Chakraborty, S., Sinha, N., Chattopadhyay, R., Sengupta, S., Mohan, P. M., and Datye, A.: Atmospheric](#)  
1482 [controls on the precipitation isotopes over the Andaman Islands, Bay of Bengal, Sci. Rep., 6, 19555,](#)  
1483 <https://doi.org/10.1038/srep19555>, 2016.

1484 [Crawford, J., Hollins, S. E., Meredith, K. T., and Hughes, C. E.: Precipitation stable isotope variability and](#)  
1485 [subcloud evaporation processes in a semi-arid region, Hydrol. Process., 31, 20–34,](#)  
1486 <https://doi.org/10.1002/hyp.10885>, 2017.

1487 [Dai, Q., Yang, Q., Han, D., Rico-Ramirez, M. A., and Zhang, S.: Adjustment of Radar-Gauge Rainfall](#)  
1488 [Discrepancy Due to Raindrop Drift and Evaporation Using the Weather Research and Forecasting Model and](#)  
1489 [Dual-Polarization Radar, Water Resour. Res., 55, 9211–9233, https://doi.org/10.1029/2019WR025517, 2019.](#)

1490 [Dansgaard, W.: Stable isotopes in precipitation, Tellus A: Dynamic Meteorology and Oceanography, 16, 436,](#)  
1491 <https://doi.org/10.3402/tellusa.v16i4.8993>, 2012.

1492 [Deshpande, R. D., Maurya, A. S., Kumar, B., Sarkar, A., and Gupta, S. K.: Rain-vapor interaction and vapor](#)  
1493 [source identification using stable isotopes from semiarid western India, J. Geophys. Res., 115, 2010JD014458,](#)  
1494 <https://doi.org/10.1029/2010JD014458>, 2010.

1495 [Draxler, R. R. and Hess, G.: Description of the HYSPLIT4 modeling system, 1997.](#)

1496 [Foote, G. B. and du Toit, P. S.: Terminal Velocity of Raindrops Aloft, J. App. Meteorol. \(1962-1982\), 8, 249–](#)  
1497 [253, 1969.](#)

1498 [Farrance and Frenkel, Clin Biochem Rev., Vol 33, 2012](#)

1499

1500 [Froehlich, K., Kralik, M., Papesch, W., Rank, D., Scheifinger, H., and Stichler, W.: Deuterium excess in](#)

1501 [precipitation of Alpine regions – moisture recycling, \*Isotopes in Environmental and Health Studies\*, 44, 61–70,](https://doi.org/10.1080/10256010801887208)  
1502 <https://doi.org/10.1080/10256010801887208>, 2008.

1503 [Gat, J. R.: Oxygen and hydrogen isotopes in the hydrologic cycle, \*Annu. Rev. Earth Planet. Sci.\*, 24, 225–262,](https://doi.org/10.1146/annurev.earth.24.1.225)  
1504 <https://doi.org/10.1146/annurev.earth.24.1.225>, 1996.

1505 [Graf, P., Wernli, H., Pfahl, S., and Sodemann, H.: A new interpretative framework for below-cloud effects on](https://doi.org/10.5194/acp-19-747-2019)  
1506 [stable water isotopes in vapour and rain, \*Atmos. Chem. Phys.\*, 19, 747–765, https://doi.org/10.5194/acp-19-747-](https://doi.org/10.5194/acp-19-747-2019)  
1507 [2019](https://doi.org/10.5194/acp-19-747-2019), 2019.

1508 [Gray, W. M.: Fundamental Importance of Convective Downdrafts and Mass Recycling Within the Tropical](https://doi.org/10.6057/2012TCRR01.14)  
1509 [Cloud Cluster and the Typhoon-Hurricane, \*Trop. Cyclone Res. and Rev.\*, 1, 130–141,](https://doi.org/10.6057/2012TCRR01.14)  
1510 <https://doi.org/10.6057/2012TCRR01.14>, 2012.

1511 [Herman, R. L., Cherry, J. E., Young, J., Welker, J. M., Noone, D., Kulawik, S. S., and Worden, J.: Aircraft](https://doi.org/10.5194/amt-7-3127-2014)  
1512 [validation of Aura Tropospheric Emission Spectrometer retrievals of HDO / H<sub>2</sub>O, \*Atmos. Meas. Tech.\*, 7, 3127–](https://doi.org/10.5194/amt-7-3127-2014)  
1513 [3138, https://doi.org/10.5194/amt-7-3127-2014](https://doi.org/10.5194/amt-7-3127-2014), 2014.

1514 [Hersbach, H., Bell, B., Berrisford, P., Hirahara, S., Horányi, A., Muñoz-Sabater, J., Nicolas, J., Peubey, C.,](https://doi.org/10.1002/qj.3803)  
1515 [Radu, R., Schepers, D., Simmons, A., Soci, C., Abdalla, S., Abellan, X., Balsamo, G., Bechtold, P., Biavati, G.,](https://doi.org/10.1002/qj.3803)  
1516 [Bidlot, J., Bonavita, M., De Chiara, G., Dahlgren, P., Dee, D., Diamantakis, M., Dragani, R., Flemming, J.,](https://doi.org/10.1002/qj.3803)  
1517 [Forbes, R., Fuentes, M., Geer, A., Haimberger, L., Healy, S., Hogan, R. J., Hólm, E., Janisková, M., Keeley, S.,](https://doi.org/10.1002/qj.3803)  
1518 [Laloyaux, P., Lopez, P., Lupu, C., Radnoti, G., De Rosnay, P., Rozum, I., Vamborg, F., Villaume, S., and](https://doi.org/10.1002/qj.3803)  
1519 [Thépaut, J.: The ERA5 global reanalysis, \*Quart. J. Royal Meteorol. Soc.\*, 146, 1999–2049,](https://doi.org/10.1002/qj.3803)  
1520 <https://doi.org/10.1002/qj.3803>, 2020.

1521 [Horita, J. and Wesolowski, D. J.: Liquid-vapor fractionation of oxygen and hydrogen isotopes of water from the](https://doi.org/10.1016/0016-7037(94)90096-5)  
1522 [freezing to the critical temperature, \*Geochimica et Cosmochimica Acta\*, 58, 3425–3437,](https://doi.org/10.1016/0016-7037(94)90096-5)  
1523 [https://doi.org/10.1016/0016-7037\(94\)90096-5](https://doi.org/10.1016/0016-7037(94)90096-5), 1994.

1524 [Hwong, Y.L. and Muller, C.J.: The unreasonable efficiency of total rain evaporation removal in triggering](https://doi.org/10.1029/2023GL106523)  
1525 [convective self-aggregation, \*Geophys. Res. Lett.\*, 51, p.e2023GL106523,](https://doi.org/10.1029/2023GL106523)  
1526 <https://doi.org/10.1029/2023GL106523>, 2024.

1527

1528 [Ingleby, B., Pauley, P., Kats, A., Ator, J., Keyser, D., Doerenbecher, A., Fucile, E., Hasegawa, J., Toyoda, E.,](https://doi.org/10.1175/BAMS-D-15-00169.1)  
1529 [Kleinert, T., Qu, W., St. James, J., Tennant, W., and Weedon, R.: Progress toward high-resolution, real-time](https://doi.org/10.1175/BAMS-D-15-00169.1)  
1530 [radiosonde reports, \*Bulletin of the American Meteorological Society\*, 97\(11\), 2149–2161,](https://doi.org/10.1175/BAMS-D-15-00169.1)  
1531 <https://doi.org/10.1175/BAMS-D-15-00169.1>, 2016

1532

1533 [IPCC, A.: Climate change 2014 synthesis report, IPCC: Geneva, Switzerland, 1059–1072, 2014.](https://doi.org/10.1017/S0028740414000101)

1534 [Jensen, M. P., Holdridge, D. J., Survo, P., Lehtinen, R., Baxter, S., Toto, T., and Johnson, K. L.: Comparison of](https://doi.org/10.5194/amt-9-3115-2016)  
1535 [Vaisala radiosondes RS41 and RS92 at the ARM Southern Great Plains site, \*Atmos. Meas. Tech.\*, 9, 3115–](https://doi.org/10.5194/amt-9-3115-2016)  
1536 [3129, https://doi.org/10.5194/amt-9-3115-2016](https://doi.org/10.5194/amt-9-3115-2016), 2016.

1537 [Kanamitsu, M.: Description of the NMC Global Data Assimilation and Forecast System, \*Wea. Forecasting\*, 4,](https://doi.org/10.1175/1520-0434(1989)004<0335:DOTNGD>2.0.CO;2)  
1538 [335–342, https://doi.org/10.1175/1520-0434\(1989\)004<0335:DOTNGD>2.0.CO;2](https://doi.org/10.1175/1520-0434(1989)004<0335:DOTNGD>2.0.CO;2), 1989.

1539 [Konwar, M., Das, S.K., Deshpande, S. M., Chakravarty, K., and Goswami, B. N.: Microphysics of clouds and](https://doi.org/10.1002/2014JD021606)  
1540 [rain over the Western Ghat, \*J. Geophys. Res.-Atmos.\*, 119, 6140–6159, https://doi.org/10.1002/2014JD021606,](https://doi.org/10.1002/2014JD021606)  
1541 [2014](https://doi.org/10.1002/2014JD021606).

1542 [Kumar, S., Resmi, E. A., Jash, D., Patade, S., Sumesh, R.K., Andrews, A., Sukumar, N., Aswini, A.R., and](https://doi.org/10.1066/43)  
1543 [Kulkarni, G.: Raindrop size distribution in stratiform precipitation: Insights from spectral bin simulations over](https://doi.org/10.1066/43)  
1544 [the high-altitude cloud physics observatory, Western Ghats, \*Journal of Atmospheric and Solar-Terrestrial\*](https://doi.org/10.1066/43)  
1545 [Physics, 277, 106643, 2025](https://doi.org/10.1066/43)

1546

1547 [Kumar, S., Hazra, A., and Goswami, B. N.: Role of interaction between dynamics, thermodynamics and cloud](https://doi.org/10.1002/2014JD021606)  
1548 [microphysics on summer monsoon precipitating clouds over the Myanmar Coast and the Western Ghats, \*Clim.\*](https://doi.org/10.1002/2014JD021606)

1549 [Dynam., 43, 911–924, https://doi.org/10.1007/s00382-013-1909-3, 2014.](https://doi.org/10.1007/s00382-013-1909-3)

1550 [Kumar, T. V. L., Durga, G. P., Rao, K. K., Nagendra, H., and Mall, R. K.: Moisture recycling over the Indian](https://doi.org/10.1016/B978-0-12-822402-1.00008-9)  
1551 [monsoon core region in response to global warming from CMIP5 models, in: Indian Summer Monsoon](https://doi.org/10.1016/B978-0-12-822402-1.00008-9)  
1552 [Variability, Elsevier, 449–466, https://doi.org/10.1016/B978-0-12-822402-1.00008-9, 2021.](https://doi.org/10.1016/B978-0-12-822402-1.00008-9)

1553 [Kurita, N.: Water isotopic variability in response to mesoscale convective system over the tropical ocean, J.](https://doi.org/10.1002/jgrd.50754)  
1554 [Geophys. Res.-Atmos., 118, https://doi.org/10.1002/jgrd.50754, 2013.](https://doi.org/10.1002/jgrd.50754)

1555 [Lee, C., Lawson, W. G., Richardson, M. I., Anderson, J. L., Collins, N., Hoar, T., and Mischna, M.: Demonstration of ensemble data assimilation for Mars using DART, MarsWRF, and radiance observations from MGS TES, J. Geophys. Res., 116, E11011, https://doi.org/10.1029/2011JE003815, 2011.](https://doi.org/10.1029/2011JE003815)  
1556  
1557

1558 [Lee, J. and Fung, I.: Amount effect of water isotopes and quantitative analysis of post-condensation processes,](https://doi.org/10.1002/hyp.6637)  
1559 [Hydrol. Process., 22, 1–8, https://doi.org/10.1002/hyp.6637, 2008.](https://doi.org/10.1002/hyp.6637)

1560 [Lekshmy, P. R., Midhun, M., Ramesh, R., and Jani, R. A.: <sup>18</sup>O depletion in monsoon rain relates to large-scale](https://doi.org/10.1038/srep05661)  
1561 [organized convection rather than the amount of rainfall, Sci. Rep., 4, 5661, https://doi.org/10.1038/srep05661,](https://doi.org/10.1038/srep05661)  
1562 [2014.](https://doi.org/10.1038/srep05661)

1563 [Lekshmy, P. R., Midhun, M., and Ramesh, R.: Influence of stratiform clouds on δD and δ<sup>18</sup>O of monsoon water](https://doi.org/10.1016/j.jhydrol.2018.06.001)  
1564 [vapour and rain at two tropical coastal stations, J. Hydrol., 563, 354–362,](https://doi.org/10.1016/j.jhydrol.2018.06.001)  
1565 [https://doi.org/10.1016/j.jhydrol.2018.06.001, 2018.](https://doi.org/10.1016/j.jhydrol.2018.06.001)

1566 [Levine, R. C. and Turner, A. G.: Dependence of Indian monsoon rainfall on moisture fluxes across the Arabian](https://doi.org/10.1007/s00382-011-1096-z)  
1567 [Sea and the impact of coupled model sea surface temperature biases, Clim. Dynam., 38, 2167–2190,](https://doi.org/10.1007/s00382-011-1096-z)  
1568 [https://doi.org/10.1007/s00382-011-1096-z, 2012.](https://doi.org/10.1007/s00382-011-1096-z)

1569 [Li, X. and Srivastava, R. C.: An Analytical Solution for Raindrop Evaporation and Its Application to Radar](https://doi.org/10.1175/1520-0450(2001)040<1607:AASFRE>2.0.CO;2)  
1570 [Rainfall Measurements, J. Appl. Meteorol., 40, 1607–1616, https://doi.org/10.1175/1520-](https://doi.org/10.1175/1520-0450(2001)040<1607:AASFRE>2.0.CO;2)  
1571 [0450\(2001\)040<1607:AASFRE>2.0.CO;2, 2001.](https://doi.org/10.1175/1520-0450(2001)040<1607:AASFRE>2.0.CO;2)

1572 [Li, X., Tang, C., and Cui, J.: Intra-Event Isotopic Changes in Water Vapor and Precipitation in South China,](https://doi.org/10.3390/w13070940)  
1573 [Water, 13, 940, https://doi.org/10.3390/w13070940, 2021.](https://doi.org/10.3390/w13070940)

1574 [Law, S.L.G., Kuok, K. K., and Trinidad, S.G.: An Experimental Study on The Correlation of Natural Rainfall](https://doi.org/10.1101/012009)  
1575 [Intensities and Raindrop Size Distribution Characteristics, 2021 IOP Conf. Ser.: Mater. Sci. Eng. 1101 012009,](https://doi.org/10.1101/012009)  
1576 [10.1088/1757-899X/1101/1/012009, 2021](https://doi.org/10.1101/012009)  
1577

1578 [Mandke, S.K., Soman, M. K., and Satyan, V.: Impact of Convective Downdrafts in a GCM on the Simulated](https://doi.org/10.2151/jmsj1965.77.5_1061)  
1579 [Mean Indian Summer Monsoon and its Variability, J. Meteorol. Soc. Jpn., 77, 1061–1082,](https://doi.org/10.2151/jmsj1965.77.5_1061)  
1580 [https://doi.org/10.2151/jmsj1965.77.5\\_1061, 1999.](https://doi.org/10.2151/jmsj1965.77.5_1061)

1581 [Midhun, M., Lekshmy, P. R., Ramesh, R., Yoshimura, K., Sandeep, K. K., Kumar, S., Sinha, R., Singh, A., and](https://doi.org/10.1029/2017JD027427)  
1582 [Srivastava, S.: The Effect of Monsoon Circulation on the Stable Isotopic Composition of Rainfall, J. Geophys.](https://doi.org/10.1029/2017JD027427)  
1583 [Res.-Atmos., 123, 5205–5221, https://doi.org/10.1029/2017JD027427, 2018.](https://doi.org/10.1029/2017JD027427)

1584 [Moerman, J. W., Cobb, K. M., Adkins, J. F., Sodemann, H., Clark, B., and Tuen, A. A.: Diurnal to interannual](https://doi.org/10.1016/j.epsl.2013.03.014)  
1585 [rainfall δ<sup>18</sup>O variations in northern Borneo driven by regional hydrology, Earth Planet. Sci. Lett., 369–370, 108–](https://doi.org/10.1016/j.epsl.2013.03.014)  
1586 [119, https://doi.org/10.1016/j.epsl.2013.03.014, 2013.](https://doi.org/10.1016/j.epsl.2013.03.014)

1587 [Munksgaard, N. C., Zwart, C., Haig, J., Cernusak, L. A., and Bird, M. I.: Coupled rainfall and water vapour](https://doi.org/10.1002/hyp.13576)  
1588 [stable isotope time series reveal tropical atmospheric processes on multiple timescales, Hydrol. Process., 34,](https://doi.org/10.1002/hyp.13576)  
1589 [111–124, https://doi.org/10.1002/hyp.13576, 2020.](https://doi.org/10.1002/hyp.13576)

1590 [Murali Krishna, U. V., Das, S. K., Sulochana, E. G., Bhowmik, U., Deshpande, S. M., and Pandithurai, G.: Statistical characteristics of raindrop size distribution over the Western Ghats of India: wet versus dry spells of the Indian summer monsoon, Atmos. Chem. Phys., 21, 4741–4757, https://doi.org/10.5194/acp-21-4741-2021, 2021.](https://doi.org/10.5194/acp-21-4741-2021)  
1591  
1592  
1593

1594 [Naik, M., Jadhav, A. V., Mukhim, S., Kumar, P. P., and Rohini, L.: Bhawar-Cloud base height variability](#)  
1595 [observed using a Laser- Based Ceilometer over a tropical station Pune, India International Journal of Remote](#)  
1596 [Sensing, 45, <https://doi.org/10.1080/01431161.2024.2402003>, 2003.](#)  
1597  
1598 [Nimya, S. S., Sengupta, S., Parekh, A., Bhattacharya, S. K., and Pradhan, R.: Region-specific performances of](#)  
1599 [isotope enabled general circulation models for Indian summer monsoon and the factors controlling isotope](#)  
1600 [biases, Clim. Dynam., 59, 3599–3619, <https://doi.org/10.1007/s00382-022-06286-1>, 2022.](#)  
1601  
1602 [Noone D.: Pairing Measurements of the Water Vapor Isotope Ratio with Humidity to Deduce Atmospheric](#)  
1603 [Moistening and Dehydration in the Tropical Mid-troposphere, Journal of climate, 25\(13\), 4476-4494,](#)  
1604 <https://doi.org/10.1175/JCLI-D-11-00582.1>, 2012.  
1605  
1606 [Pathak, A., Ghosh, S., and Kumar, P.: Precipitation Recycling in the Indian Subcontinent during Summer](#)  
1607 [Monsoon, J. Hydrometeorol., 15, 2050–2066, <https://doi.org/10.1175/JHM-D-13-0172.1>, 2014.](#)  
1608  
1609 [Pattanaik, D., Mandal, R., Dey, A., Phani, R., Chattopadhyay, R., Joseph, S., Sahai, A., and Mohapatra, M.:](#)  
1610 [Extended Range Forecast \(ERF\) During Southwest Monsoon 2019, 2019.](#)  
1611  
1612 [Pfahl, S., Wernli, H., and Yoshimura, K.: The isotopic composition of precipitation from a winter storm – A](#)  
1613 [case study with the limited-area model COSMO<sub>iso</sub>, Atmos. Chem. Phys., 12, 1629–1648,](#)  
1614 <https://doi.org/10.5194/acp-12-1629-2012>, 2012.  
1615  
1616 [Pradhan, R., Singh, N., and Singh, R. P.: Onset of summer monsoon in Northeast India is preceded by enhanced](#)  
1617 [transpiration, Sci. Rep., 9, 18646, <https://doi.org/10.1038/s41598-019-55186-8>, 2019.](#)  
1618  
1619 [Pranindita, A., Wang-Erlandsson, L., Fetzer, I., and Teuling, A. J.: Moisture recycling and the potential role of](#)  
1620 [forests as moisture source during European heatwaves, Clim. Dynam., 58, 609–624,](#)  
1621 <https://doi.org/10.1007/s00382-021-05921-7>, 2022.  
1622  
1623 [Pruppacher, H. R., and Klett, J. D.: Microstructure of Atmospheric Clouds and Precipitation, in: Microphysics](#)  
1624 [of Clouds and Precipitation, vol. 18, Springer Netherlands, Dordrecht, 10–73, \[https://doi.org/10.1007/978-0-\]\(https://doi.org/10.1007/978-0-306-48100-0\_2\)](#)  
1625 <https://doi.org/10.1038/s41597-024-04308-7>, 2024.  
1626  
1627 [Rajaveni, S. P., Nimya, S. S., Sengupta, S., Datye, A., and Sarma, D.: Three Years of Stable Water Isotope Data](#)  
1628 [of Daily Rain Samples Collected from Three Geomorphic Regions of India, Sci. Data, 11, 1445,](#)  
1629 <https://doi.org/10.1002/2016JD025352>, 2016.  
1630  
1631 [Rajaveni, S. P., Nimya, S. S., Sengupta, S., Datye, A., and Sarma, D.: Three Years of Stable Water Isotope Data](#)  
1632 [of Daily Rain Samples Collected from Three Geomorphic Regions of India, Sci. Data, 11, 1445,](#)  
1633 <https://doi.org/10.1038/s41597-024-04308-7>, 2024.  
1634  
1635 [Rao, Y.P.: Southwest Monsoon, Meteorological Monograph Synoptic Meteorology No.1., India Meteorological](#)  
1636 [Department, 1976.](#)  
1637  
1638 [Risi, C., Bony, S., and Vimeux, F.: Influence of convective processes on the isotopic composition \( \$\delta^{18}\text{O}\$  and](#)  
1639  [\$\delta\text{D}\$ \) of precipitation and water vapor in the tropics: 2. Physical interpretation of the amount effect, J. Geophys.](#)  
1640 [Res., 113, 2008JD009943, <https://doi.org/10.1029/2008JD009943>, 2008.](#)  
1641  
1642 [Risi, C., Bony, S., Vimeux, F., and Jouzel, J.: Water-stable isotopes in the LMDZ4 general circulation model:](#)  
1643 [Model evaluation for present-day and past climates and applications to climatic interpretations of tropical](#)  
1644 [isotopic records, J. Geophys. Res.-Atmos., 115, <https://doi.org/10.1029/2009JD013255>, 2010.](#)  
1645  
1646 [Risi, C., Galewsky, J., Reverdin, G., and Briant, F.: Controls on the water vapor isotopic composition near the](#)  
1647 [surface of tropical oceans and role of boundary layer mixing processes, Atmos. Chem. Phys., 19, 12235–12260,](#)  
1648 <https://doi.org/10.5194/acp-19-12235-2019>, 2019.  
1649  
1650 [Risi, C., Muller, C., and Blossey, P.: Rain Evaporation, Snow Melt, and Entrainment at the Heart of Water](#)

1640 [Vapor Isotopic Variations in the Tropical Troposphere, According to Large-Eddy Simulations and a Two-](#)  
1641 [Column Model, \*J. Adv. Model Earth Syst.\*, 13, e2020MS002381, <https://doi.org/10.1029/2020MS002381>, 2021.](#)

1642 [Risi, C., Muller, C., Vimeux, F., Blossey, P., Védeau, G., Dufaux, C., and Abramian, S.: What Controls the](#)  
1643 [Mesoscale Variations in Water Isotopic Composition Within Tropical Cyclones and Squall Lines? Cloud](#)  
1644 [Resolving Model Simulations in Radiative-Convective Equilibrium, \*J. Adv. Model Earth Syst.\*, 15,](#)  
1645 [e2022MS003331, <https://doi.org/10.1029/2022MS003331>, 2023.](#)

1646 [Salamalikis, V., Argiriou, A. A., and Dotsika, E.: Isotopic modeling of the sub-cloud evaporation effect in](#)  
1647 [precipitation, \*Sci. Total Environ.\*, 544, 1059–1072, <https://doi.org/10.1016/j.scitotenv.2015.11.072>, 2016.](#)

1648 [Saranya, P., Krishan, G., Rao, M. S., Kumar, S., and Kumar, B.: Controls on water vapor isotopes over Roorkee,](#)  
1649 [India: Impact of convective activities and depression systems, \*J. Hydrol.\*, 557, 679–687,](#)  
1650 [https://doi.org/10.1016/j.jhydrol.2017.12.061, 2018.](#)

1651 [Sarkar, M., Bailey, A., Blossey, P., de Szoek, S. P., Noone, D., Quiñones Meléndez, E., Leandro, M. D., and](#)  
1652 [Chuang, P. Y.: Sub-cloud rain evaporation in the North Atlantic winter trade winds derived by pairing isotopic](#)  
1653 [data with a bin-resolved microphysical model, \*Atmos. Chem. Phys.\*, 23, 12671–12690,](#)  
1654 [https://doi.org/10.5194/acp-23-12671-2023, 2023.](#)

1655 [Sengupta, S., Bhattacharya, S. K., Parekh, A., Nimya, S. S., Yoshimura, K., and Sarkar, A.: Signatures of](#)  
1656 [monsoon intra-seasonal oscillation and stratiform process in rain isotope variability in northern Bay of Bengal](#)  
1657 [and their simulation by isotope enabled general circulation model, \*Clim. Dynam.\*, 55, 1649–1663,](#)  
1658 [https://doi.org/10.1007/s00382-020-05344-w, 2020.](#)

1660 [Sengupta, S., Bhattacharya, S. K., Sunil, N. S., and Sonar, S.: Quantifying Raindrop Evaporation Deficit in](#)  
1661 [General Circulation Models from Observed and Model Rain Isotope Ratios on the West Coast of India,](#)  
1662 [Atmosphere, 14, 1147, <https://doi.org/10.3390/atmos14071147>, 2023.](#)

1663 [Sinha, N. and Chakraborty, S.: Isotopic interaction and source moisture control on the isotopic composition of](#)  
1664 [rainfall over the Bay of Bengal, \*Atmos. Res.\*, 235, 104760, <https://doi.org/10.1016/j.atmosres.2019.104760>,](#)  
1665 [2020.](#)

1666 [Sodemann, H., Aemisegger, F., Pfahl, S., Bitter, M., Corsmeier, U., Feuerle, T., Graf, P., Hankers, R., Hsiao, G.,](#)  
1667 [Schulz, H., Wieser, A., and Wernli, H.: The stable isotopic composition of water vapour above Corsica during](#)  
1668 [the HyMeX SOP1 campaign: insight into vertical mixing processes from lower-tropospheric survey flights,](#)  
1669 [Atmos. Chem. Phys., 17, 6125–6151, <https://doi.org/10.5194/acp-17-6125-2017>, 2017.](#)

1670 [Stewart, M. K.: Stable isotope fractionation due to evaporation and isotopic exchange of falling waterdrops:](#)  
1671 [Applications to atmospheric processes and evaporation of lakes, \*J. Geophys. Res.\*, 80, 1133–1146,](#)  
1672 [https://doi.org/10.1029/JC080i009p01133, 1975.](#)

1673 [Song, H., Kim, S., Lee, H., and Kim, K.: Climatology of Tropospheric Relative Humidity over the Korean](#)  
1674 [Peninsula from Radiosonde and ECMWF Reanalysis, \*Atmosphere\* 2020, 11\(7\),](#)  
1675 [704; <https://doi.org/10.3390/atmos11070704>](#)

1676 [Tao, W., Chen, J., Li, Z., Wang, C., and Zhang, C.: Impact of aerosols on convective clouds and precipitation,](#)  
1677 [Rev. Geophys., 50, 2011RG000369, <https://doi.org/10.1029/2011RG000369>, 2012.](#)

1678 [Trenberth, K. E.: Atmospheric Moisture Recycling: Role of Advection and Local Evaporation, \*J. Climate\*, 12,](#)  
1679 [1368–1381, \[https://doi.org/10.1175/1520-0442\\(1999\\)012<1368:AMRROA>2.0.CO;2\]\(https://doi.org/10.1175/1520-0442\(1999\)012<1368:AMRROA>2.0.CO;2\), 1999.](#)

1680 [Utsav, B., Deshpande, S. M., Das, S. K., and Pandithurai, G.: Statistical Characteristics of Convective Clouds](#)  
1681 [over the Western Ghats Derived from Weather Radar Observations, \*J. Geophys. Res.-Atmos.\*, 122,](#)  
1682 [https://doi.org/10.1002/2016JD026183, 2017.](#)

1683 [Vimeux, F., Tremoy, G., Risi, C., and Gallaire, R.: A strong control of the South American SeeSaw on the intra-](#)  
1684 [seasonal variability of the isotopic composition of precipitation in the Bolivian Andes, \*Earth and Planet. Sci.\*](#)  
1685 [Let., 307, 47–58, <https://doi.org/10.1016/j.epsl.2011.04.031>, 2011.](#)

1686 [Wang, B., Ding, Y., and Sikka, D.: Synoptic systems and weather, \*The Asian Monsoon\*, 131–201, 2006.](#)

1687 [Wang, R., Gentine, P., Yin, J., Chen, L., Chen, J., and Li, L.: Long-term relative decline in evapotranspiration](#)  
1688 [with increasing runoff on fractional land surfaces, \*Hydrol. Earth Syst. Sci.\*, 25, 3805–3818,](#)  
1689 <https://doi.org/10.5194/hess-25-3805-2021>, 2021.

1690 [Wang, S., Zhang, M., Che, Y., Chen, F., and Qiang, F.: Contribution of recycled moisture to precipitation in](#)  
1691 [oases of arid central Asia: A stable isotope approach, \*Water Resour. Res.\*, 52, 3246–3257,](#)  
1692 <https://doi.org/10.1002/2015WR018135>, 2016.

1693 [Worden, J., Noone, D., Bowman, K. et al.: Importance of rain evaporation and continental convection in the](#)  
1694 [tropical water cycle, \*Nature\*, 445, 528–532, <https://doi.org/10.1038/nature05508>, 2007.](#)

1695 [Worden, J., Noone, D., Galewsky, J., Bailey, A., Bowman, K., Brown, D., Hurley, J., Kulawik, S., Lee, J., and](#)  
1696 [Strong, M.: Estimate of bias in Aura TES HDO/H<sub>2</sub>O profiles from comparison of TES and in situ HDO/H<sub>2</sub>O](#)  
1697 [measurements at the Mauna Loa observatory, \*Atmos. Chem. Phys.\*, 11, 4491–4503, \[https://doi.org/10.5194/acp-\]\(https://doi.org/10.5194/acp-11-4491-2011\)](#)  
1698 [11-4491-2011](#), 2011.

1699 [Wu, Y., Gao, J., Zhao, A., Niu, X., Liu, Y., Ratnasekera, D., Gamage, T. P., and Samantha, A. H. R.: One-year](#)  
1700 [continuous observations of near-surface atmospheric water vapor stable isotopes at Matara, Sri Lanka, reveal a](#)  
1701 [strong link to moisture sources and convective intensity, \*Atmos. Chem. Phys.\*, 25, 4013–4033,](#)  
1702 <https://doi.org/10.5194/acp-25-4013-2025>, 2025.

1703

1704 [Xiao, F., Zhu, B., and Zhu, T.: Inconsistent urbanisation effects on summer precipitation over the typical climate](#)  
1705 [regions in central and eastern China, \*Theor. Appl. Climatol.\*, 143, 73–85, \[https://doi.org/10.1007/s00704-020-\]\(https://doi.org/10.1007/s00704-020-03404-z\)](#)  
1706 [03404-z](#), 2021.

1707 [Xie, X., Evaristo, R., Troemel, S., Saavedra, P., Simmer, C., and Ryzhkov, A.: Radar Observation of](#)  
1708 [Evaporation and Implications for Quantitative Precipitation and Cooling Rate Estimation, \*J. Atmos. and Ocean.\*](#)  
1709 [Technol.](#), 33, 1779–1792, <https://doi.org/10.1175/JTECH-D-15-0244.1>, 2016.

1710 [Xing, M., Liu, W., and Hu, J.: A set of methods to quantitatively evaluate the below-cloud evaporation effect on](#)  
1711 [precipitation isotopic composition: a case study in a city located in the semi-arid regions of Chinese Loess](#)  
1712 [Plateau, <https://doi.org/10.5194/acp-2020-312>, 26 May 2020.](#)

1713 [Xu, H., Guo, J., Tong, B., Zhang, J., Chen, T., Guo, X., Zhang, J., and Chen, W.: Characterizing the near-global](#)  
1714 [cloud vertical structures over land using high-resolution radiosonde measurements, \*Atmos. Chem. Phys.\*, 23,](#)  
1715 [15011–15038, <https://doi.org/10.5194/acp-23-15011-2023>, 2023.](#)

1716 [Yoshimura, K., Kanamitsu, M., Noone, D., and Oki, T.: Historical isotope simulation using Reanalysis](#)  
1717 [atmospheric data, \*J. Geophys. Res.\*, 113, 2008JD010074, <https://doi.org/10.1029/2008JD010074>, 2008.](#)

1718 [Zaitchik, B. F., Macalady, A. K., Bonneau, L. R., and Smith, R. B.: Europe’s 2003 heat wave: a satellite view of](#)  
1719 [impacts and land–atmosphere feedbacks, \*Int. J. Climatol.\*, 26, 743–769, <https://doi.org/10.1002/joc.1280>, 2006.](#)

1720 [Zhang, F., Huang, T., Man, W., Hu, H., Long, Y., Li, Z., and Pang, Z.: Contribution of Recycled Moisture to](#)  
1721 [Precipitation: A Modified d-Excess-Based Model, \*Geophys. Res. Lett.\*, 48, e2021GL095909,](#)  
1722 <https://doi.org/10.1029/2021GL095909>, 2021.

1723 [Zhu, G., Zhang, Z., Guo, H., Zhang, Y., Yong, L., Wan, Q., Sun, Z., and Ma, H.: Below-Cloud Evaporation of](#)  
1724 [Precipitation Isotopes over Mountains, Oases, and Deserts in Arid Areas, \*J. Hydrometeorol.\*, 22, 2533–2545,](#)  
1725 <https://doi.org/10.1175/JHM-D-20-0170.1>, 2021.

1726

1727